

**Pseudo-Homogeneous CSTR Simulation of a Fluidized Bed
Reactor operating in condensed-mode including Sanchez-
Lacombe n-hexane co-solubility effect predictions**

Pedro Alexandre Oliveira Rainho

Thesis to obtain the Master of Science Degree in Chemical Engineer

Chemical Engineer

Supervisors: Prof. Maria do Rosário Ribeiro, Dr. Timothy F. L. McKenna

Examination Committee

Chairperson: João Carlos Moura Bordado

Supervisor: Maria do Rosário Gomes Ribeiro

Members of the Committee: Carla Isabel Costa Pinheiro

November, 2014

Acknowledgements

It was a great pleasure to have had the opportunity to make my master thesis internship in LCPP, Lyon. I left happy with my work. But I wouldn't have developed my activity so peacefully if I haven't had a kind and friendly group of people day in day out. During my internship I have dealt with very skilful people that were ready to help every time. I'd for sure recommend this workplace. Thanks to a good integration in workplace everything else went faster. And this is a crucial basis to feel good in a new country and somehow to better endure the distance from family and friends.

I have to thank to my co-supervisor Alizadeh Arash for closely monitoring me and help me in specific jobs. I thank my supervisor Timothy F.L. McKenna for providing me this internship and for giving me the general guidelines in my work. I have special thanks for my Portuguese supervisor Maria do Rosário. She was the one who enabled this training abroad. You were all very professional and gentle.

I want to leave a message for the Portuguese friends who went with me to this journey. They are Cristina, Rui and Margarida. It's always refreshing to have some people whom one can speak in native language. Unless they're not nice. Fortunately you weren't that case. And in a whole I think we made a good representation of Portugal.

I also have to mention some people in LCPP that I closely related to. They are, among others, Aaron, Julien, Fatima, Benoit, Nessrine, Islem, Barbara, Thiago, Thaissa, Layla, Ana Carolina, Solmaz, PierreLuc, Alain, Cyntich, Sebastian, Laura. It was a pleasure to be with you.

The last but not the least. Family is always a bedrock. After a day of work, getting home and talk to them in *skype* was just the best end of the day. I won't forget it's much because of them I could take this experience.

Gratification and confidence for the future are my last acknowledgments words.

Abstract

This thesis explores the impact of the **inert condensing agent (ICA) n-hexane** in the production of **Polyethylene** via gas-phase **condensed mode** bed reactor. The gas loaded to these reactors contains mainly ethylene, nitrogen and other reaction agents like hydrogen. But it includes also condensed inert agents like n-hexane. They have an important role in **cooling down** the bed of the reactor not only because they have a relevant heat capacity but primarily because they can be in a condensed state. As the gas-liquid mixture enters the reactor, the condensed liquid content vaporizes and removes latent heat that way allowing bigger productions. ICA's like n-hexane seem, in addition, to **solubilize** the **ethylene** gas in the **amorphous polyethylene** of the **growing polymer phase** (co-solubility effect) enabling even higher polymerization rates.

For an accurate prediction of ethylene solubilisation in polymer phase it is necessary to have an appropriate thermodynamic model. The **Sanchez-Lacombe** equation of state has been successfully applied to **polymer systems**. The reacting system under analysis in this thesis, intended to simulate the gas-phase ethylene polymerization process, is composed by a **gas phase** of **ethylene/n-hexane/nitrogen** and a **polymer phase** of **ethylene/n-hexane/amorphous polyethylene**. This system was evaluated at **7 bar** ethylene, **1 bar** nitrogen and within a range of **0.00-1.00 bar n-hexane**. The reactor simulations were based on a simple pseudo-homogeneous **CSTR** approach and the reaction rate ethylene concentration was given by the Sanchez-Lacombe equation of state. The calculations include **CSTR mass and heat balances** and they are solved for several **steady states** with different operation conditions such as **catalyst flowrates, inlet gas temperature** and **kinetic rate constants**.

The global results show that from **no n-hexane** in reactor to a pressure of 0.10bar hexane there's a variation of polyethylene production of about **2%** (n-hexane co-solubility effect). And as total pressure adds **0.1bar** hexane, the polyethylene production variation approximately follows this trend; it is like this as far as **inlet stream cooling capacity** is not too high (declining reactor temperature and, by extension, kinetics) that it subordinates n-hexane co-solubility effect. Regarding reactor temperature, there are two distinct behaviours: if the reactor operates in a non-condensed mode (less than **0.4bar** hexane), there's a moderate decrease of temperature (**2%** maximum) with rising hexane pressure. It falls down much faster when the reactor starts to operate in a condensed-mode reaching a **8%** variation for each 0.1bar hexane increasing step. In a **sensitive analysis** performed to some parameters of mass and heat balances, highlights focus on a variation of **-8.3°C** in reactor temperature when **heat capacity of gas** deviates **+20%**; a variation of **+3.3°C** in temperature and **+5.7%** in production when **ethylene concentration** in polymer phase changes only **+5%**. And a significant variation of **+6.5°C** in temperature when **reaction enthalpy** only varies **+10%**. Hexane equilibrium gas fraction has a reasonable impact too: when it changes **+15%**, it causes a variation of **+5.0°C** in temperature.

Keywords: Condensed-mode; inert condensing agent; n-hexane; gas-phase ethylene polymerization; FBR with CSTR approach; Sanchez-Lacombe; polymer phase solubility

Table of Contents

List of Tables	7
List of Figures	8
Glossary	9
List of abbreviations	9
List of definitions	9
List of symbols	11
0. Thesis structure and reading orienting	14
1. Introduction	15
1.1. Quick Overview on Polyethylene	15
1.1.1. Generalities	15
1.1.2. Polyethylene industrial production process	18
1.2. Main aims with this thesis	21
2. Literature Review	23
2.1. Thermodynamics considerations	23
2.1.1. Sanchez-Lacombe for hexane co-solubility effect in Polymer phase	25
2.1.2. SAFT research on light gases solubility in amorphous polyethylene	28
2.2. Gas-Phase Fluidized Bed Reactor (FBR)	30
2.2.1. Fluidized bed reactor for LLDPE production	30
2.2.2. Gas-phase ethylene polymerization modelling	33
2.2.3. Condensed mode gas-phase reactor operation	38
2.3. Brief outlook on olefin catalysts	41
3. Reactor Model	44
3.1. Detailed model	44
3.2. Summary of important data used in simulation	53
3.3. Results and sensitive analysis	56
3.3.1. Results	56
3.3.1.1. Plot Results	59
3.3.2. Sensitive analysis	70
3.4. Conclusions & Perspectives	73
3.5. References	75
4. Appendix	80
A. Thermodynamics considerations	80

A.1. Thermodynamics parameters related to polymer particle (amorphous polymer phase)	80
A.2. Inlet flow thermodynamic condition	82
A.3. Ethylene vaporization enthalpy fitting.....	85
B. Outputs concerning Simulation results	86

List of Tables

Table 1 – summary of different topics related to the main types of PE, mentioned in last paragraphs.	17
Table 2 – Summary of the typical operation condition in a FBR for LLDPE production already exposed in last paragraphs	32
Table 3 – General parameters/constants used in model simulations.	53
Table 4 – Working thermodynamic conditions relating to polymer phase ethylene concentration, polymer phase hexane concentration, gas density, polymer particle density and gas heat capacity. The half below of the table indicates the liquid fraction of inlet flow at different inlet temperatures, for the working hexane pressures.....	55
Table 5 – Simulation results for 3 different reference propagation kinetic constants, $k_p^{80^\circ\text{C}}$	58
Table 6 – Relative variation of polyethylene mass rate and reactor temperature for each hexane pressure with respect to simulation 1	61
Table 7 – comparison between simulation 3 results and an industrial patent. Patent partial pressures are calculated using ideal gas law given the molar fractions in its examples. Z, Y, W, L and M mean a certain numerical value.....	66
Table 8 – comparison between simulation 3 results and an industrial patent. Patent partial pressures are calculated using ideal gas law given the molar fractions in its examples. In patent case 1, the ICA is isopentane. In patent case 2, the ICA is n-butane	68
Table 9 – vaporization heat and heat capacity for the ICA's compared in patents (isopentane, n-butane and n-hexane). They are referred to the boiling point temperature at 1 bar pressure.	68
Table 10 – Sensitive analysis output for simulation 1	71

List of Figures

Figure 1 – Pellets of PE with different colours.....	15
Figure 2 – Total PE demand by end use in 2010. Plot made in Excel® whose data was extracted from IHS (Rappaport, 2011)	17
Figure 3 – Polyethylene net exports in the principal regions around the world. Plot made in Excel® whose data was extracted from IHS (Rappaport, 2011)	18
Figure 4 – General configuration of gas-phase FBR ethylene polymerization. (Chemistry Department at the University of York, 2014)	19
Figure 5 – illustration of general polymer particle growth.....	21
Figure 6 - Schematic representation of ethylene-polyethylene binary system (1) and ethylene-n-hexane-polyethylene ternary system (2) at different scale levels. (Alizadeh A. , 2014, Figure 4.3)	25
Figure 7 – bubble, cloud and wake phase illustration	30
Figure 8 – Gas-phase FBR illustration for ethylene polymerization	31
Figure 9 – representation of macro-scale, micro-scale and surface scale view of the polymerization phenomena. (Alizadeh A. , 2014, Figure 2.3).....	33
Figure 10 – Particle and reactor view (left and right image respectively).....	45
Figure 11 – Polyethylene mass rate steady-state simulations 1 results given the condition in plot title. Numerical output is in table 5. No result for $k_p = 1200\text{m}^3\text{mol-site}^{-1}\text{s}^{-1}$ curve at 1.0bar hexane pressure due to thermodynamic constraint.	60
Figure 12 – Reactor temperature result simulation 1 given the conditions in plot title. Simulation output is in table 5	60
Figure 13 – Polyethylene mass rate steady-state simulations 2 results given the conditions in plot title. Simulation output is in appendix B	62
Figure 14 – Reactor temperature result simulation 2 given the conditions in plot title. Simulation output is in appendix B	63
Figure 15 – Polyethylene mass rate steady-state simulations 3 results given the conditions in plot title. Simulation output is in appendix B.	64
Figure 16 – Reactor temperature result simulation 3 given the conditions in plot title. Simulation output is in appendix B	64

Glossary

List of abbreviations

CMO – Condensed-mode operation
CSTR – Continuous Stirred Tank Reactor
EOS – Equation of State
FB – fluidized bed
FBR – Fluidized bed reactor
HB – Heat balance
HDPE – High density polyethylene
ICA – Inert condensing agent
LCB – Linear chain branching
LDP – Low density polyethylene
LLDPE – Linear low density polyethylene
MAO – Methylaluminoxane
MI – Melt index
MW – Molecular weight
MWD – Molecular weight distribution
PE – Polyethylene
PEMB – Polyethylene mass balance
RKS – Redich-Kwong-Soave
SCB – Short chain branching
SL – Sanchez-Lacombe
TMB – Total mass balance
Z-N – Ziegler-Natta catalyst

List of definitions

Amorphous polymer – polymer part that has no long range order characteristic of a crystalline polymer.

Catalyst support - material, usually a solid with a high surface area, to which a catalyst is affixed.

Cristalinity - Crystallinity is an indication of amount of crystalline region in polymer with respect to amorphous content. It influences polymer properties such as Hardness, tensile, stiffness, crease, melting point.

Fluidization - Process in which solids are caused to behave like a fluid by blowing gas or liquid upwards through the solid-filled reactor.

Lattice model - is a physical model that is defined on a lattice, as opposed to the continuum of space.

Melt index - It is the weight of resin flowing out from a standard die for 10 minutes under a given temperature and pressure.

Mixing index - normalized quantity (ranging between 0 and 1) which gives a measure of the particle mixing within a reactor

Multimodal polyethylene - Multimodal means that two or more peak molecular weights can be seen by gel permeation chromatography. Multimodal PE can be transformed into articles by injection molding, blow molding, rotational molding, and film extrusion. One of the advantages of multimodal PE over mono-modal PE is its easier and faster processing with reduced energy requirement and increased output.

Net exports - Relationship between a nation's imports and exports

Pellet – material compressed and or molded in a particular shape

Polymer Agglomeration - Process in which dispersed molecules or particles assemble rather than remain as isolated single molecules or particles.

Polymer swelling - increasing of volume of polymer due to absorption of a solvent

Space-time yield - It's usually defined as the quotient of product quantity flowrate divided by reacting volume.

Supercritical fluid - substance at a temperature and pressure above its critical point, where distinct liquid and gas phases do not exist

Tailoring – adapting requirements or specification to a current polymer through deletion, modification and/or supplementation without deviating from determined standards

List of symbols

Kinetic list

C^* - total active sites concentration in total catalyst (mol-active-site/ m^3_c)

C_0^* - total initial active sites concentration in total catalyst (mol active site/ m^3_c)

C_{et}^P - ethylene equilibrium concentration in (amorphous) polymer phase (mol/ m^3_p)

C_{hex}^P - hexane equilibrium concentration in (amorphous) polymer phase (mol/ m^3_p)

E_a – activation energy for catalyst propagation (J/mol)

E_d – activation energy for catalyst deactivation (J/mol)

$K_d^{Texp.}$ – catalyst deactivation constant at experimentation temperature (s^{-1})

K_d – catalyst deactivation constant (s^{-1})

$K_p^{Texp.}$ – propagation polymerization constant at a experimentation temperature (m^3_p /mol-active-site.s)

K_p – propagation polymerization constant (m^3_p /mol-active-site.s)

P_{et} – ethylene pressure in the reactor (bar)

P_{hex} – hexane pressure in the reactor (bar)

P_{N_2} – nitrogen pressure in the reactor (bar)

R_p – Average rate of polymerization ($kg_{pol.}/m^3_c.h$)

Operations list

b – reactor base area (m^2)

%Conv. – conversion percentage of ethylene

d – reactor diameter (m)

h_b – reactor bed height (m)

$m_{et,0}$ – inlet mass flowrate of ethylene in gas-phase (kg/h)

m_{et} – outlet mass flowrate of ethylene in gas-phase (kg/h)

$m_{et,d}$ – dissolved mass flowrate of ethylene in polymer phase (kg/h)

m_g – outlet mass flowrate of gas-phase (kg/h)

$m_{hex,0}$ – inlet mass flowrate of hexane in gas-phase (kg/h)

m_{hex} – outlet mass flowrate of hexane in gas-phase (kg/h)

$m_{hex,d}$ – dissolved mass flowrate of hexane in polymer phase (kg/h)

$m_{N_2,0}$ – inlet mass flowrate of nitrogen (kg/h)

m_{N_2} – outlet mass flowrate of nitrogen (kg/h)

m_p – polymer phase mass flowrate (ton/h)

m_{Pet} – polyethylene mass flowrate (ton/h)

$Q_{c,0}$ – inlet catalyst flowrate (g/s)

Q_c – outlet catalyst flowrate (g/s)

$Q_{g,0}$ – inlet gas volumetric flowrate (m^3/h)

Q_g – outlet gas volumetric flowrate (m^3/h)

Q_p – polymer particle volumetric outflow rate (m^3/h)

u_g – superficial gas velocity (m/s)

V_b – reactor bed volume (m^3)
 V_c – Total catalyst volume in the reactor (m^3)
 V_p – total volume of polymer particles in the reactor
 σ_p – average particle residence time (h)
 ε – porosity in the reactor (volume of gas in total volume of bed reactor)
 ρ_p – polymer particle density (kg/m^3)
 ρ – bulk density of the fluidized bed (kg/m^3)

Thermodynamic list

$C_{p,g}$ – heat capacity of gas-phase ($J/kg.K$)
 $C_{p,p}$ – heat capacity of polymer phase ($J/kg.K$)
 $C_{p,c}$ – heat capacity of catalyst ($J/kg.K$)
 F – total molar inlet flowrate (mol/s)
 G – gas molar inlet flowrate (mol/s)
 L – liquid molar inlet flowrate (mol/s)
 $M_{et.}$ – ethylene molar mass (g/mol)
 M_F – molecular weight of total inlet gas flowrate (g/mol)
 m_{Gas} – gas mass in inlet gas flowrate (kg/s)
 M_{Gas} – molecular weight of gas in inlet gas flowrate (g/mol)
 $M_{hex.}$ – hexane molar mass (g/mol)
 $m_{Liq.}$ – liquid mass in inlet gas flowrate (kg/s)
 $\%m_{Liq.}$ – liquid mass fraction in inlet gas flowrate (mass of liquid by total mass)
 $M_{Liq.}$ – molecular weight of liquid in inlet gas flowrate (g/mol)
 M_{N_2} – nitrogen molar mass (g/mol)
 R – ideal gas constant ($kJ.mol^{-1}.K^{-1}$)
 T – reactor temperature ($^{\circ}C$)
 T_0 – temperature of the reactor inlet flows ($^{\circ}C$)
 $T^{DewPoint}$ – inlet gas flowrate dew point temperature ($^{\circ}C$)
 $T_{exp.}$ – experimentation temperature ($^{\circ}C$)
 $x_{et.}$ – liquid phase equilibrium fraction of ethylene
 $x_{hex.}$ – liquid phase equilibrium fraction of hexane
 $x_{hex.}^{DewPoint}$ – liquid phase equilibrium fraction of hexane in dew point
 $y_{et.}$ – gas phase equilibrium fraction of ethylene in inlet flowrate
 $y_{hex.}$ – gas phase equilibrium fraction of hexane in inlet flowrate
 $y_{hex.}^{DewPoint}$ – gas phase equilibrium fraction of hexane in dew point
 $y_{N_2.}$ – gas phase equilibrium fraction of nitrogen in inlet flowrate

$\Delta H_{\text{hex.}^{\text{v}}}$ – vaporization enthalpy of hexane (kJ/mol)

$\Delta H_{\text{r}}^{\text{T}}$ – reaction enthalpy at the temperature of reaction (kJ/mol)

$\Delta H_{\text{r}}^{\text{T}^{\text{exp}}}$ – reaction enthalpy at the experimentation temperature (kJ/mol)

Δc_p – variation in specific heat of reaction media (J/kg.K)

ρ_c – catalyst density (kg/m³)

ρ_g – gas density (kg/m³)

ρ_p – polymer phase density (kg/m³)

Note: the units of the quantities may be different, in some cases, from the ones expressed here in Glossary. They were already mentioned for a quick perception in what they physically represent

0. Thesis structure and reading orienting

This thesis is divided into 3 chapters – **Introduction**, **Literature review** and **Reactor simulation**.

In the **introduction**, there's a brief exposition of the world of polyethylene covering different aspects such as its market, main production processes and some other generalities. To finish this chapter there's a topic where it is expressed the main intents and what's expected to achieve with this thesis.

The chapter of **literature review** will make the necessary framework providing the reader a series of relevant subjects and works related to the polyethylene production in gas-phase using a fluidized bed reactor. First it will be introduced the main contributions of Sanchez-Lacombe equation of state in predicting the co-solubility effect of hexane for ethylene solubility in the polymer phase. Particularly a study where it had been done equilibrium simulations with Sanchez-Lacombe equation of state for the ethylene/n-hexane/polyethylene ternary system. There's a special attention to this work once ethylene concentration polymerization rate values used in the current thesis are extracted from it. There will be also some reference to the statistical associating fluid theory (SAFT) once it's been also used satisfactorily in this field. A literature review on fluidized bed reactors for ethylene polymerization in terms of its more general modelling and other common approaches is also presented. Emphasis will be given to the condensed-mode operation together with Sanchez-Lacombe equation of state. In the end there's a small topic on the catalysts used for these processes and the corresponding advantages and characteristics.

The results come in chapter of **Reactor simulation**. It starts with the description and assumptions of the model. There are 3 sets of simulations corresponding to 3 pairs of plots (showing polyethylene production and reactor temperature). To analyse the impact of some parameters of the model in output simulations (production and temperature) it is made a sensitive analysis to some of them such as heat capacities and equilibrium conditions. It was also attempted to make some comparison between a simulation performed in this thesis and a related industrial patent.

The references cited on text are according *American Psychological Association* (APA) style. All bibliography is in the last chapter of the thesis.

1. Introduction

1.1. Quick Overview on Polyethylene

1.1.1. Generalities

The literature on polyethylene (PE) is vast. Here is given the most important information on characteristics, applications and PE market, in a concise way. These main topics will be summarized in tables or plots after the corresponding texts.

As it is well known, the PE is the most produced and best known polymer in the world. It's easily found in our daily lives. For example, everyone uses purchase supermarket bags made of polyethylene. But its existence is spread in lots of other products. Its versatility and reliability makes possible to build materials of different design and dimensions with a wide range of applications (see table 1). Generally we can say PE is a good raw-material for soft, though, hard and sturdy materials. And it is typically appreciated by, among others, its insulating capacity, resistance against aggressive substances and damage, "unbreakability", reliability, lightness and the fact it can work from warm temperatures to colder ones (negative ones).

Polyethylene products are commonly classified by their **melt index** and **density**. The melt index provides a general indication of a product's molecular weight (MW) and processability. The fluid nature of polyethylene depends on the melt-index. A higher melt index resin will typically have a lower molecular weight and processes/flows easier. On the opposite, a higherr MW decreases its physical properties and polyethylene will flow poorly. In what concerns density it may be regarded as a measure of crystallinity. On the other hand, producing polyethylene under **high pressure** leads to a **low density** material because the mixture of branches and side branches formed makes the structure not to be so well packed. As a result the PE gets lighter.

All resultant PE products are turned into pellets composed by additives and processing aids that will lately give the desired properties to the final product. PE can sometimes be processed as it is in its



Figure 1 – Pellets of PE with different colours

natural state but usually it needs some additives to make it more suitable for certain applications. These substances are projected, for example, to prevent objects that are exposed to the open air from fading or becoming weather beaten. Sometimes a substance is added to make a film extra smooth, or to prevent the films from sticking together. Often substances are added to reduce flammability. Colours are also frequently added. (see figure 1).

From an environmental point of view, polyethylene is a friendly material. For the world production of polyethylene, not even 1% of the total production of crude oil and natural gas is used annually. The production of polyethylene is relatively clean and efficient since the emission of harmful substances is minimal and there is approximately zero waste. PE

is a thermoplastic material being very suitable for reuse and recycling. It can be melted down and used for making products virtually indefinitely. Nowadays many carrier bags and dust bin bags are made from recycled polyethylene in this way. When polyethylene is collected after use and it cannot be processed again, it supplies a high-grade fuel for the provision of energy. (Sabic, 2005) (Nowlin, 2014)

Three main density PE categories – HDPE, LDPE and LLDPE

In terms of **density** there are 3 main categories industrially produced: high density polyethylene (HDPE), Low density polyethylene (LDPE) and linear low density polyethylene (LLDPE).

HDPE products exhibit the highest density and crystallinity in the PE family. HDPE can be produced by using slurry, solution, or gas phase reactor technologies. HDPE manufacturing processes also use transition metal catalysts to make linear polymer chains with less branching than LLDPE. With HDPE, the molecular weight distribution (MWD) can vary depending on the catalyst and reactor technology used in production. For example, chromium-catalyzed products typically produce broader MWD products. The broader MWD is advantageous for some applications such as blow molding due to higher melt strength.

LDPE is produced by autoclave or tubular reactor technology. The high level of long-chain branching of LDPE causes the polymer to have low crystallinity and low density ranging from **0.915** to **0.935** g/cc. Vinyl acetate (VA) can be added to produce copolymer products that can have increased clarity (at low VA levels) and increased flexibility. As a result of the low crystallinity of LDPE, the end use applications are flexible and soft.

LLDPE is the category of particular interest in this thesis. The study in this work is somehow related to this PE family once solubility data used in later simulations came from solubility predictions made for a polymeric system composed by LLDPE. LLDPE is typically made by using a transition-metal catalyst in a gas-phase reactor that operates at low pressures (around 20-40bar) relative to the high pressures (2000-3500bar) used in the production of LDPE. Comonomers such as butene, hexene or octene are added with ethylene to create linear polymer chains with short chain branches and low densities. Solution and some slurry reactor technologies can be utilized to produce LLDPE as well. While LDPE has high levels of linear chain branching (LCB), there is little LCB in LLDPE. However there are high levels of short-chain branching (SCB) contributed by the incorporated comonomer. Even though the densities of LDPE and LLDPE are similar, LLDPE displays better tear and impact film properties than LDPE due to decreased levels of LCB and narrower MWD. Nevertheless, due to the lack of LCB and narrower MWD, film processability decreases. Rotomolding of large parts such as toys and tanks usually uses LLDPE resins. Other typical applications include heavy-duty shipping sacks, industrial packaging, flexible food packaging, storage boxes and thin-wall lids. (Lyondel Chemical, 2014); (Greene, 2014)

	Density (g/cm ³)	Some Characteristics	Applications
HDPE	0.940-0.965	<ul style="list-style-type: none"> - Higher crystallinity - Higher stiffness - broader or narrower MWD depending on catalyst - Less branching than LLDPE 	Detergent bottles; milk bottles; pails; thin-wall containers; drink cups; cases and crates; grocery bags and produce bags
LDPE	0.915-0.935	<ul style="list-style-type: none"> - highly long-chain branched - low crystallinity - flexible and soft - less tear and impact film 	High clarity film; flexible food packaging; heavy duty films; caps and closures
LLDPE	0.915-0.930	<ul style="list-style-type: none"> - little long-chain branching - high level of short-chain branching - better tear and impact film than LDPE - Narrower MWD than LDPE - It maintains its shape 	Rotomolding of toys and tanks; heavy-duty shipping sacks; industrial packaging; flexible food packaging; storage boxes; thin-wall lids

Table 1 – summary of different topics related to the main types of PE, mentioned in last paragraphs.

PE worldwide production and future perspectives on this market

According to IHS (Rappaport, 2011), in 2010 the 3 main types of PE represented 38% of the total global consumption of plastics. In 2nd place came propylene (PP) with 25% of the total global consumption. In terms of total PE demand by end use we can see the figure 2.

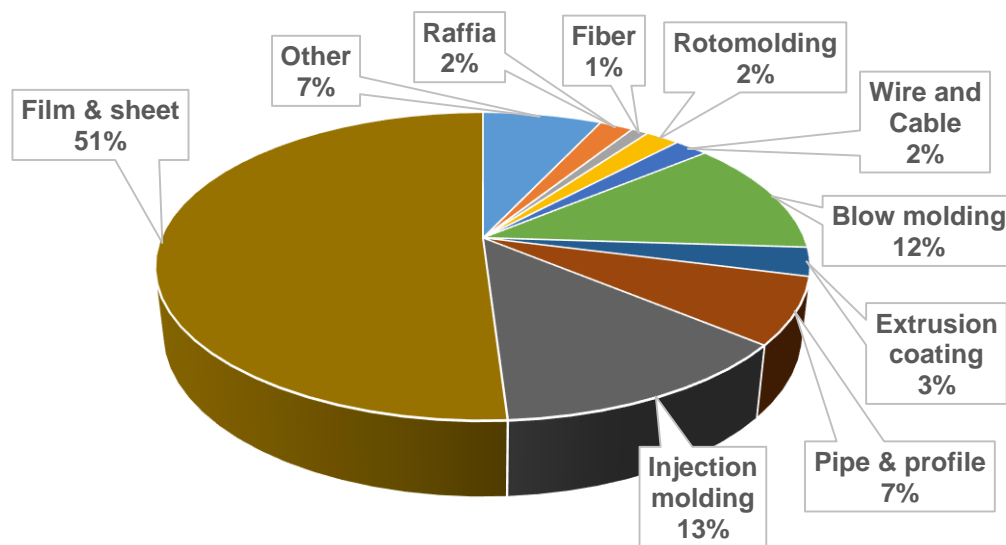


Figure 2 – Total PE demand by end use in 2010. Plot made in Excel® whose data was extracted from IHS (Rappaport, 2011)

The figure 2 evidences the clear importance that **film & sheet** end use have in PE market. In 2nd and 3rd place come injection molding and blow molding respectively. The IHS also compares the capacity of Top global PE producers in 2002 and 2015 and it expects an impressive increasing of about 78%. This increasing is due to Middle East market.

In terms of the net exports for 2010 and 2015 forecast, they follow in figure 3.

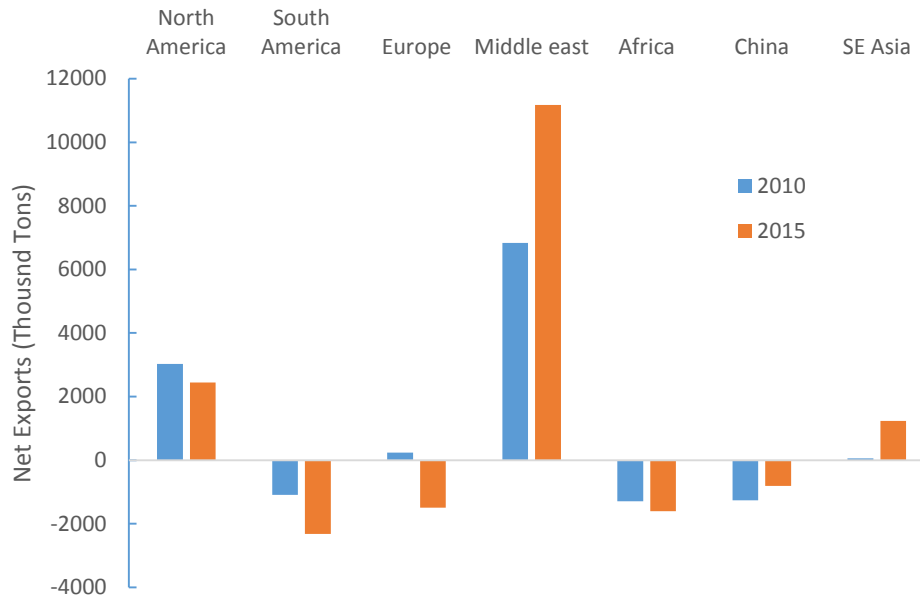


Figure 3 – Polyethylene net exports in the principal regions around the world. Plot made in *Excel®* whose data was extracted from IHS (*Rappaport, 2011*)

China is becoming self-sufficient (increasing of net exports in 2015) and Middle-east will have a very significant increasing in their net exports. Some relevant bigger net exports also will occur in South East Asia. For instance, for the LLDPE only, the market demand is expected to grow by 6.2 percent per year over the period to 2015. This is in fact mainly due to their lower production cost and a range of achievable properties which can find a variety of applications in the different industrial sectors.

1.1.2. Polyethylene industrial production process

The enormous global market of polyolefins and the projection for future demand of these materials is quite a reason for the leaders in this field to invest on research and development. Innovative materials with more desirable properties for specific applications are being synthesized through state of the art tailoring the microstructure of the polymer chains. New, more flexible processes are continuously being developed in order to make possible for the companies to produce polymers with specific properties to meet the requirements of different end-use products. Intensification for enhancement of process energy efficiency has been practiced like in **condensed mode operation** (CMO) of gas phase polymerization.

Companies also know more than ever that the environmental requirements come to play a stronger role in the process design and operation.

The most common processes for producing olefins use supported catalysts. And there are a lot of studies covering a broad type and nature of them once such topics have a great influence on polymerization. On some of these catalysts, PE resins are produced through fluidizing ethylene. The most appropriate reactor configuration to be used in or as a part of the process to produce the final polymeric product relies on production capacity of process, equipment and operating costs of process. The configuration should also take into account some flexibility in producing different grades of polymer depending on the changes in the market demand. And finally it has to be able to produce polymers with such a properties meeting the specific end-use product.

Types of production

The catalytic polymerization of olefins is carried out in three main types of processes depending on the phase of the continuous medium in which the polymerization reaction takes place. They are **solution**, **slurry** and **gas phase** processes. In the solution process, the polymerization reaction is carried out at the temperature about 200 °C. It is mainly used to produce low molecular weight polymers. In slurry process, the solid catalyst and growing polymer particles are dispersed in the continuous phase of a hydrocarbon diluent. In the gas phase polymerization process, the catalyst and polymer particles are dispersed in continuous motion inside the reactor by an agitator or a fluidizing gas flow depending on the reactor configuration.

Gas-phase technology is popularly used for producing LLDPE. The process is capable to produce broader melt index and density than others. Therefore, it can adjust to follow market needs being this a huge advantage towards other processes. In fact, gas-phase can be used for every PE density categories. And that's a particular reason for being utilized so widely and even more and more. For example, the amorphous content of a PE (responsible for PE low density) may be produced in gas-phase process and then it may follow to slurry process given its solubility in such a media. The polymerization of ethylene on supported catalyst in gas phase fluidized bed reactors (FBRs) also

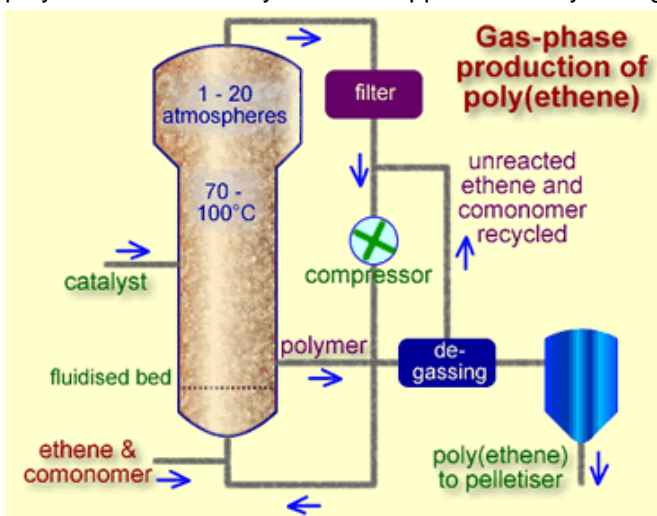


Figure 4 – General configuration of gas-phase FBR ethylene polymerization. (Chemistry Department at the University of York, 2014)

represents a considerable portion of the installed HDPE plants worldwide.

A basic configuration of the most common gas-phase ethylene polymerization is illustrated in figure 4. The feed stream contains ethylene and other gases including inert ones. This feed stream is injected into the reactor and the liquefied portion of it (in the form of small droplets) rapidly heat up and vaporize in the reactor. In this manner the latent heat of vaporization is used to absorb a significant amount of the heat of reaction especially in the bottom part of the reactor.

This is actually a way of making higher polymerization rates possible. The remaining/leaving gas in the top of the reactor is afterwards recycled being first partially liquefied in an external heat exchanger by cooling it below the dew point. In what concerns the polymer product, this leaves near by the bottom of the reactor and then it goes under some gas and impurities removal operation. In the end of the process it is usually blended with some additives and finally pelletized.

Proper fluidizing bed conditions for an efficient process

In a gas-phase ethylene polymerization fluidized bed reactor it is critical to prevent agglomeration or formation of chunks of polymer that cannot be removed as product. This is accomplished through control of the temperature of the gaseous stream in the reaction bed, setting the temperature below the fusion or sticking one of the polymer particles produced during the polymerization reaction. It is presumed that the amount of polymer produced in a fluidized bed polymerization process is related to the amount of heat that can be withdrawn from the reaction zone. Also in a steady state fluidized bed polymerization wherein the heat generated by the polymerization reaction is substantially proportional to the rate of polymer production, the heat generated is equal to the heat absorbed by the gaseous stream and lost by other means such that the bed temperature remains constant. Another requirement of a fluidized bed process is that the velocity of the gaseous recycle stream is sufficient to maintain the fluidized bed in a fluidized state.

The liquid phase of the two-phase gas/liquid recycle stream mixture in condensed mode remains entrained or suspended in the gas phase of the mixture. The space time yields are function of cooling capacity of the recycle stream. In turn, this cooling capacity of recycle stream is due to the greater temperature differential between the entering recycle stream plus the fluidized bed temperature and to the vaporization of condensed liquid entrained in the recycle stream. The condensed liquid in the recycle gas should not exceed 20% weight and should preferably be between 2 and 12% weight of the total feed. (US Patente N° 5.462.999, 1995) However, more recently these limits have been proposed to be allowed significantly higher. (US Patente N° 5.436.304, 1995)

1.2. Main aims with this thesis

Like said in previous topics, the rate of polymer production in gas-phase ethylene polymerization FBR's is significantly limited by the heat rate removal of polymerization. And one way of increasing the heat removal, and achieving higher production rates, is to use a condensed mode cooling operation. The CMO has proven to have also a side effect in terms of ethylene solubility in **amorphous polymer phase**, this is, a higher thermodynamic availability of ethylene monomer to react in growing polymer phase. To study and simulate this phenomena it's necessary to understand how the ethylene is leading to higher activity in polymerization as polymer chains are growing. The gas fed to the FBR contains, besides ethylene and other reaction agent gases, a mixture of inert condensing n-alkanes gases. When they enter the reactor, they almost immediately vaporize and stay in the gas phase being able to diffuse

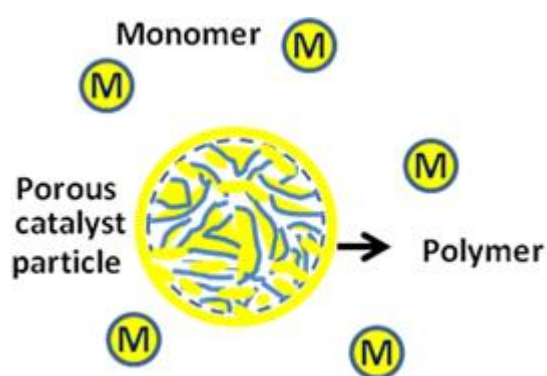


Figure 5 – illustration of general polymer particle growth

into polymer particles. As soon as ethylene gets in touch with catalyst particles, it diffuses into their pores and it starts to polymerize. By this time, catalyst particle **fragments** into smaller fragments. As the reaction proceeds, the ethylene has to start sorbing into the polymer phase in order it can achieve the active sites. As the polymer layer covering the active sites is essentially made of **amorphous polyethylene**, the rate of reaction will be determined by the concentration of ethylene in the amorphous phase of the semi-crystalline PE. The fact ICA's, like n-hexane, also solubilizes in polymeric particle seems to enhance the ethylene concentration somehow.

Science and engineering needed

Most of the solubility measurements regarding this subject were conducted for the sorption of a single solute (like ethylene) in a polymer (like polyethylene) as a binary system. But, as mentioned, the real process contains not only polyethylene and ethylene but a mixture of different components with different functionalities. If the co-solubility n-alkane functionality is to be studied, there will be sorption in polymer not only by ethylene but also by n-alkane. So for more realistic modelling it should be included at least ternary phase in polymer solubility species studies. Some thermodynamics models have been tested to predict and account this solubilisation. The **Sanchez-Lacombe** equation of state (EOS) is one of the most widely applied models in simulation of polymerization phase thermodynamics. In this thesis it will be used its most lately results concerning ethylene solubility and concentration in growing polymer phase when n-hexane is present. It aims to capture the global effect of having an increasing ethylene concentration in polymer phase derived by the co-solubility effect of n-hexane.

Several studies for LLDPE production have included particle growth models that led to a better understanding of the reactor behavior as well as properties of the polymer produced. Modelling at the particle level requires not only thermodynamics but naturally transfer phenomena too. Nevertheless it has been established in the literature that, under many conditions, heat transfer and diffusional

resistances do not play an important role at the particle level in gas-phase polyethylene reactors when this particle is already in a mature/developed state (Kosek, Grof, Novák, Stepánek, & Marek, 2001). Under this statement, and since it meets the purposes of this work, it will be considered only thermodynamics.

To perform the **reactor simulations** it will be written mass and energy balances in a simplified pseudo-homogeneous CSTR approach. The polymerization rate term follows the widely used general ethylene polymerization kinetics (Floyd, Choi, Taylor, & Ray, 1986) where ethylene concentration in amorphous polymer phase comes from SL predictions. A set of steady-state simulations to obtain the **polyethylene mass rate** and **reactor temperature** will be done then.

2. Literature Review

2.1. Thermodynamics considerations

A deep understanding of the phase behaviour of polymer-solvent systems is of crucial practical importance in polymer production and processing. The gas-phase ethylene polymerization is one particular case of interest. One needs to be able to measure the solubility of ethylene in the amorphous phase of polyethylene and describe it with an appropriate thermodynamic model. These tools will allow a comprehensive understanding about the effect of process conditions on the rate of polymerization. In a gas-phase polymerization, all the monomers are in gaseous (or supercritical) form, whereas the polymerization is occurring in the liquid phase (let's say polymer phase). Thus, during a gas-phase polymerization reaction, the monomers must be absorbed into and diffuse through the growing polymer particle to reach the catalytic sites. In consequence, thermodynamic analysis of the process involves the phase equilibrium of the monomer + polymer phase. Industrially there are even other light gases in the reactor and analysis then involves the multi-component phase equilibrium of gases + polymer.

In the commercial gas-phase manufacture of LLDPE, at least a ternary mixture of ethylene, n-alkane, and polyethylene coexist in the reactor during polymerization. To a more rigorous understanding of the kinetics of this polymerization, precise knowledge of the solubility and diffusion of ethylene and the n-alkane in polyethylene is required at reaction conditions. Experimental studies of sorption of multicomponent gas mixtures in polyolefins under reactor conditions are expensive and time-consuming. Furthermore, safety considerations can add significantly to the cost of such work. Industrial applications have traditionally relied on empirical correlations and semi theoretical equations-of-state to generate solubility information on such solutes and their mixtures in relevant polymeric systems. Hereupon, thermodynamic models like Sanchez-Lacombe can be a safer, cheaper and reliable alternative.

There are two major classes of thermodynamic equations of state which have been subject to substantial improvements during the course of last decades and currently have found a wide range of application fields in the polymer industry due to their excellent predictive capabilities: (a) perturbation theory models with the **Perturbed Chain Statistical Association Fluid Theory (PC-SAFT)** model as its most recent and widely applied version and (b) **lattice models** with **Sanchez-Lacombe EOS** (Sanchez & Lacombe, 1978) as its most widely applied version. In the lattice models, it is assumed that the molecules have one or more segments and the partition function of system can be calculated by counting the number of possible configurations when these segments are arranged in hypothetical cells which resemble the crystal lattice of a solid. The thermodynamic properties then can be obtained by using formalism of statistical mechanics. The lattice can be considered to be compressible or incompressible. The incompressible lattices are generally used to model liquids at low pressures while the compressible lattices result in the equations of state based on lattice model like the lattice fluid theory of Sanchez and Lacombe. The Sanchez-Lacombe EOS is similar and can be considered as the continuation of Flory-Huggins theory (Frederic, Agnes, & McBrewster, 2010). The most important

improvement is that Sanchez-Lacombe theory introduces holes into the hypothetical lattice to account for the variation in compressibility and consequently density.

The statistical associating fluid theory (SAFT) provides an EOS based on the continuum approach for chain molecules developed by Wertheim Chapman. The more recent versions of the SAFT EOS include the **variable-range** - SAFT-VR - and the **perturbed-chain** - PC-SAFT - descriptions. The differences between these arise from the specific treatment of the **attractive inter-segment interactions** and the **choice of reference fluid**. In the case of SAFT-VR the reference is a hard-sphere fluid, while in that of PC-SAFT the reference is a hard-sphere-chain fluid. Recently, simplified PC-SAFT has been developed for one-fluid mixing rule and applied to the reference hard-chain fluid. Since the simplification takes the form of a mixing rule, the simplified EOS reduces to original PC-SAFT in the pure-component limit. However, the modification greatly simplifies the form of the reference radial distribution function, without loss of accuracy and with a reduction in computing times. The SAFT-VR EOS describes a fluid of associating chain molecules with the segments of the chain interacting through attractive interactions of variable range (typically a square-well potential). The reference system of attracting monomers is used to build up the chain. In the SAFT-VR approach, the molecules are modelled as flexible chains formed from m tangent spherical segments. Each segment in a chain has the same diameter, σ , but segments belonging to different species can have different diameters. The dispersive interactions between the segments can be modelled using any standard attractive pair potential of depth, ϵ , and variable range, λ . For further details and fundamentals of SAFT theories, reader shall consult (Chapman, Gubbins, Jackson, & Radosz, 1989), (Gross & Sadowski, 2001).

2.1.1. Sanchez-Lacombe for hexane co-solubility effect in Polymer phase

The rate law of ethylene polymerization adopted in this thesis is the one proposed by Floyd (Floyd, Choi, Taylor, & Ray, 1986). It's a catalytic **single-site** and **first order** rate with respect to the ethylene concentration at the active sites. The local rate of polymerization inside a polymer particle is expressed as:

$$R_{p,loc} = k_p C^* C_m^* \quad (1)$$

k_p - rate propagation constant

C^* - local concentration of active sites in some catalyst fragment

C_m^* - ethylene local concentration in the amorphous phase of polymer surrounding catalyst fragment

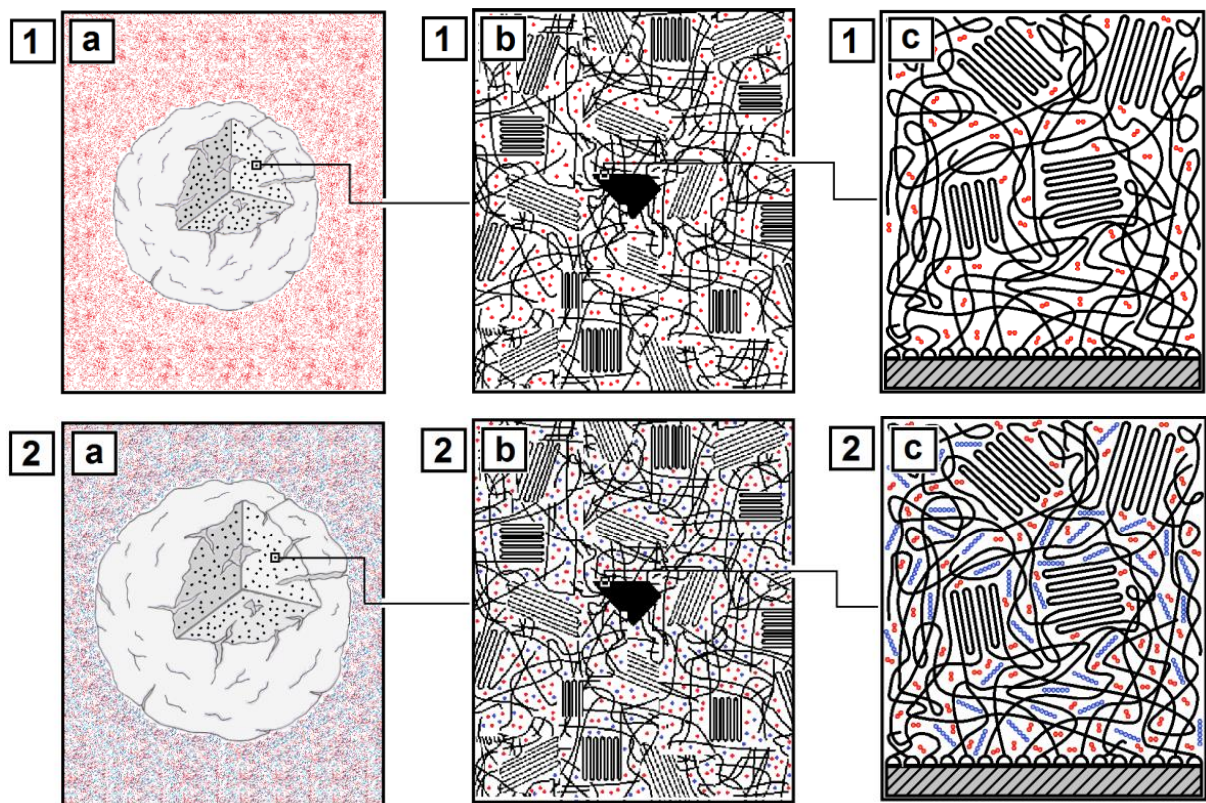


Figure 6 - Schematic representation of ethylene-polyethylene binary system (1) and ethylene-n-hexane-polyethylene ternary system (2) at different scale levels. (Alizadeh A. , 2014, Figure 4.3)

The figure 6 illustrates a polymer particle in a binary system (1) and ternary system (2). In both of them, the structure surrounded by a gas phase (a) is zoomed until a catalyst fragment surrounded by produced semi-crystalline polyethylene (b) which in turn is zoomed till polymer chains being immobilized on the surface of catalyst fragment (c). In system (1) there's only ethylene gas (in red) in polymer particle whereas in system (2) both ethylene and n-hexane (in blue) are present.

To predict satisfactorily the ethylene concentration in amorphous polymer phase, C_m^* , in eq. 1, a thermodynamic model has to be capable of detecting the effect of n-hexane on the ethylene solubility and the polymer swelling. The predictive capabilities of SL EOS depend on **binary interaction parameters** which some are found to be **temperature-dependent**. These parameters can be used to predict the solubility of multicomponent systems like in the current ethylene/polyethylene/n-hexane system.

Hutchinson and Ray (Ray & Hutchinson, 1990) have developed thermodynamic models to predict equilibrium monomer concentrations at the catalyst sites from external gas-phase monomer concentrations in the vicinity of the polymer particles. Kosek (Kosek, Grof, Novák, Stepánek, & Marek, 2001) explored the advantage of the steady-state modeling as the possibility of dependence of temperature and concentrations in the particle on model parameters. He found that for many catalyst systems in which heat and mass transfer resistances do not influence monomer concentrations and temperatures within the polymer particles, the monomer concentration at the catalyst sites is determined by the equilibrium sorption of the monomer within the polymer particles. Yang (Yao, Hu, & Yang, 2007) measured the solubility of ethylene/isopentane and ethylene/n-hexane in semicrystalline PE of crystallinity of 48.6%, at temperatures of 70, 80, and 90°C, 2 MPa total pressure, 80–190KPa isopentane pressure and 20-90KPa n-hexane pressure. He concluded isopentane and n-hexane increase the solubility of ethylene in the corresponding ternary system. On the contrary, the solubility of isopentane or n-hexane remains unchanged with an increase of the ethylene partial pressure. Bashir et al. (Bashir, Ali, Kanellopoulos, & Seppälä, 2013) used SL EOS predictions in the multicomponent system of ethylene/1-hexene/LLDPE-1-hexene mixture at 70°C, 90°C and 150°C. Their predictions were in good agreement with the experimental data. They also noted the solubility enhancement is co-monomer-type dependent.

Alizadeh (Alizadeh A. , 2014) extended the application of Sanchez-Lacombe EOS from the binary system of ethylene/PE to the ternary system of ethylene/n-hexane/PE in order to describe the change in concentration of ethylene in the amorphous phase of polyethylene. He fitted his SL predictions with the sorption equilibrium data acquired by group of Yang (Yao, Hu, & Yang, 2007), (Yao, Hu, & Yang, 2007) by adjusting the binary interaction parameters (k_{ij}). Yang's team used some commercial LLDPE for binary and ternary system as well, at three equilibrium temperature of 70, 80, and 90 °C, up to 20 bar total pressure and up to 1 bar n-hexane. In a global conclusion, the trend predictions of ternary Sanchez-Lacombe are according to experimental data but they overestimate the solubility of both ethylene and n-hexane except for ethylene solubility at 90 °C and 5bar total pressure. But as the equilibrium temperature increases, the predicted solubility magnitude overestimation for both ethylene and n-hexane is decreased.

ETHYLENE + LLDPE and n-HEXANE + LLDPE binary systems (Alizadeh A. , 2014)

In the **binary ethylene/LLDPE** system, the average of absolute deviation percentage of SL prediction from Yang's data was 0.59%, 0.65%, 0.66% and 0.46% at 60°C, 70°C, 80°C and 90°C respectively. On the other way, SL overestimated the solubility of n-hexane at lower pressures and underestimated the solubility values at higher pressures. There was average of absolute deviation of 16.6%, 29.0%, 23.9% and 33.7% at 70°C, 80°C, 85°C e 90°C.

ETHYLENE + n-HEXANE + LLDPE ternary system (Alizadeh A. , 2014)

For having SL predictions for this ternary system, Alizadeh "perturbed" the initial ethylene/LLDPE binary system with n-hexane. And then he perturbed the n-hexane/LLDPE binary system with ethylene. In his calculations, he defined **normalized functions** for solubility, volume, and concentration. These functions are basically ratios of such quantities in the ternary system to quantities in the initial binary system (e.g. normalized solubility of ethylene in amorphous polymer is defined as: the ethylene solubility in the ternary system divided by the ethylene solubility in the initial binary system). These functions were used as a measure of enhancement of ethylene solubility, volume of amorphous polymer, and concentration of ethylene in amorphous polymer in the mentioned ternary system. Normalized pressure of n-hexane was also defined: it is the n-hexane pressure divided by its vapour pressure at the equilibrium temperature at which the ternary system is being studied.

First Alizadeh simulated the effect of n-hexane on the ethylene solubility, amorphous polymer swelling, and ethylene concentration by addition of 10 bars of ethylene in equilibrium with LLDPE at 80 °C. He noticed that the normalized solubility, volume and concentration started to increase as a function of normalized partial pressure of n-hexane. He pointed out that at each specific normalized pressure, the extent of increase in the normalized solubility is higher than the extent of the increase in the normalized volume due to the sorption of n-hexane. This results in an increase of the normalized concentration and, accordingly the concentration of ethylene in the amorphous phase of polyethylene in presence of n-hexane rises.

Analogous for ethylene, he varied ethylene pressure between 5 to 15 bar and he saw that, in all cases, it does not have any effect in normalized solubility, normalized volume, and normalized concentration due to presence of n-hexane. However, at higher limit of normalized pressure of n-hexane, the normalized solubility and normalized volume predicted at each partial pressure of ethylene start to diverge one from the other. The maximum divergence of **normalized solubility** at higher ethylene pressures of 10 and 15 bars with respect to the **normalized solubility at 5 bars ethylene** is about 26%. On the other hand, the maximum divergence of **normalized volume** at higher ethylene pressures of 10 and 15 bars with respect to the predicted **normalized volume at 5 bars ethylene** is about 17%. The pattern of divergence of predicted normalized solubility and normalized volume at different partial pressures of ethylene were similar. This happens because the change in the volume of the amorphous phase is directly related to the mass of solutes sorbed into it. For this reason, and since the normalized concentration is proportional to the ratio of normalized solubility to normalized volume, the magnitude

of increase in dimensionless concentration as a function of dimensionless pressure of n-hexane still remains approximately independent of partial pressure of ethylene in higher limit of normalized pressure of n-hexane. The maximum divergence of predicted normalized concentration at higher ethylene pressures of 10 and 15 bars with respect to the predicted normalized concentration at 5 bars ethylene is about 7%, which can be considered to be negligible.

At a 10bar partial pressure of ethylene, in the lower limit of normalized pressure of n-hexane up to about 0.5, the different 70, 80 and 90°C equilibrium temperatures do not affect the magnitude of the enhancement in the normalized solubility, volume, and concentration as a function of normalized pressure of n-hexane. At higher limit of normalized pressure of n-hexane, the Sanchez-Lacombe model predicts that the magnitude of enhancement in normalized solubility, volume, and concentration would decrease by increasing the temperature at which the gas-polymer system is in equilibrium.

When the equilibrium temperature increased from 70 to 90 °C, with a 0.5 normalized partial pressure of n-hexane at each equilibrium temperature, the effect of ethylene on the solubility of n-hexane is attenuated. However the trend for the dependency of n-hexane solubility to the partial pressure of ethylene remains the same: the solubility of n-hexane starts to increase with partial pressure of ethylene until it reaches a maxima in solubility of n-hexane. After this point the solubility of n-hexane decreases by increasing the partial pressure of ethylene. Similar trends are predicted for the effect of equilibrium temperature for the ternary system of ethylene/n-hexane/LLDPE in which the normalized partial pressure of n-hexane is equal to 0.25 and 0.75.

2.1.2. SAFT research on light gases solubility in amorphous polyethylene

Shyamal (Nath, Banaszak, & de Pablo, 2001) performed some simulations for ternary ethylene, 1-hexene, and amorphous polyethylene (C70) at temperatures of 65, 85, and 105 °C, and at various partial pressures of the solvent ethylene and 1-hexene molecules. They simulated the solubility of pure ethylene in C70 at all three temperatures and at pressures of 6.9, 10.3, and 13.8 bar, respectively. These binary simulations correspond to results at zero 1-hexene partial pressure. They then added 1-hexene molecules to the simulation boxes and conduct calculations with 1-hexene partial pressures of up to about 1.4bar. They were interested in generating data at fixed partial pressures of ethylene and 1-hexene. However, since they used a Gibbs ensemble, they could only control the total pressure, and consequently, their results were only within 5% of the target ethylene partial pressure. Results of simulations show that, within the range of simulation pressures and temperatures, the solubility of pure ethylene could be approximated with Henry's law. From the Monte-Carlo simulation of ternary mixtures, they concluded that the presence of 1-hexene molecules slightly increases the solubility of ethylene in polyethylene. The simulation results were compared with predictions from the SAFT equation-of-state. They found that SAFT predicts the same general trends as the simulation results. However, SAFT appears to overpredict ethylene solubilities and mixture densities as compared to the simulation results. Also, SAFT appears to overpredict the ethylene solubility dependency on ethylene partial pressure for the ternary mixtures and the temperature dependency of the binary mixture densities as compared to

the simulations. The diffusion of ethylene and 1-hexene in C70 in their ternary mixture is also studied. From their simulations they found that the diffusion coefficient of ethylene is about 2.2 times higher than the diffusion coefficient of 1-hexene in C70. Results have indicated that ethylene molecules tend to form aggregates of their own in the mixture, and both ethylene and 1-hexene exhibit a tendency to reside in the vicinity of the end groups of C70 molecules. This aggregation may be relevant for molecules of longer chain lengths and/or with multiple branches.

The absorptions of the gases in a multi-component mixture with amorphous PE are predicted to be at their highest values at the saturation pressure of the gaseous mixture. Absorption of one or more of the light gases present (such as C2 and n-C4) may therefore be achieved by controlling the pressure at which this saturation occurs; this will be approximately when the partial pressure of the least-volatile gas approaches its (pure-component) saturation pressure. Andrew et al. (Haslam, et al., 2006) calculated that the absorption of alkenes may thus be increased approximately by a factor of 2. This may be achieved either by altering the temperature or pressure of the entire system or, perhaps more conveniently, by altering the composition of the gaseous mixture itself. They proposed the co-solubility effect to be explained like: hexane-1 is a much less-volatile gas than ethylene. At reactor temperature, its saturation pressure is quite close to that of n-pentane. When hexene is added to the reactor gas mixture, the effect should therefore be similar to that produced by the addition of n-pentane which is predicted to substantially increase the solubility of the ethylene. Therefore the large differences in observed rate increases would be expected since when the reactor pressure is close to the gas-mixture saturation pressure, the steepness of the solubility curves for all the gases present rise very sharply.

2.2. Gas-Phase Fluidized Bed Reactor (FBR)

2.2.1. Fluidized bed reactor for LLDPE production

FLUIDIZED REACTOR MODELING BASICS

The fluidized reactor model mostly accepted relies on Kunni & Levenspiel Fluidized bed theory (Kunni & Levenspiel, 1991). In their model, the gas flows up the reactor in the form of **bubbles** exchanging gas with reactive particles (like catalysts). The product formed in these particles then returns back into a bubble and leaves the bed when it reaches the top of the reactor. The rate at which the reactants and products transfer in and out of the bubble as well as the time bubble takes to pass through the bed affects the conversion. The velocity at which the bubbles move through the column and the rate of transport of gases in and out of bubbles need accurate characterization.

At low gas velocities (but already in a fluidized media), the rising bubbles contain very few solid particles. The remainder of the bed – **emulsion phase** – has a much higher concentration of solids in it. The **cloud phase** is an intermediate phase between the bubble and emulsion phases. It's the region penetrated by gas from a rising bubble.

At gas flow rates above the point of **minimum fluidization**, bubbles of gas rise rapidly and burst on

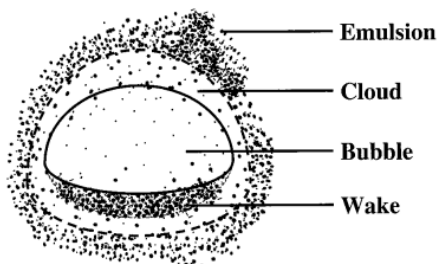


Figure 7 – bubble, cloud and wake phase illustration

its surface while the emulsion phase is thoroughly agitated. The bubbles form very near the bottom of the bed, close to the distributor plate. And this is why its design has a significant effect on fluidized-bed characteristics.

The gas within a particular bubble remains largely within that bubble, only penetrating a short distance into the surrounding emulsion phase.

In order to have a practical and useable model of fluidized-bed behaviour, kunni and Levenspiel made the following assumptions:

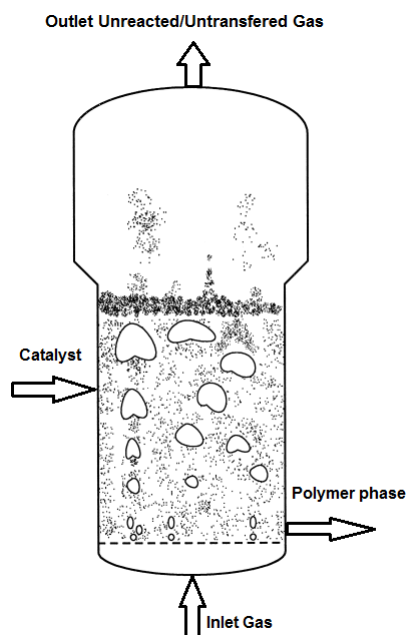
- ✓ Unique size bubbles
- ✓ The solids in the emulsion phase flow downward essentially in plug flow
- ✓ The emulsion phase exists at minimum fluidizing conditions.
- ✓ In the wakes, the concentration of solids is equal to the concentration of solids in the emulsion phase, and therefore the gaseous void fraction in the wake is also the same as in the emulsion phase.

The details of their model and other specific considerations are not decisive for the purposes of this work and they're left for literature checking.

GAS-PHASE ETHYLENE POLYMERIZATION GENERAL DESCRIPTION

The basic industrial operation on supported catalyst in gas phase FBR is:

- Injection of a feed gas below the distributor plate. It is designed to appropriately distribute the gas in the reactor zone. The gas rises up through the bed in a more or less plug-flow-like manner.
- As it rises, it fluidizes the mixture of solid particles in the bed.
- The particles, which are a mixture of freshly injected catalysts or prepolymers plus the growing particles, circulate in the bed with a CSTR-like residence time distribution.
- The top of the reactor is wider than the main reaction zone. This is to cause the velocity to drop and it is intended to help preventing any fine particles from leaving the reactor.



A small amount of high activity catalyst particles, with diameter of 10–50 μm , is supplied continuously or semi-continuously to the reactor carried by an inert gas like nitrogen. Before they enter the reactor, they can be pre-activated and/or prepolymerized. Catalyst injection rates are in the range of 0.001-0.05 g/s depending on catalyst activity and reactor capacity. Since the catalyst particles are the smallest/less dense in the reactor they move upwards. But at the same time they are moving upward by the fluidizing gas, they are increasing their size due to the polymerization. The gas feed should be designed in order to not elutriate the particles having in account their maximum weight (which depends on their residence time). As these catalyst particles are exposed to monomer or monomer mixture in the reactor, polymerization occurs almost immediately and the catalyst particles are quickly encapsulated by the newly formed polymers to a size of around 300–1000 μm . Their sizes (naturally depending on their residence

Figure 8 – Gas-phase FBR illustration for ethylene polymerization

time in the reactor) range from the initial catalyst particle diameter to the large particle in the bed, composed by that time mostly of polymer. In the first stage of particle life, the polymer starts to fill the pores of the supported catalyst particle and a gradual fragmentation of the catalyst support takes place. Yet, the fragments are kept together by the polymer. The time-scale of the fragmentation process ranges from fractions of a second to a few seconds. Fully-grown polymer particles are withdrawn continuously or intermittently from the bottom portion of the reactor (above distributor plate) while keeping the bed level approximately constant. The superficial gas velocity can vary from 3 to 8 times the minimum fluidization velocity. (US Patente N° 4.303.771, 1981) The reaction heat is dissipated from the growing polymer particles by a fast rising gas stream. This leads to low monomer conversion per pass (<5%) and a large amount of unreacted gas leaves the reactor. It is then cooled, compressed, and recycled back to the reactor. An inert hydrocarbon liquid may also be added to the recycle gas stream to increase the reactor heat removal capacity (condensed mode operation) and hence to increase the polymer throughput. Overall conversion is about 98% (McAuley, Talbot, & Harris, 1994). Industrial fluidized bed

reactors typically operate at temperatures of 75-110°C and pressures of 20-40 bar (Xie, McAuley, Hsu, & Bacon, 1994). The pressure drop across the bed is slightly higher than the weight of the particles divided by the cross sectional area.

Catalyst size (μm)	30-50	Temperature ($^{\circ}\text{C}$)	75-110
Particle size (μm)	300-1000	Pressure (bar)	20-40
Conversion/pass	2-5%	Gas velocity (m/s)	0.5-0.9
Overall Conversion	98%	Bed Porosity, ϵ	0.55
Catalyst flowrate (g/s)	0.005-0.01	Mixing index	0.4-0.5
Bed height (m)	10-15		

Table 2 – Summary of the typical operation condition in a FBR for LLDPE production already exposed in last paragraphs

The **instability** of fluidization means generally that a bed of particles fluidizes badly and even disrupts or collapses with apparent agglomeration and channeling in the bed. There exist two types of instability in the gas-phase fluidized-bed polymerization process when the reactor structure is designed properly. The first kind of instability is called “high temperature instability”, in which the hot point of the temperature forms locally within the bed resulting from a higher feeding rate of the active catalyst and insufficient heat transfer. The hot point will make particles molten and will agglomerate. The second kind of instability is due to the occurrences of condensable composition in a fluidizing medium, which will make particles stickier and result in big agglomerates. When an agglomerate exists in the fluidized bed, a pair of forces will act on it: the sticky force, due to the liquid between solid particles, and the drag force due to the motion of the fluidizing gas. If the dynamics of agglomerate formation and breakup are in equilibrium, and the size of agglomerate does not grow beyond certain limits, the fluidized bed will remain stable. This equilibrium is possible if the sticky force is just balanced by the drag force. In general, the sticky force increases with the mass fraction of the liquid in the particle, and the drag force increases with the fluidizing velocity. In a practical gas-phase polyethylene operation, the fluidizing velocity is usually fixed, so the mass fraction of liquid in the particle should be less than a definite value in order to keep the bed stable. The extreme conditions of defluidization is that the agglomerate occupies almost the entire cross section of the bed. However, it is reasonable that defluidization will occur before this extreme condition is reached in large-scale fluidized-bed reactors. It is appropriate that the maximal size of the agglomerate permissively existing in the bed is estimated as the size of the discharge port of the polymer product in the reactor.

2.2.2. Gas-phase ethylene polymerization modelling

For entirely describing the phenomena occurring in the gas-phase ethylene polymerization it's necessary to understand what's happening at different levels. Several studies for LLDPE production have included particle growth models that led to a better understanding of the reactor behaviour as well as properties of the polymer produced. Ray (Ray & Hutchinson, 1990) considered a modeling hierarchy as microscale, mesoscale and macroscale, based on the characteristics of the polymerization reactor systems. In such approach, overall mass and energy balance and heat removal from the reactor is considered in macroscale level. Particle growth, intraparticle and interparticle mass and energy balance occur at the mesoscale level, while the kinetics of polymerization corresponds to microscale level. The figure 9 is a typical (and good) illustration of the whole phenomena occurring in gas-phase ethylene polymerization FBR.

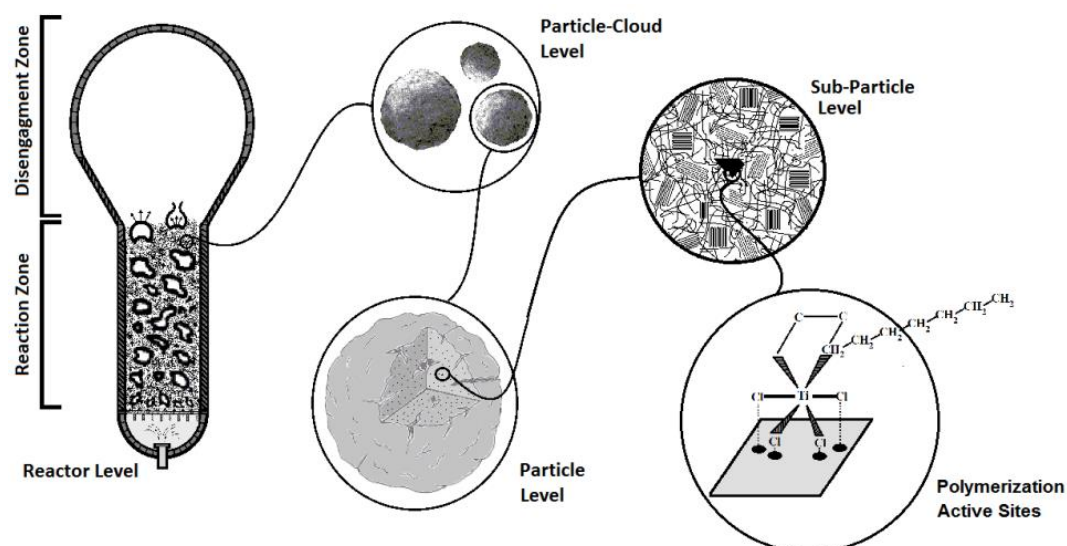


Figure 9 – representation of macro-scale, micro-scale and surface scale view of the polymerization phenomena. (Alizadeh A. , 2014, Figure 2.3)

It has been established that, under many conditions, heat transfer and diffusional resistances **do not play an important role** at the **particle level** in gas-phase polyethylene reactors (Floyd, Choi, Taylor, & Ray, 1986). For many catalyst systems in which heat and mass transfer resistances do not influence monomer concentrations and temperatures within the polymer particles, the monomer concentration at the catalyst sites is determined by the **equilibrium sorption** of the **monomer within the polymer particles**. This equilibrium sorption may be measured and predicted with SL as already discussed in chapter of thermodynamics considerations and with Alizadeh work. Another important work on it was the one of Hutchinson and Ray (Ray & Hutchinson, 1990) where they have developed thermodynamic models to predict equilibrium monomer concentrations at the catalyst sites from external gas-phase monomer concentrations in the vicinity of the polymer particles.

Nevertheless, for very young particles with highly active catalysts, heat and mass transfer resistances can become significant, leading to particle overheating. Modelling at the particle level is useful for predicting polymer particle growth and morphology. And, if diffusional or temperature gradients within the particles are significant, it's also important to model for predicting the effects of intraparticle temperature and concentration gradients on the molecular properties of the polyethylene produced. Kosek (Kosek, Grof, Novák, Stepánek, & Marek, 2001) explored the advantage of the steady-state modeling as the possibility of a systematic investigation of the dependence of temperature and concentrations in the particle on model parameters

The fluidized bed reactors for LLDPE production have been modelled as **single, two, or three-phase** reactors. Modeling fluidized-bed polymerization reactors is not simple since many interactions between phases need to be taken into account.

In the next paragraphs it will be pointed out the main contributions in terms of the 3 types of reactor modelling as well as some important other issues like Particle Size Distribution and Segregation.

SINGLE-PHASE MODELLING

In case of low to moderate activity of the catalyst, heat transfer and diffusion resistances do not play an important role at the particle level in the gas-phase polyethylene reactors. In the limiting case, where either bubbles are small or interphase mass and energy transfer rates are high and catalyst is at low to moderate activity, intraparticle temperature and concentration gradients are negligible (Floyd, Choi, Taylor, & Ray, 1986). In this case, LLDPE production fluidized bed reactors could be modelled as a CSTR proposed by McAuley et al. (McAuley, Talbot, & Harris, 1994). He considered the polymerization reactor to be a well-mixed one. For this to be a well-mixed reactor, the mixing index – particles degree of mixing in a reactor – should be near by 1. (Wu & Baeyens, 1998) McAuley et al. revised Choi and Ray's model (Choi & Ray, 1985), establishing a maximum stable bubble size and making new assumptions regarding material and heat transfer mechanisms within the bed. In both works, the emulsion phase is assumed to behave as a CSTR fully mixed. This latter assumption is good for small fluidized-beds that are violently fluidized and have a height to diameter ratio close to one, as it was demonstrated by Lynch and Wanke (Lynch & Wanke, 1991). However for a typical ethylene polymerization reactor, mixing index is about 0.4-0.5. This indicates a low reactor mixing and makes a single CSTR a not very realistic approach. Alizadeh (Alizadeh, Mostoufi, Pourmahdian, & Sotudeh-Gharebagh, 2004) employed a tanks in series model to represent a pseudo-homogeneous media for predicting the performance of an industrial-scale gas-phase polyethylene production reactor. Weijuan et al. (MENG, LI, CHEN, & LI, 2013) simulated the steady-state behavior of industrial slurry polymerization of ethylene in 2 continuous stirred tank reactors. He studied the effects of various operating conditions on the molecular structure and properties of polyethylene. The model demonstrated that changing the catalyst flow rate, changes simultaneously the mean residence-time in both reactors, which plays a significant role on the establishment of polyethylene architecture properties such as molecular mass and polydispersity index.

TWO-PHASE MODELLING

Choi & Ray (Choi & Ray, 1985) divided the reactor into two sections: emulsion phase and bubble phase with constant size. The reactions take place only in the emulsion phase due to the assumptions that the bubbles are solid-free. In these two-phase model, temperature and concentration gradients within the gas bubble phase throughout the bed is assumed as well as an interaction of separate emulsion and bubble phases.

Hatzantonis (Hatzantonis, Yiannoulakis, & Yiagopoulos, 2000) considered the effect of varying bubble size on the dynamic and steady state behavior of reactor as well as product properties. They also divided the reactor into emulsion phase and bubble phase sections. They had assumed that the emulsion phase is perfectly mixed while the bubble phase was divided into N well-mixed compartments in series. In their model, the size of each compartment was set equal to the bubble diameter at the corresponding bed height. They have shown that the model has a better agreement with industrial data than single-phase and two-phase models with constant bubble size. It was shown that since the bubble-growth model assumes a more realistic bubble-phase mixing pattern, improved emulsion-to-bubble heat transfer rates are obtained, and, thus, the maximum stable bubble size does not significantly affect the emulsion temperature predictions. Also the mass transfer rate from bubbles to the emulsion phase did not affect the dynamic behaviour of the FBR. The well-mixed and constant bubble size models were found to be limiting cases of the bubble-growth model. The constant bubble size model was found to overpredict the emulsion phase temperature, ethylene conversion and average molecular weights. Furthermore, the constant bubble size model predicted a narrower safe operation window compared to that calculated by the bubble growth model. On the other hand, the well-mixed and bubble-growth model predictions were in better agreement under typical operating conditions of commercial interest. The effect of the particle size on the dynamic behaviour of the reactor was not considered although it was shown that it is an important reactor parameter.

Jafari (Jafari, Sotudeh-Gharebagh, & Mostoufi, 2004) divided a fluidized bed for polyethylene production into several bed segments. Each segment consists of an emulsion and bubble phase and the reaction is considered to progress in both phases. The bubble phase flow pattern is assumed to be plug flow while the emulsion phase is considered to be a completely mixed CSTR. This model has the privilege of being a two-phase model with the reactions considered to take place in both phases. They concluded the model is able to favourably predict the real performance of the FBR's over a wide range of bubbling and turbulent regimes of fluidization.

Kiashemshaki (Kiashemshaki, Mostoufi, & Sotudeh-Gharebagh, 2006) adopted the reactor procedure developed by Jafari just saw. The model is able to predict monomer concentration profiles, polymer productivity and reactor temperature, as well as molecular weight distribution and polydispersity index. They have shown that about 20% of the polymer is produced inside the bubble phase and as such cannot be neglected in modeling such reactors.

Farag (Farag, Ossman, & Farid, 2013) presented the developments in modeling gas-phase catalyzed olefin polymerization fluidized bed reactors (FBR) using chromium catalyst technique. Like

the previous authors, Farag assumed a bed divided into several sequential sections with a bubble phase and emulsion phase. In addition he included the bubble size, particle size distribution, and catalyst properties in dynamic simulation of the reactor in order to obtain better understanding of the reactor performance. He assessed the effect superficial gas velocity, catalyst injection rate, catalyst particle growth, and minimum fluidization velocity on the dynamic behaviour of the FBR. Its simulations indicated that the single-pass ethylene conversion is sensitive to catalyst particle diameter, number of compartment, and bed voidage. On the contrary, changing superficial gas velocity has no significant effect on the conversion.

THREE-PHASE MODELLING

Fernandes et al. (Fernandes & Lona, 2001) used a heterogeneous three-phase model that considers bubble, emulsion and a new differentiating particulate phases (plug flow was assumed for all phases), combining mesoscale (particle growth and intraparticle transfer processes) and macroscale modeling. Since gas diffusion to the interior of the catalyst/polymer particle is not instantaneous, they proposed intraparticle gas diffusion in modelling fluidized bed reactors. The full heterogeneous model should be used for low residence times (up to 1200 s) whereas the simplified heterogeneous model can be used for high residence times without compromising simulation results. They showed that the average molecular weight and polydispersity of the polymer increase more intensely at the beginning of the polymerization, slowing down after a given time. And when fast fluidizing systems are used, the range of particle diameters inside the reactor is much greater.

Ibrehem (Ibrehem, Hussain, & Ghasem, 2009) included the catalyst phase and considered all three phases as compared to the other models (constant bubble size model, well-mixed model and the bubble growth model). His model took into account the presence of particles participating in the reaction with emulsion and catalyst phases whose amount was shown to depend on superficial gas velocity and catalyst feed. In addition, heat and mass transfer between the bubble and the cloud as well as between the cloud and the emulsion phases were considered. Simulations indicated the model is capable of predicting reactor performance indicators as well as calculating the changes of polymer particles size throughout the transience of the reaction.

SEGREGATION, PARTICLE GROWTH and PARTICLE SIZE DISTRIBUTION

Although polymer particles in a fluidized bed polymerization reactor are generally modelled as being very well mixed, particle segregation may occur to some extent. The difference in particle size and/or density is a direct reason for segregation, as described in detail by Kunni and Levenspiel. Particle segregation occurs in the reactor according to particle weight. Naturally the full-grown polymer particles are removed at the base of the reactor. For example, the size distribution of polymer particles removed from the bottom of the reactor may differ from the polymer particle size distributions in other locations of the reactor. Axial temperature gradients often observed in industrial fluidized bed polyolefin reactors are believed to be a strong function of the axial solids mixing. Also, the feed catalyst particles are not always of uniform size but have a certain size distribution. Since the size of a polymer particle produced

in the reactor is determined by the particle's residence time in the reactor, the polymer particles in a gas phase olefin polymerization reactor exhibit a broad particle size distribution. In wide particle-size systems, a good mixing of the particles is only achieved under very specific hydrodynamic conditions. The same bubbles cause segregation while denser or larger particles tend to fall preferentially through the disturbed region behind each bubble. Even denser or larger particles carried up in the bubbles wake from the bottom segregated layer will be shed from the wake and descend rapidly.

Wu (Wu & Baeyens, 1998) observed that a bed may be well fluidized in the sense that all the particles are fully supported by the gas but they may still be segregated in the sense that the local bed composition does not correspond with the overall average. Segregation is likely to occur when there is a substantial difference in the drag/unit weight between different particles. Particles having a higher drag/unit weight migrate to the surface whereas those with a lower drag/unit weight migrate to the distributor. In polymer systems where particles present a wide size distribution, a tendency towards segregation is found with larger particles migrating to the bottom of the fluidized bed whereas smaller particles go preferably concentrate in the top section of the bed.

Yiannoulakis (Yiannoulakis, Yiagopoulos, & Kiparissides, 2001) presented a steady-state population balance model developed for the prediction of the particle size distribution in ethylene copolymerization FBR's operating under moderate particle agglomeration conditions. He employed the polymeric flow model to calculate the growth rate of a single particle under internal and external heat and mass transfer limitations. This model was solved together with a steady-state particle population model to predict the particle size distribution in the FBR. Under complete mixing conditions of solids in the bed and a uniform catalyst feed, it was shown that internal and external mass and heat transfer limitations can have a strong impact on the calculated particle size distributions in the bed.

Mckenna et al. (McKenna & Soares, 2001) reviewed the state-of-the-art models for single particle olefin polymerization with respect to particle growth, polymerization rates, concentration and temperature radial profiles, polymer microstructure, and particle morphology. It was discussed that these models can be conveniently classified as polymer property and particle morphology models, according to their most important predictive abilities.

Kim et al. (Kim & Choi, 2001) noticed that in a wide particle-size systems, a good mixing of the particles is only achieved under very specific hydrodynamic conditions. They investigated the effects of various reactor operating conditions on the particle size distribution in the reactor. They saw that particle segregation effect becomes pronounced as the fluidizing gas velocity is lowered. When the catalyst activity is increased by ten times, polymer production rate increases and the amount of large polymer particles increases. Increased catalyst feed rate decreases particle residence time due to increased production rate and hence the polymer particle size distribution goes to smaller sizes. The particle size distribution also becomes narrower as catalyst feed rate is increased. When catalyst deactivation occurs, the particle size distribution shifts to smaller sizes. For a rapidly deactivating catalyst, the particle size distribution becomes quite broad. It is also observed that the particle size distributions in the top and bottom compartments are significantly different for such catalysts. They finally observed that the shape of product particle size distribution is qualitatively similar to that of feed catalyst size distribution but not quite a replica of the catalyst size distribution.

Kanellopoulos et al. (Kanellopoulos, Dompazis, Gustafsson, & Kiparissides, 2004) analyzed the effects of initial catalyst size, catalyst morphology and hydrodynamic conditions on the growth and overheating of highly active Ziegler-Natta catalyst particles. As the initial catalyst size increases, the polymerization rate initially decreases due to mass transfer limitations. However particle overheating increases due to heat transfer limitations. They also plotted the particle overheating with respect to time for three values of PE crystallinity. They saw polymerization rate decreases as the extent of crystallinity in the prepolymerized particle increases despite the effective active metal concentration increases.

Grosso (Grosso & Chiovetta, 2005) introduced the restriction posed on the overall polymerization process by the particle separation system in the discharge chamber. The model recognizes the fact the chamber was added precisely to select the larger particles and, hence, to force a given particle distribution at the exit point. It was found that said distribution is relevant in establishing the properties of the bed and an additional element to adjust the reactor operation. Grosso used the three-phase model to account the changes suffered by the particles in the bed. Simulations showed that it's necessary to include the impact of both the product and bed particle diameter distribution when analysing reactor performance. Narrow particle distribution in the product render maximum utilization of the reactor volume. Smaller particles in the product stream are predicted when higher catalyst activities are introduced, since the latter imply higher catalyst mass fractions in the bed.

2.2.3. Condensed mode gas-phase reactor operation

The condensed mode operation in the gas-phase fluidized bed ethylene polymerization process is apparently increasing the space-time yield of polymer production. By decreasing the reactor temperature and solubilizing more ethylene in polymer phase. The cooling capacity of the recycle gas stream is increased by addition of non-polymerizing condensable agents in order to increase the dew-point temperature of the stream. An even further increasing in cooling capacity is achieved in the super-condensed mode operation (US Patente N° 8.669.334 B2, 2014). This is actually a mean of expanding the plant capacity without resizing the reactor. In gas-phase ethylene polymerization FBR's, heat removal is a central factor for the productivity. Usually the gas unreacted is compressed and cooled being recycled with fresh feed to the reactor. This cooling will determine the reaction production by its capacity of removing heat. It is possible to increase the rate of heat removal from particles with the convection mechanism by increasing the gas superficial velocity. However, there is a limit for the increase of gas flow rate because of higher possibility of the entrainment of catalyst and polymer particles out of bed at higher gas flow rates. One can also increase the heat capacity of the gas phase by changing its composition which would lead to higher capacity of gas phase in order to evacuate the polymerization heat from the growing particles inside the bed. If this recycle stream contains some ICA's, it will raise its dew-point and the condensation of liquid will take place. This way can remove heat by vaporizing when it goes into the reactor. There are different ways proposed in the patents like increasing the pressure or decreasing the percentage of non-condensable and the latter is the usual choice. The preferred inert condensable components are saturated C5 and C6. Great care should be commercially

taken in condensed mode operation to avoid conditions that can lead to the formation of chunks or, worse, an unstable fluidized bed, which collapses or causes polymer particles to fuse together. There is no generally accepted view as to what causes chunking or sheeting at present. This situation limits the further scale-up of polymerization reactors and the innovation of new process technology. When there is occurrence of condensable materials in a fluidizing medium, particles will stick together and result in big agglomerates. ICA's with low solubility in polymer resin will optimize the relationship between the tendency to promote stickiness and the ability to remove heat, allowing increased production rates in the reactor. This relationship is a trade-off between limiting the stickiness of the produced resin and the heat removal capability. With a relatively high total solubility of ICA's, and comonomer(s), and other components in the gaseous stream dissolved into the resin, the resin becomes sticky. Above a certain stickiness limit or total solubility in the resin, agglomerates form at different parts of the reactor, causing sheeting on interior wall of the reactor and/or recycle system, chunks and/or plate pluggage. It's very important to keep the gas-liquid inlet stream at droplet level. This is, the inlet stream should have only an optimal entrained liquid.

There are different methods for introducing the generated liquid phase to the FBR which has been described in a range of patents. Despite all the differences in the proposed and practiced configurations in the related condensed mode patents for gas phase ethylene polymerization in FBR, all of these condensed mode configurations are designed and developed in a manner to meet the following requirements for the operation of the process:

- (a) the liquid phase should be vaporized quickly in the fluidized bed;
- (b) the liquid accumulation should be prevented because of the possibility of production of polymer agglomerates;
- (c) liquid should be introduced to bed in a manner to have the minimum effect in the fluidization behavior and stable operation of the bed;
- (d) the properties of the polymer product must be consistent during the condensed mode operation

Jiang et al. (Jiang, McAuley, & Hsu, 1997) studied the effects of changing the operating conditions on the cooling capacity of the recycle gas for polyethylene reactor systems. The possible production and heat-removal benefits obtainable from operating with metallocene catalysts at higher reactor temperatures without sticking are approximately 1.1% per °C. They also noticed that makeup ethylene should be added after the heat exchanger and makeup hexene should be added before the heat exchanger to maximize heat removal.

Ramanathan (Ramanathan, 1998) used a CSTR with a polymer phase very well-mixed and a residence-time for polymer particle of several hours. The catalyst was present in the polymer phase and the solubility of monomers and other reactants were predicted by SL. In his simulation with 3 different catalysts he concluded that the polymer produced, cooler duty and the amount of condensation in recycle stream are the same for dry or wet mode. There is about 160 % increase in productivity if 10 mole % of liquid is present in the recycle stream. The catalyst with a very short half-life will result in almost no change in ash content and catalyst activity when a switch is made to condensed mode operation.

Yang et al. (Yang, Yang, Chen, & Rong, 2002) developed a model on the basis of force balance of agglomerate to predict the maximal mole fraction of the condensed isopentane permitted in the fluidizing gas stream which can be subsequently used as a criterion to distinguish the unstable operating zone of the fluidized bed. It was proposed that absorption of heavy components on the polymer particles would make particles stickier and result in a liquid bridge at the contact point between the two particles in condensed mode operation. The theoretical calculation agreed with the industrial operation data very well.

(Mirzaei, Kiashemshaki, & Emani, 2007) used Peng-Robson EOS for flash calculations to evaluate the liquid fraction as well as the gas and liquid composition in the inlet stream to the reactor and SL EOS for calculation of the concentration of monomers, hydrogen and condensable components in the polymer particles using the concentration of the components in the gas phase. Their results were according to some patent they used for comparison.

The introduced liquefied portion of the feed stream is expected to vaporize fast in order to have minimum effect on the stable fluidization of the reactor. Consequently, the inert condensable components will be present in the vapor phase for a much longer time than they are in the liquid phase. Arash and McKenna (Alizadeh & McKenna, Condensed Mode Cooling in Ethylene Polymerization: droplet evaporation, 2013) thought the liquid to evaporate at hot spots in the bed. Parameters like droplet size, size distribution, heat of vaporisation and properties of solid particle phase as well as eventual contact between these two phases will control the overall vaporisation process of the liquid droplet in the presence of fluidising solid particles. They analysed time scales for droplet heat up and vaporisation compared in case of homogenous vaporisation of the droplet. Based on their assumptions and calculations they expected the major part of the liquid injected through the bottom of an FBR to vaporise at a height of between 1 and 2m. Since the evaporation process is quite rapid, the gas phase will be quite rich in the heavier ICA and so in the polymer.

Ye-feng Zhou et al. (Zhou, Wang, Yang, & Wu, 2013) attempted to improve the classical emulsion-bubble two-phase model for FBRs by introducing coexisting multi-temperature zones, namely, the gas-liquid-solid and gas-solid zones, in one reactor. As the condensed-liquid content increases, the gas-liquid-solid zone expands upward to a greater height in the bed, and the heat-transfer capacity in this zone becomes enhanced. At different liquid contents, the simulation temperature profile derived from the improved model fits the industrial temperature measurements satisfactorily.

2.3. Brief outlook on olefin catalysts

METALLOCENE catalyst

Metallocene catalysts are based on **metallocene compounds** of group **4 transition metals** with methylaluminoxane (MAO). These catalysts exhibit a high activity for olefin polymerization and higher productivities translating to lower catalyst cost and cleaner polymer. The control of polymer particle morphology is an important aspect of PE production for practical purposes. By manipulating the metallocene compound structure one can produce polymer with tailor-made structure for specific applications. The custom properties include greater stiffness and impact strength, greater stretch and improved sealability. The polymer particles produced using metallocene catalysts can have higher sticking temperatures than the polyethylene produced using Ziegler-Natta catalysts. Therefore gas-phase reactors can be safely operated at slightly higher temperatures with metallocenes without risking of particle agglomeration. Metallocene catalysts lead to polymers with a **very narrow molecular weight distribution**. The fact they allow less low-molecular weight resins than other ones makes them to produce better properties materials than, for instance, those of Ziegler-Natta. This reduces the smoke, taste and other process difficulties associated with low molecular weight polymers. On the other side, polymers with narrow molecular weight distribution are usually difficult to process in existing equipment. They also require less comonomer to achieve the same density and that in turn reduces the production cost of the low-density polymer. Combining various metallocenes in one reactor can produce high performance bimodal resins with molecular weight and comonomer segregation. (Shamiri, et al., 2014)

Many industrial applications require the catalyst to be supported on a carrier. The most commonly used supports are **SiO₂** or **Al₂O₃** and lately **polymer ones**. The use of polymer as support can facilitate the control of particle morphology without involving a prepolymerization step. It also reduces inorganic residues in the final products. Furthermore, manipulating the functional groups in polymer support opens the possibility of influencing the molecular structure of the polymer. Harrison (Harrison et al., 1998) have developed supported catalysts that combine high productivity of polymers and copolymers with narrow MW and composition distributions. They reacted hydroxylated silica and alumina supports with MAO in toluene suspension providing chemically modified supports suitable for use in slurry and gas-phase polymerizations of ethylene or propylene. At lower temperatures, leaching of active catalyst from these alumina supports does not occur to an appreciable extent but the morphology and bulk density of the polymer formed is unsuitable for use in a gas-phase process. Their studies indicated that less comonomer is incorporated using these supported metallocene catalysts than their soluble analogues under otherwise identical conditions.

Chung et al. (Chung, et al., 2002) used hydroxylated styrene/divinylbenzene copolymer as a support for different metallocene catalysts in the polymerization of ethylene in gas phase and their correlations of the average activities of 3 catalysts indicated that temperature is the most important factor affecting the polymerization. The pressure seemed to show a negative effect and the MAO level in the range studied had rather weak effect on polymerization. The kinetic analysis reveals that the catalysts probably contain two types of active sites and the high active sites decay ten times faster than the low active sites.

Chiovetta (Chiovetta & Estenoz, 2004) studied support-catalyst polymer particles composed of millions of microparticles arranged in cells and having silica nuclei covered with MAO. Main variables were the changing particle morphology and the kinetic-diffusion effects determining local monomer availability during residence time. The cells near the macroparticle center are always in a less convenient position when compared with those located closer to the liquid bulk-phase, in terms of reaching the final, accessible microparticle configuration that emerges after fragmentation and subsequent rearrangement. The relative extent of the time needed to attain this final stage when compared with macroparticle residence time in the reactor indicates the actual participation of a cell at any given location within the support-catalyst-complex. One kinetic analysis showed that increasing the kinetic constant should not necessarily produce a proportional increase in polymer production.

It's utmost that catalysts yield products with excellent morphology, namely spherical product particles without the formation of fines. Such properties are required for use in gas-phase FBR. Wu et al. (Wu, Zhou, Lynch, & Wanke, 2005) presented results on the activity and product morphology of catalysts made by supporting $(n\text{-BuCp})_2\text{ZrCl}_2$ and MAO on polymeric supports they previously prepared. A comonomer effect was observed for all catalysts but the magnitude of this effect and the 1-hexene concentration at which the comonomer effect was the highest varied significantly among catalysts. Low Al:Zr ratios resulted in high 1-hexene incorporation. Products produced with catalysts which had high MAO contents contained considerable amounts of fines. These fines are produced by the detachment of loosely held polymer nodules formed on the exterior surface of the growing polymer particles. These small variations in molar masses among catalysts indicate that the nature of the active sites were similar in the different catalysts and the main cause for variation in the polymerization rates was due to differences in accessibility of monomers to active sites probably caused by the difference in fracturing characteristics of the different catalysts.

ZIEGLER-NATA and PHILLIPS catalysts Generalities

A Ziegler-Natta (ZN) catalyst is formed by reacting a metal alkyl or alkyl halide (cocatalyst) with a transition metal salt. Most of the Ziegler-Natta polymerization reactions are based on titanium catalyst systems. The commercial catalysts usually are based on TiCl_4 on MgCl_2 carrier with triethylaluminium cocatalyst (TEAL). Since these catalysts usually comprise multiple active sites, they lead to the production of polymers having broad and, often bimodal, molecular weight and copolymer composition distributions. Industrially the most important parameters that have to be taken into consideration to make different, tailor-made polyolefin products with special properties, are reaction temperature, concentration of monomer, comonomer, cocatalyst, hydrogen and residence time in the reactor. Hydrogen concentration is used as MWD controller substance and it also affects the productivity of the catalyst differently for different monomers. Because all base properties are in connection with Mw, this will also make difference in every properties of the final product. The cocatalyst not only eliminates impurities from the different reaction components but also activates the catalyst (reduces Ti^{4+} to Ti^{3+}) form. With increasing amounts, as more impurities can be eliminated, and more active sites can be formed, the productivity of the catalyst increases. Concerning monomer concentration, as the ratio of

monomer/active sites is increasing, the productivity of the catalyst increases, and also the molecular weight. (Suba, Árvai, & Németh, 2007), (Lloyd, 2011)

Phillips type catalysts are based on **organochromium** compounds or on **chromium oxides**, supported on an **amorphous material** such as silica. The first type is made by calcining a high surface area support, and then depositing an organochromium compound, such as chromocene onto it anhydrously. The catalyst preparation consists in the impregnation of a silica support, made by precipitation of silica gel, with a soluble chromium salt. This material is catalytically inactive, and further calcination at higher temperature is necessary. Siloxyl chromium complexes are formed by the reaction of chromic oxide with the hydroxyl groups on the silica surface, as the catalyst is activated prior to operation. (Weckhuysen & Schoonheydt, 1999), (Lloyd, 2011)

These catalysts are able to polymerize olefins which have no branching closer than the 4-position to the double bond and which contain no more than about eight carbon atoms. Thus, propylene, 1-butene, 1-pentene, and 1-hexene are polymerized to branched, high molecular weight polymers ranging from solids to viscous liquids. From ethylene, a broad range of solid polymers are produced, which are characterized by a linear backbone without long-chain branching (like HDPE). Copolymerization of ethylene with mostly C4-C8 olefins gives a branched polymer, in which the number of branches per molecule and the number of carbon atoms per branch depend on the amount and nature of the comonomer. Chromium-based catalyst always produce a resin with a broad distribution of individual polymer molecules, each one contributing to the overall properties of the resin. Besides molecular weight distribution, the amount, type and pattern of branching also influences the properties of the resin. The success of the Phillips polymerization process originates from its diversity. They are able to make more than 50 different types of polyethylene, and a whole battery of chromium-based catalysts are developed, each of which are able to produce a different type of HDPE or LLDPE. (Lloyd, 2011)

3. Reactor Model

3.1. Detailed model

The reactor model developed in this work consist in a **pseudo-homogeneous CSTR** type. It's assumed that all bed operates in such approach. It's a "box" model chiefly intending to get the global effect of n-hexane in the production of polyethylene taking into account its co-solubility functionality. There are no concerns about mass or heat transfer phenomena nor real fluidizing bed reactor characteristics. Based on this, it will be assumed a simple model in steady-state that can give important indications on how the temperature and polyethylene production vary with different hexane pressures and for different sets of conditions such as different kinetic constants, catalyst flowrates and inflow temperatures.

In the next pages, the model equations are written, briefly explained and finally the results of equation solving are shown in plots. The main model assumptions are firstly enumerated.

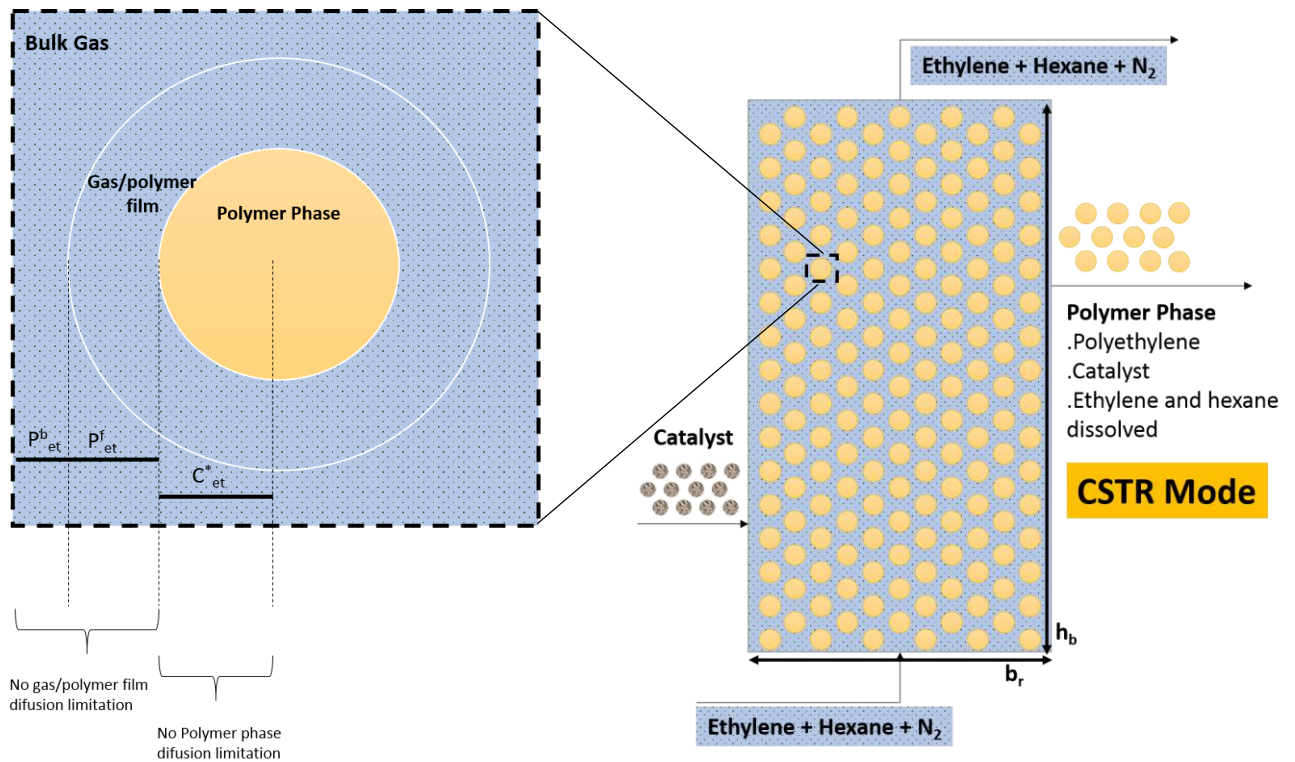
Model **ASSUMPTIONS**

- ✓ Single-phase CSTR approach
- ✓ 1 inlet flow containing a mixture of **ethylene, n-hexane** and **nitrogen**
- ✓ 1 inlet solid flow containing the catalyst
- ✓ 1 outlet gas flow containing ethylene, n-alkane and all nitrogen
- ✓ 1 outlet solid flow containing the **polymer phase** which includes **catalyst, polyethylene, dissolved ethylene** and **n-alkane**. Dissolved nitrogen in the particle is negligible and it's considered to be zero.
- ✓ Equilibrium is **instantaneous** and particles are mature (no mass or heat transfer phenomena in every volume of reactor and particles)
- ✓ The **absorbing latent heat species** (n-hexane and ethylene) do it **instantaneously**
- ✓ Elutriation of solids is neglected at the top of the bed
- ✓ No pressure gradient or even difference pressure between reactor inlet and outlet
- ✓ The catalyst particle size is spherical shape and **mono-dispersed**
- ✓ Fast catalyst activation
- ✓ Spherical and Constant mean particle size

Figure 10 is representing the **Model Assumptions** just described. The **left image** is a zooming of particle scale where it is evidenced the absence of ethylene mass gradients through the different layers. The same is analogous for hexane and heat transfer although not explicitly represented. So the pressure of bulk gas is the same as in gas/polymer film and the concentration in polymer phase is just a thermodynamic function. The temperature is also equal in every volume of the reactor.

The **right image** shows a macro view of the reactor. It represents a pseudo-homogeneous media of polymer particles fluidized by gas. All of them have the same residence time (steady-state CSTR).

The reacting volume is the catalyst volume. There's an inflow of catalyst and an inflow of gas of ethylene, n-hexane and nitrogen. The outflows are composed by the polymer phase and the gas not reacted and not dissolved as well in polymer phase. The reactor is also characterized by a bed height, h_b , and a base area, b .



P_{et}^b – Ethylene pressure in gas bulk phase
 P_{et}^f – Ethylene pressure in gas/polymer film
 C_{et}^* – ethylene concentration in polymer phase (solubility)

Figure 10 – Particle and reactor view (left and right image respectively)

Model EQUATIONS

Given the previous model assumptions, the set of equations that will allow to simulate the productivity and temperature are exposed. They are essentially:

- mass balance for polyethylene
- mass balance for ethylene
- mass balance for n-hexane
- mass balance for nitrogen
- mass balance for activated catalyst
- heat balance

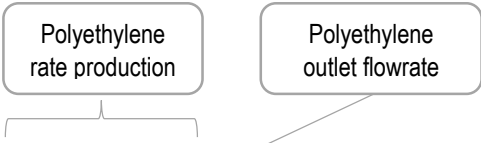
In the end the two equations to be computed will be the **polyethylene mass balance** and **heat balance**. The other balances are substituted in the mentioned ones.

The different terms of these equations such as vaporization rate, catalyst activity, reaction heat are also briefly discussed.

Mass Balances (MB's) (Steady-State operation)

- Polyethylene mass balance (PEMB)

The polyethylene production, \dot{m}_{Pet} , is evaluated through mass balance according to:



$$R_p(T, P)V_c - \dot{m}_{Pet} = 0 \quad (2)$$

The reaction rate, R_p , is an extrapolation of eq.1 for every particle in the reactor. It's an average polymerization rate.

$$R_p(T, P) = k_p(T)C^*(T)C_{et}^p(P)M_{et} \quad (3)$$

In eq. (3), it's pointed that the ethylene concentration in **amorphous** polymer phase, C_{et}^p , (mentioned from now on as just polymer phase) is a function of pressure, more exactly the hexane pressure. Its variation was predicted in Alizadeh work (Alizadeh A. , 2014) with SL EOS and such data is in table 4.

The kinetic parameter, k_p , has an Arrhenius dependence on temperature according to:

$$k_p(T) = k_p^{T_{\text{exp}}} \cdot e^{\frac{E_a}{R} \left(\frac{1}{T_{\text{exp}}} - \frac{1}{T} \right)} \quad (4)$$

The concentration of active sites, C^* , in eq. (3) is obtained with activated catalyst mass balance (see eq. (8)).

- **Ethylene mass balance**

$$\dot{m}_{\text{et},0} - \dot{m}_{\text{et}} - [R_p(T, P)]V_c - \dot{m}_{\text{et},d} = 0 \quad (5)$$

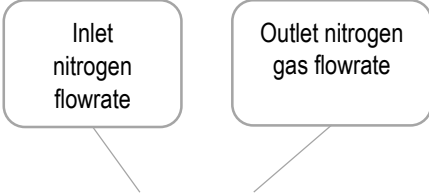
The mass balance to the ethylene (eq. 5) is intended to be used in heat balance. One should expect outlet ethylene gas flowrate, \dot{m}_{et} , to be similar to the inlet one once conversion is low (no more than 5%).

- **n-Hexane mass balance**

$$\dot{m}_{\text{hex},0} - \dot{m}_{\text{hex}} - \dot{m}_{\text{hex},d} = 0 \quad (6)$$

The n-hexane mass balance is also intended to be used in heat balance. Again, since the contact of the gas with polymer particles is very low, and so the conversion, the outlet hexane gas rate, \dot{m}_{hex} , will be no much different from the inlet one.

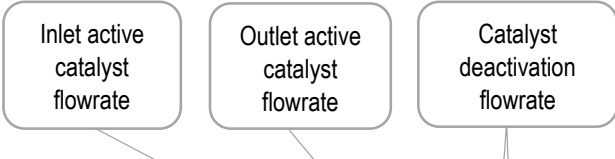
- **Nitrogen (N₂) mass balance**



$$\dot{m}_{N_{2,0}} - \dot{m}_{N_2} = 0 \quad (7)$$

The nitrogen goes into the reactor and leaves it at the same rate. As said in the model assumptions, nitrogen doesn't dissolve in the polymer particle and stays always in the gas phase.

- **Activated catalyst mass balance**



$$Q_{c,0} C_0^* - Q_c C^* - k_d(T) C^* V_c = 0 \quad (8)$$

This mass balance to the number of mols of active sites in the reactor is solved for active sites concentration, C^* , and then substituted in the polymerization rate law (eq.3).

The catalyst deactivation constant, k_d , has an Arrhenius dependence on temperature:

$$k_d(T) = k_d^{T_{exp}} \cdot e^{\frac{E_d}{R} \left(\frac{1}{T_{exp}} - \frac{1}{T} \right)} \quad (9)$$

The fact there are 2 temperature dependent parameters with exponential laws in MB's make polyethylene mass rate very sensitive to the temperature.

- **Heat Balance (HB) (Steady-State operation)**

Reference State:

- $T_{ref.} = T_0$ (reactor inlet stream temperature)
- Gaseous both ethylene and n-hexane; gaseous nitrogen; amorphous polyethylene; solid catalyst
- Work pressure, P

$$(-\Delta H_r^T) \dot{m}_{Pet} - (T - T_0) [\dot{m}_g \bar{c}_{p,g} + \dot{m}_p \bar{c}_{p,p}] - (F_{hex,0}^L \Delta H_{v,hex}^{T_0} + F_{et,0}^L \Delta H_{v,et}^{T_0}) = 0 \quad (10)$$

The heat balance (eq.10) is accommodating the global heat exchanged between the reactor and the gas streams. The first term – heat of polymerization rate – expresses the heat released in polymerization and represents a large numerical value.

The heat of polymerization, ΔH_r^T , is more generally:

$$(-\Delta H_r^T) = (-\Delta H_r^{T_{exp.}}) + \Delta C_p (T - T_{exp.}) \quad (11)$$

T is the reaction/reactor temperature and $(-\Delta H_r^{T_{exp.}})$ is the polymerization heat admitted in Alizadeh work at his $T_{exp.} = 80^\circ\text{C}$ predictions.

The outlet gas mass rate, \dot{m}_g , in eq. 10 is the sum of the three existing gases:

$$\dot{m}_g = \dot{m}_{et.} + \dot{m}_{hex.} + \dot{m}_{N_2} \quad (12)$$

And each of its terms are (through specie mass balance):

$$\dot{m}_{et.} = \dot{m}_{et,0} - \dot{m}_{Pet.} - \dot{m}_{et,d} \quad (13)$$

$$\dot{m}_{hex.} = \dot{m}_{hex,0} - \dot{m}_{hex,d} \quad (14)$$

$$\dot{m}_{N_2} = \dot{m}_{N_2,0} \quad (15)$$

With ethylene and hexane dissolved mass rate in polymer phase, $\dot{m}_{et,d}$ and $\dot{m}_{hex,d}$ respectively, equal to:

$$\dot{m}_{et,d} = C_{et}^p \frac{M_{et.}}{\rho_p} \dot{m}_{Pet.} \quad (16)$$

$$\dot{m}_{hex,d} = C_{hex}^p \frac{M_{hex.}}{\rho_p} \dot{m}_{Pet.} \quad (17)$$

$M_{et.}$ and $M_{hex.}$ are ethylene and hexane molar masses, respectively.

\dot{m}_p (eq. 10) is the total mass flowrate of polymer phase. It includes polyethylene mass rate, $\dot{m}_{Pet.}$, catalyst mass rate, \dot{m}_c , and n-hexane plus ethylene gas dissolved mass rate ($\dot{m}_{hex,d}$ and $\dot{m}_{et,d}$). Again with the respective MB's it's possible to conveniently write:

$$\dot{m}_p = (\dot{m}_{Pet.} + \dot{m}_c + \dot{m}_{et,d} + \dot{m}_{hex,d}) = \dot{m}_{Pet.} \left(1 + \frac{C_{et.}^p (P) M_{et.}}{\rho_p} + \frac{C_{hex.}^p (P) M_{hex.}}{\rho_p} \right) + \dot{m}_c \quad (18)$$

The 2nd and 3rd term between brackets in eq. 18 have very low numerical values. For writing convenience, this quantity is named by letter f .

$$\left(1 + \frac{C_{et.}^p (P) M_{et.}}{\rho_p} + \frac{C_{hex.}^p (P) M_{hex.}}{\rho_p} \right) \equiv f \approx 1 \quad (19)$$

In what concerns latent heat terms in eq.10, the ethylene and hexane liquid amounts were calculated based on thermodynamic condition of inlet gas flow (see appendix A.2). It was chosen to consider ethylene in liquid phase as well according to the respective Redlich-Kwong-Soave (RKS) phase diagram prediction. For full considerations on the procedure for these thermodynamics calculations, check appendix A.2.

To calculate the enthalpy of vaporization for n-hexane it was used a Watson type correlation (NIST, 2014):

$$\Delta H_{hex.}^V = 45.61 \left(1 - \frac{T}{507.43} \right)^{0.401} ; P = 1 \text{ bar}; 342 \leq T(K) \leq 480 \quad (20)$$

For ethylene it was fit a polynomial equation to a set of data for 10bar (J. Smulaka, 2001)

$$\Delta H_{et.}^V(10\text{bar}) = -0.0202T^2 - 72.836T + 11172; -168.15 \leq T(^{\circ}\text{C}) \leq -53.15 \quad (21)$$

The fitting of this equations can be checked in appendix A.3.

A small caveat about **ethylene presence in vaporization process** and its **vaporization heat correlation** (eq. 21) shall be said. Although pure ethylene is clearly a gas, it was here included in vaporization process simply because that's what RKS model predicted at work conditions. And to maintain consistent argument, it was assumed ethylene to take also part in inlet stream gas-liquid equilibrium. RKS model estimates there is about a 10-15% liquid ethylene fraction in the range of work conditions. This is a measurable amount. Concerning vaporization heat correlation, one notices that at 10bar total pressure, ethylene will boil at -53.15°C. Therefore using eq. 21 out of the temperature range is admitting a pseudo-liquid state for ethylene at higher temperatures. It may not be the most corrected consideration but assumed the prediction of RKS model of an ethylene liquid state in the working conditions it becomes necessary to have some estimation of it.

After the mathematical treatment discussed, the PEMB and HB are both explicated in polyethylene mass rate, \dot{m}_{Pet} , resulting in the final solving form:

$$\left\{ \begin{array}{l} PEMB.: \dot{m}_{Pet} = \left[k_p^{T_{ref.}} e^{\frac{Ea}{R} \left(\frac{1}{T_{ref.}} - \frac{1}{T} \right)} \frac{C_0^*}{1 + k_d^{T_{ref.}} e^{\frac{Ed}{R} \left(\frac{1}{T_{ref.}} - \frac{1}{T} \right)} \sigma_c} C_{et}^p M_{et} \right] V_c \\ HB.: \dot{m}_{Pet} = \frac{(F_{hex0}^L \Delta H_{v,hex}^{T_0} + F_{et0}^L \Delta H_{v,et}^{T_0}) + (T - T_0) [(\dot{m}_{et0} + \dot{m}_{hex0} + \dot{m}_{N20}) \bar{c}_{p,g} + \dot{m}_c \bar{c}_{p,p}]}{\Delta H_r^T - (T - T_0) f(\bar{c}_{p,p} - \bar{c}_{p,g})} \end{array} \right. \quad (22)$$

The 2 equations to solve consist in a non-linear system. The only way to solve is numerically. Since the range of work temperatures of interest are between [40 - 110°C] (this takes into account the values used in industry as well as the polyethylene melting temperature) it was chosen to write them both in order to polyethylene mass rate (\dot{m}_{Pet}) and solve them for the mentioned range of temperatures, checking then when they are equal. This method is eventually better to test/adjust some parameters. It wouldn't be this prompt if it was used a tool like *matlab*® or some other analogous. For example, adjusting the inlet gas flow and the inlet catalyst mass to the reactor would be much more laborious.

It might exist other solutions out of the considered temperature range. But that's, for the reasons already exposed, irrelevant in this problem. So no need for studying all the solutions of the system.

The step of temperature simulation was 0.25 degree. Despite this step might not be relevant in industrial scale, the polyethylene mass flowrate rate is highly sensitive to temperature (at least, for the reactor model used). Actually a solution between, for example 80.25 and 80.50°C may represent a difference of 20kg/h of polyethylene. So the step should not be bigger. Anyway the big intent with these simulations are showing the general behaviour of polyethylene mass rate and reactor temperature. This is will be focused in Plot results chapter.

3.2. Summary of important data used in simulation

The following tables – table 3 and table 4 – show the constant values used in simulations. The way they were calculated or set are also briefly explained.

General Thermodynamic Parameters			
$T_{exp.}$ (°C)	$P_{et.}$ (bar)	P_{N_2} (bar)	R (kJ.mol ⁻¹ .K ⁻¹)
80	7.00	1.00	8.315x10 ⁻³
$C_{p,c}$ (J.kg ⁻¹ .K ⁻¹)	$(-\Delta H_r^{80°C})$ (J/mol _{et.})	$C_{p,p}$ (J.kg ⁻¹ .K ⁻¹)	
2000	107 600	2000	
Molecular masses			
$M_{et.}$ (g/mol)	$M_{hex.}$ (g/mol)	M_{N_2} (g/mol)	
28.05	123	14	
Catalyst Parameters			
$T_{exp.}$ (°C)	$k_d^{80°C}$ (s ⁻¹)	E_d (kJ/mol)	E_a (kJ/mol)
80	1.00x10 ⁻⁴	42	42
ρ_c (kg/m ³)	C_0^* (mol/m ^{3c})	d_c (µm)	V_c (L)
2300	0.55	30	13
Reactor Parameters			
d (m)	b (m ²)	h_b (m)	V_b (m ³)
4.0	12.6	10.7	134
ϵ	V_p (m ³)	d_p (µm)	
0.55	60.4	500	

Table 3 – General parameters/constants used in model simulations.

Data in table 3 is divided in groups of thermodynamic parameters, molecular masses, catalyst parameters and reactor parameters. The thermodynamics and catalyst parameters were taken from Alizadeh Phd Thesis (Alizadeh A. , 2014). The experimentation temperature, $T_{exp.}$, is the temperature at which the concentration of ethylene and hexane in polymer phase (table 4) were predicted by the Sanchez-Lacombez EOS in his work. Since the simulations were made in the same conditions, all the relevant numerical quantities he has available it will be used.

In terms of reactor parameters, the bed volume was calculated with the usual formula:

$$V_b = bh_b = \pi 4^{-1} d^2 h_b \quad (23)$$

The diameter and height of the fluidized bed reactor were adjusted to be in a usual range of industrial reactors. According some patents they are [10-15]m for bed height and [2.44-4.4]m for bed diameter (US Patente N° 4,588,790, 1986).

For a typical fluidizing porosity, ε , the volume of particles in the bed was calculated by:

$$V_p = V_b(1 - \varepsilon) \quad (24)$$

The catalyst volume, V_c , needed for this particle volume, V_p , was calculated assuming particles are **spherical shaped**. First it was computed the number of polymer particles, n_p , summing total particle volume, V_p .

$$V_p = n_p \frac{\pi}{6} d_p^3 \Leftrightarrow n_p = \frac{6}{\pi} V_p d_p^{-3} \quad (25)$$

Also assuming each catalyst particle will turn into a polymer particle, n_c is equal to n_p and the catalyst volume comes:

$$V_c = n_p \frac{\pi}{6} d_c^3 \quad (26)$$

The catalyst and particle diameter were chosen according reference values. They are [30-50] μm for catalyst particle and [300-1000] μm for polymer particle (McAuley, Talbot, & Harris, 1994).

Table 4 contains, in the first half, equilibrium data for the concentration of ethylene and n-hexane in polymer phase. The original data was extracted from Alizadeh work (Alizadeh A. , 2014) and it consisted in 4 predictions of the mentioned concentrations at **4 hexane pressures** – 0.0, 0.3, 0.6 and 0.8 bar. Then these values were interpolated. The correlation obtained was also extrapolated for 0.9 and 1.0 bar hexane. The intent was to have a more continuous range of hexane pressure conditions. The made correlations are in appendix A.I.

The 2nd half of the table shows the mass liquid fraction, $m_{liq.}$, of inlet stream at 40, 45 and 50°C. It is also indicated the dew-point at given conditions. Below 0.40 bar n-hexane (including) there's no liquid phase (dew-point is below the inlet flow temperature). On the other hand, the maximum percentage of liquid mass in the flow is at 1bar hexane. To see how these values were calculated, see appendix A.II.

At 40°C inlet flow, there is no liquid until hexane pressure reaches 0.5bar. From this level on until 1 bar hexane, the amount of liquid is always increasing. At 45°C, only at 0.60 bar hexane pressure starts to exist liquid in inlet flow. Finally the 50°C temperature flow only starts to have liquid at 0.70 bar hexane pressure. The liquid quantity fractions, at the same hexane pressure, decreases with increasing temperature.

T _{ref.} (°C)	Working Thermodynamic Conditions				
P _{hex.} (bar)	C _{et.P} (mol/m ³ _p)	C _{hex.P} (mol/m ³ _p)	ρ _p (kg/m ³)	C _{p.g} (J.kg ⁻¹ .K ⁻¹)	ρ _g (kg/m ³)
0.00	84.29	0.00	920.4	1553.4	8.00
0.10	86.03	38.17	919.0	1565.9	8.30
0.20	87.96	79.20	917.4	1577.7	8.60
0.30	90.07	123.08	915.8	1588.9	8.90
0.40	92.37	169.82	914.0	1599.4	9.20
0.50	94.86	219.42	912.1	1609.3	9.50
0.60	97.53	271.86	910.1	1618.5	9.80
0.70	100.39	327.16	908.0	1627.1	10.10
0.80	103.44	385.32	905.7	1635.1	10.40
0.90	106.67	446.33	903.4	1642.3	10.70
1.00	110.08	510.20	900.9	1649.0	11.00
	Inlet mass liquid fraction, m _{liq.}				
	Inflow temperature, T ₀ (°C)				
P _{hex.} (bar)	40.0°C	45.0°C	50.0°C	T ^{dew point} (°C)	
0.40	0.00%	0.00%	0.00%	38.8	
0.50	3.91%	0.00%	0.00%	43.6	
0.60	8.66%	3.46%	0.00%	48.1	
0.70	13.02%	8.04%	2.61%	52.3	
0.80	17.03%	12.26%	7.06%	56.1	
0.90	20.89%	16.27%	11.23%	59.7	
1.00	24.17%	19.77%	14.97%	63.1	

Table 4 – Working thermodynamic conditions relating to polymer phase ethylene concentration, polymer phase hexane concentration, gas density, polymer particle density and gas heat capacity. The half below of the table indicates the liquid fraction of inlet flow at different inlet temperatures, for the working hexane pressures.

It should be recalled that these calculations were performed using thermodynamic models that have their deviations towards reality. Even so, with regards to co-solubility effect prediction, the trends such models evidence are agreeable and they may be assumed to be satisfactory to include in reactor model simulations. As remarked in literature review, the Sanchez-Lacombe model predictions overestimate the solubility of both ethylene and n-hexane until 90°C. The best performance achieved was actually at higher temperatures. So in the range of temperatures expected in the fluidized bed reactor – [50-90]°C – there should be some overestimation of solubility of ethylene in polymer phase and, by extension, in polyethylene production. The extent of these differences may be discussed later with some sensitive analysis. The biggest deviations might come from the gas-liquid phase equilibria predictions. Again, in the absence of comparable literature, a sensitive analysis may provide some information on it.

3.3. Results and sensitive analysis

3.3.1. Results

The resolution of the system of two equations (eq. 22) for the different conditions are shown in the next pages. For one set of conditions, table 5 shows the numerical values of the simulation. The figures 11 and 12 show it graphically. For other conditions it will be represented just the graphical results. The respective tables were left in appendix for not overloading the text.

Besides **reactor temperature, T**, and **polyethylene production rate, \dot{m}_{Pet}** , the simulation tables (table 5 and the other 2 simulation tables left in appendix) also show the **conversion, space time-yield** (or polymerization rate, R_p), **gas superficial velocity, $u_{g,0}$** , and σ_p . There was the concern to have these outputs in a range compatible with the industrial gas-phase ethylene polymerization operations. The formulas for them come next:

$$\%Conv. = \frac{\dot{m}_{Pet}}{\dot{m}_{et,0}} 100 \quad (27)$$

The conversion has the usual formal definition. Usually a single pass monomer conversion vary from 2-5%. (Xie, McAuley, Hsu, & Bacon, 1994)

$$R_p = k_p(T)C_0^*C_{et}^p \quad (28)$$

The space time-yield, or polymerization rate in this situation, is basically the polymer produced per time and reaction volume.

$$Q_{g,0} = \frac{\dot{m}_{g,0}}{\rho_g} \quad (29)$$

The way this density was evaluated was already mentioned and its calculations are in appendix A.1.

The volumetric inlet gas flowrate is useful to check the proper range of superficial gas velocity value. Since the base area, b , of reactor is already fixed, the superficial velocity of gas can be estimated by:

$$u_{g,0} = \frac{Q_{g,0}}{b} \quad (30)$$

According some patents (US Patente N° 5.462.999, 1995) these velocities are around $0.48 < u_{g,0} < 1$ m/s.

The average particle residence time, σ_p , is defined as the quotient of particle volume in the reactor, V_p , by the volumetric inflow rate, Q_0 , which comprises catalyst volumetric inlet flowrate, $Q_{c,0}$, and gas volumetric inlet flowrate that contributes to polymerization, $Q_{g,0}$. Q_0 is numerically the same as the polymer volumetric outlet rate, Q_p .

$$\sigma_p = \frac{V_p}{Q_0} = \frac{V_p}{Q_{c,0} + Q_{g,0}} = \frac{V_p}{Q_p} \quad (31)$$

The bulk density of the fluidized bed, ρ , is estimated by:

$$\rho = \frac{m_b}{V_b} = \frac{(1-\varepsilon)bh_b\rho_p + \varepsilon bh_b\rho_g}{bh_b} = (1-\varepsilon)\rho_p + \varepsilon\rho_g \quad (32)$$

Or equivalently:

$$\rho = \rho_p + \varepsilon(\rho_g - \rho_p) \quad (33)$$

Its value is around $300 < \rho < 500 \text{ kg/m}^3$ according to some patents. (US Patente N° 5.462.999, 1995), (US Patente N° 4,588,790, 1986)

The simulation I results in table 5 fix total molar flow, F , inlet temperature, T_0 , and catalyst flowrate, Q_c , for 3 different values of k_p (at the experimentation temperature, T_{exp}). In the particularly set of conditions with $k_p = 1200 \text{ m}^3_{\text{pet}} \text{ mol}^{-1} \text{ ac} \cdot \text{s}^{-1}$ one can see there are no values for **1bar** hexane pressure. This is a particular case of thermodynamic constraint. The dew point of such inflow is above the reactor temperature. So there is no total vaporization making the gas-phase have a different composition from the intended one. In each simulation it's always expected the liquid portion of inflow to completely vaporize and, additionally, in a flash way. This ensures the gas phase has the desired composition/concentration. In simulations where the dew-point of inlet flow is above reactor temperature it leads (at least in this work simulations) to no simulation solution. Anyway there was only one case like this.

Simulation Results						
Molar Gas flow rate, F (mol/s) 2000		T ₀ (°C) 40.0		Catalyst flow rate (g/s) 0.222		
	k _p ^{80°C} (m ³ _{Pet.} mol-site ⁻¹ .s ⁻¹) 1200					
P _{hex.} (bar)	m _{Pet} (ton/h)	T (°C)	% Conv.	R _P (kg _{Pet.} m _c ⁻³ .h ⁻¹)	u _{g,0} (m/s)	σ _P (h)
0.00	5.295	107.8	2.62	405334	0.52	10.5
0.10	5.409	105.8	3.10	412928	0.53	10.2
0.20	5.502	103.8	3.19	422200	0.53	9.93
0.30	5.620	102.3	3.30	431409	0.53	9.65
0.40	5.771	101.3	3.43	441506	0.54	9.33
0.50	5.855	93.8	3.52	448443	0.54	9.11
0.60	5.922	85.0	3.60	453336	0.54	8.93
0.70	5.954	76.8	3.66	456482	0.54	8.79
0.80	5.961	69.0	3.71	457212	0.54	8.69
0.90	5.921	61.3	3.72	453394	0.54	8.65
1.00	-	-	-	-	-	-
	k _p ^{80°C} (m ³ _{Pet.} mol-site ⁻¹ .s ⁻¹) 1350					
0.00	5.987	116.3	3.39	458938	0.52	9.26
0.10	6.115	114.0	3.50	468509	0.53	9.00
0.20	6.241	112.0	3.62	478461	0.53	8.76
0.30	6.370	110.3	3.74	489017	0.53	8.52
0.40	6.528	109.0	3.88	500509	0.54	8.24
0.50	6.640	101.5	3.99	509745	0.54	8.04
0.60	6.759	93.0	4.11	517857	0.54	7.82
0.70	6.845	85.0	4.21	525129	0.54	7.65
0.80	6.934	77.8	4.31	531551	0.54	7.47
0.90	6.978	70.5	4.39	535426	0.54	7.34
1.00	7.019	64.3	4.46	538299	0.54	7.21
	k _p ^{80°C} (m ³ _{Pet.} mol-site ⁻¹ .s ⁻¹) 1500					
0.00	6.685	124.8	3.78	512309	0.52	8.29
0.10	6.827	122.3	3.91	523141	0.53	8.06
0.20	6.965	120.0	4.04	534385	0.53	7.85
0.30	7.126	118.3	4.18	546370	0.53	7.61
0.40	7.291	116.8	4.33	559274	0.54	7.38
0.50	7.457	109.5	4.48	570809	0.54	7.16
0.60	7.577	100.8	4.61	581568	0.54	6.98
0.70	7.743	93.3	4.76	592699	0.54	6.76
0.80	7.859	86.0	4.89	603368	0.54	6.59
0.90	6.389	79.5	5.04	613947	0.54	6.39
1.00	8.145	73.8	5.17	624621	0.54	6.21

Table 5 – Simulation results for 3 different reference propagation kinetic constants, k_p^{80°C}.

3.3.1.1. Plot Results

In general, all the simulations show an increasing of polyethylene production with increasing hexane pressure. However, as the hexane pressure increases, the relative variation of production tends to get smaller. The opposite trend for reactor temperature: increasing hexane gas pressure means decreasing temperature. More n-hexane implies more liquid content and therefore more heat removal, either in the form of latent or sensitive heat (for its heat capacity). This last contribution may not be as relevant as the first one but given the huge flow of gas and even its velocity, it also plays an important role in removing heat. Vaporization occurs when the reactor is working in condensed mode. In this condition, the graphical results seem to show that higher production is allowed at usual polyethylene reaction temperatures. So in a whole, this is in line with global expectations.

The figures 11 and 12 exhibit the results of table 5. The figure 11 shows the steady-state mass flowrate production, $\dot{m}_{\text{Pet.}}$, (vertical axes) for the different hexane pressures (horizontal axes). In turn, figure 12 shows the steady-state temperature in the reactor, T , as a function of the same hexane pressures. The title of both plots contains the fixed conditions. The label contains the changing parameters. Ex.: in the figure 11 and 12, Q_c , F and T_0 are the fixed conditions. And as changing parameters there are 3 different reference k_p 's. For each set of conditions there are always one plot for **polyethylene mass rate** and one for **reactor temperature** following.

In results analysis, there will be often comparisons in terms of relative variation quantities. This general relative variation, Δq_r , is defined as:

$$\Delta q_r (\%) = \frac{q_{i+1} - q_i}{q_i} 100, i \equiv \text{reference value} \quad (34)$$

For example, if q_3 is related to some output at 0.4bar hexane, q_4 will be related to the same output at 0.5bar hexane. The relative variation can be positive (if actual value is bigger than reference one) or negative (if actual value is smaller than reference one).

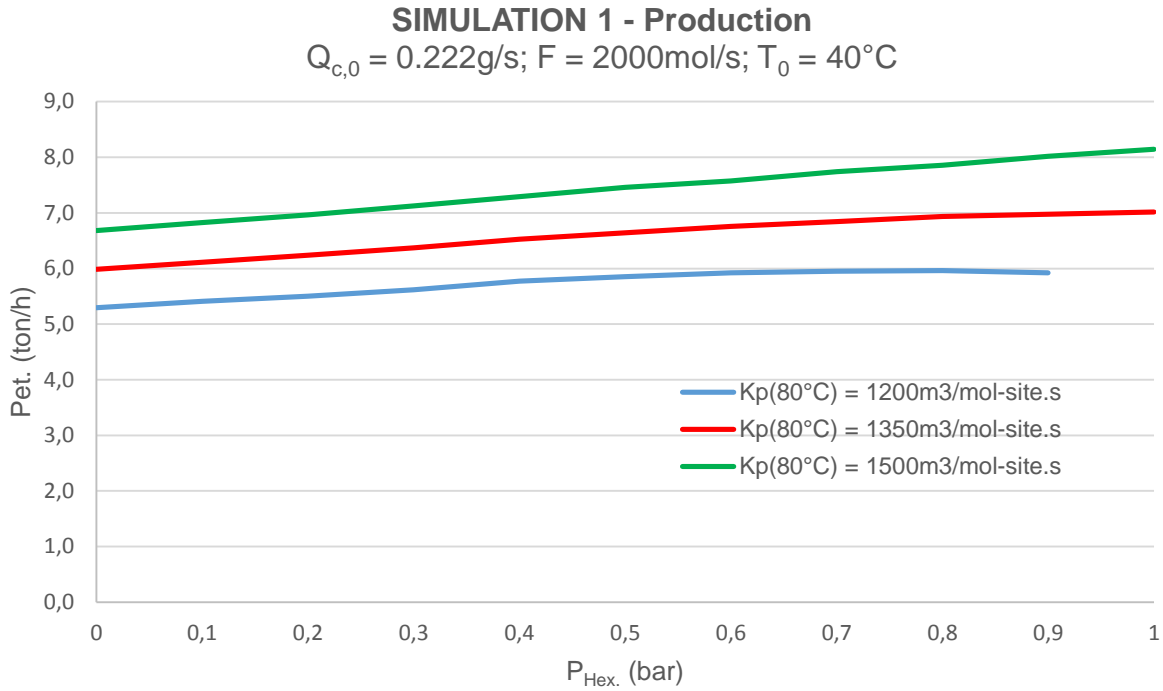


Figure 11 – Polyethylene mass rate steady-state simulations 1 results given the condition in plot title. Numerical output is in table 5. No result for $k_p = 1200\text{m}^3\text{mol-site}^{-1}\text{s}^{-1}$ curve at 1.0bar hexane pressure due to thermodynamic constraint.

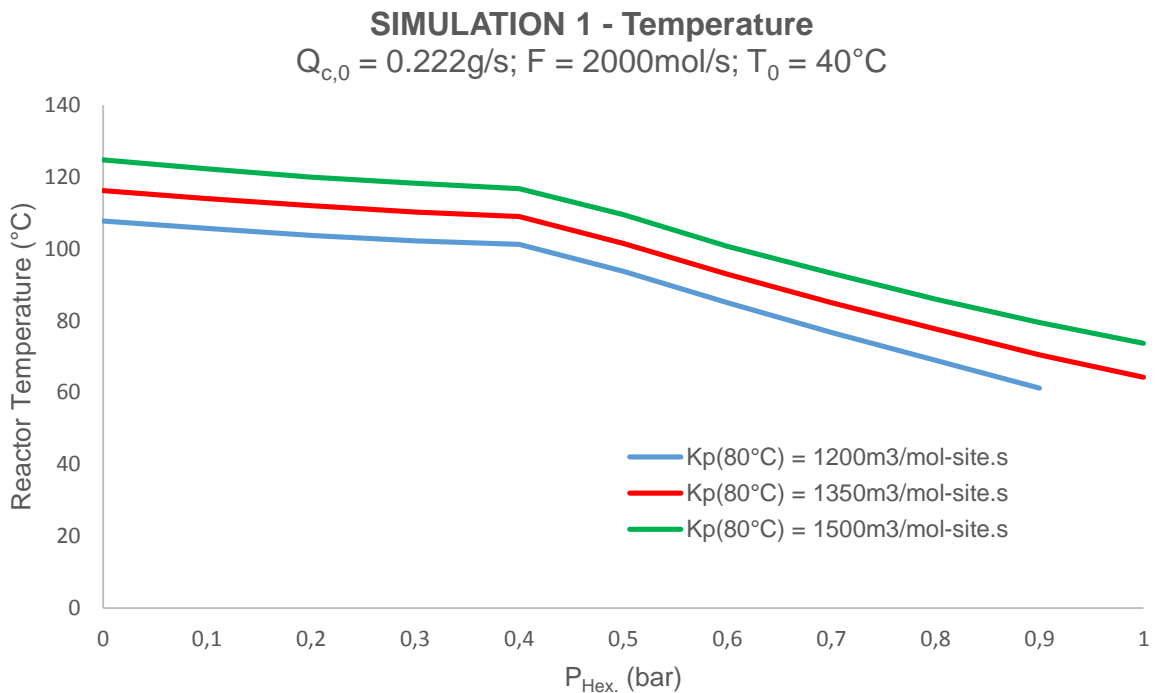


Figure 12 – Reactor temperature result simulation 1 given the conditions in plot title. Simulation output is in table 5

The progress of curves in figure 11 show an increasing polyethylene rate production with increasing hexane pressure/concentration in polymer phase. Moreover, curves appear to have a smaller relative variation in production as the hexane pressure increases, specially from starting of condensing mode

(table 6 confirms it numerically). The three curves differ in propagation constant rate, $k_p^{80^\circ\text{C}}$. Higher ones lead naturally to bigger production rates. As mentioned before, there's no result at 1.0bar hexane pressure for $k_p = 1200\text{m}^3\text{mol-site}^{-1}\text{s}^{-1}$. Since the dew-point temperature at such conditions is about 63°C and the simulation result would be below this value, there's no mathematical solution. The figure 12 shows a global decreasing temperature with increasing hexane pressure. From no hexane in inlet stream to a pressure of 0.4bar hexane, the temperature gradually decreases (due to heat capacity of gases) and after it, a more abrupt lowering of temperature proceeds thanks to vaporization of condensed species. The condensed species in these simulations were assumed to be not only n-hexane but also ethylene (following from phase-equilibria predictions – appendix A.2). For the three k_p 's tested there are an average relative variation between them of about **15%** for polymer production. For temperature, there's a relative variation of about **10%** (in condensed-mode). It's also noticed a trend of decreasing of production and temperature relative variation between k_p 's with increasing k_p . This is, in the k_p 's presented, the biggest relative variations occurred between simulation sets of k_p 's = $1200\text{ m}^3\text{mol-site}^{-1}\text{s}^{-1}$ and k_p 's = $1350\text{ m}^3\text{mol-site}^{-1}\text{s}^{-1}$. Between k_p 's = $1350\text{ m}^3\text{mol-site}^{-1}\text{s}^{-1}$ and k_p 's = $1500\text{ m}^3\text{mol-site}^{-1}\text{s}^{-1}$ is lesser.

Table 6 shows the relative variation of polyethylene mass rate and reactor temperature for Simulation 1, from no hexane in inlet stream to starting condensed mode (0.50bar hexane) and so on. From **0.00-0.40bar hexane**, the reactor would operate in a **Dry-mode** and from that point on, in a **condensed-mode**. Table indicates that from **no hexane** until existence of hexane – **0.10bar hexane** – there's a relative variation of about **2%** in polyethylene production.

SIMUL.1	m _{Pet.} Relative variation (%)			T relative variation (%)			Operation-mode
	K _p ^{80°C} (m ³ _{Pet.} mol-site ⁻¹ .s ⁻¹)						
P _{hex.} (bar)	1200	1350	1500	1200	1350	1500	
0.10	2.14	2.14	2.13	-1.86	-1.94	-2.00	DRY
0.20	1.73	2.07	2.02	-1.89	-1.75	-1.84	DRY
0.30	2.15	2.06	2.31	-1.45	-1.56	-1.46	DRY
0.40	2.67	2.48	2.32	-0.98	-1.13	-1.27	DRY
0.50	1.47	1.72	2.28	-7.41	-6.88	-6.21	COND.
0.60	1.13	1.79	2.21	-9.33	-8.37	-7.99	COND.
0.70	0.55	1.27	2.19	-9.71	-8.60	-7.44	COND.
0.80	0.12	1.30	1.50	-10.10	-8.53	-7.77	COND.
0.90	-0.67	0.64	1.53	-11.23	-9.32	-7.56	COND.
1.00	-	0.59	1.60	-	-8.87	-7.23	COND.

Table 6 – Relative variation of polyethylene mass rate and reactor temperature for each hexane pressure with respect to simulation 1

Table 6 seems to show that polyethylene mass flowrate relative variation increases during dry-mode operation and then it starts to decrease. This is pronouncedly for set of $k_p^{80^\circ\text{C}} = 1200 \text{ m}^3\text{mol}\cdot\text{site}^{-1}\text{s}^{-1}$. As the hexane pressure increases, the liquid amount gets higher and the reactor temperature will drop due to considerable cooling capacity. At a certain value of hexane pressure, the reactor temperature gets too low and kinetics is clearly affected. For the other k_p 's, since they are bigger, the related productions are more "slowly" affected. The fact the k_p sets of values are not exactly all in descending order will be due to solving simulation step. Sometimes the exact solutions may be a bit above or below the solutions proposed and this reflects in subsequent calculations like relative variations.

Temperature decreases with a smooth rate until 0.4bar hexane pressure and from this value on, it decreases more rapidly. For example, for $k_p = 1300 \text{ m}^3\text{mol}\cdot\text{site}^{-1}\text{s}^{-1}$, from 0.1-0.4bar hexane pressure, the average rate of decreasing is about 1.5% and from 0.5 bar on is about 9%. As already discussed in respective graphical results, this significant rate difference from 0.5bar hexane pressure lies in the fact reactor starts operate in a condensed-mode.

Next plots – figure 13 and figure 14 – show results of simulation 2. Each curve has a different catalyst flowrate.

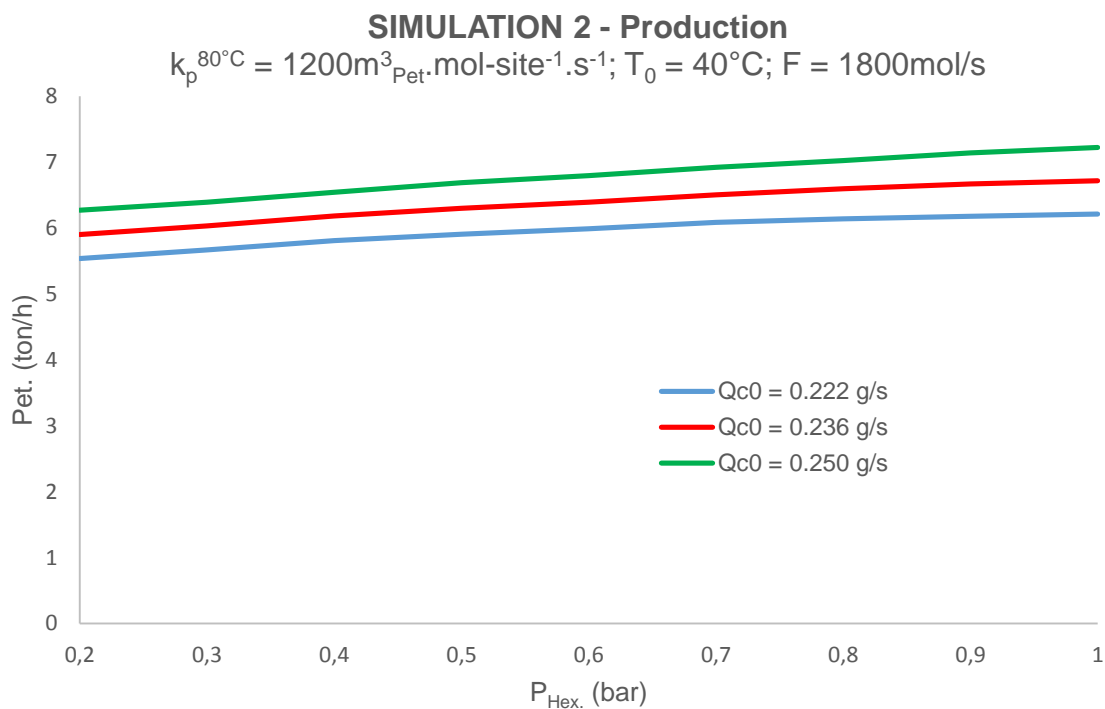


Figure 13 – Polyethylene mass rate steady-state simulations 2 results given the conditions in plot title. Simulation output is in appendix B

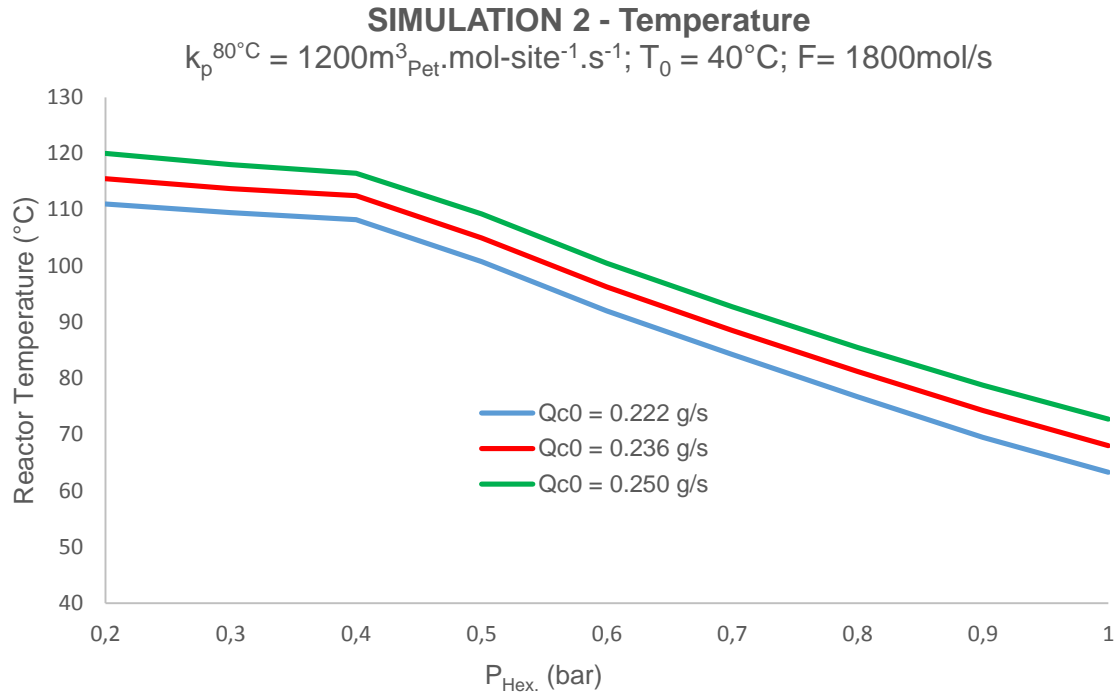


Figure 14 – Reactor temperature result simulation 2 given the conditions in plot title. Simulation output is in appendix B

The simulation 2 (figure 13 and 14) appears to have similar trends to the simulation 1. But here, because catalyst flowrates has not the same impact on temperature as kinetic constant, k_p , the highest relative variation between them is for production. For the three catalyst flow rates (Q_c) tested, there are a relative variation between them of about **9%** for polymer production and **7%** (as hexane pressure increases) for temperature when reactor operates in condensed-mode. Since the trends are quite the same as the case of simulation 1, this may lead immediately to the question of what preferably to boost: catalyst kinetic constant or catalyst flowrate for analogous productivity?! The cost factor might be the natural “decision variable”. But in principle, catalyst kinetic constant is not immediately available to change unlike the catalyst flowrate. In addition, the fact catalyst flowrate makes temperature changing slowly might consider it safer. The three curves differ in feeding catalyst flowrate, Q_{c0} . When this flowrate is bigger, essentially catalyst active-sites concentration is bigger in the reactor and so the production rates. Recalling that catalyst active-site concentration (in CSTR steady-state) is:

$$C^* = \frac{C_0^*}{1 + k_d \frac{V_c}{Q_{c,0}}} \quad (35)$$

This makes mathematically clear why production rate will increase with catalyst flowrate.

The progress of curves in figure 13 show an increasing polyethylene rate production with increasing hexane concentration in polymer phase and they seem to have lesser relative variations with increasing hexane pressure as well.

The figure 14 shows a global decreasing temperature with increasing hexane pressure. The behaviour of its curves are very similar to the ones of simulation 1. From 0.2 to 0.4bar hexane pressure, the temperature gradually decreases and then a stronger decreasing of temperature goes on when it

starts to occur heat vaporization of condensed species. Temperature decreases with a smooth rate until 0.4bar hexane pressure and from this value on, it has a manifest decreasing. For example, for $Q_{c,0} = 0.236\text{g/s}$, from 0.2-0.4bar hexane pressure, the average rate of decreasing is about 1.5% and from 0.5 bar on is about 8% (see appendix B, tables B.6).

Next plots – figure 15 and figure 16 – show results of simulation 3. Each curve has a different inlet Temperature, T_0 .

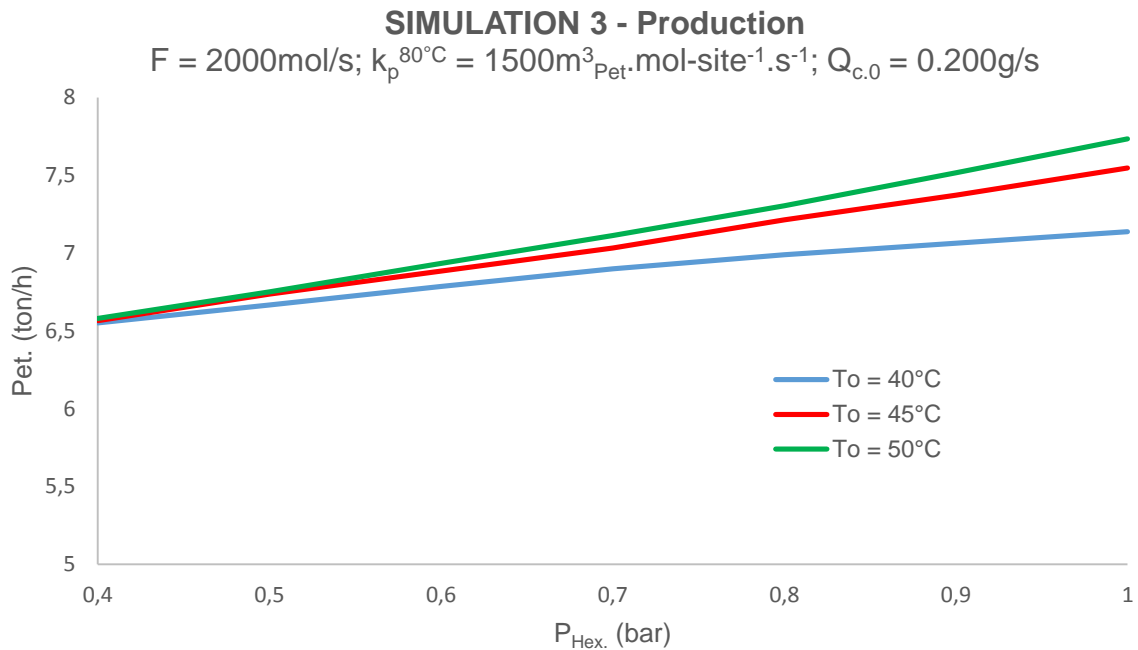


Figure 15 – Polyethylene mass rate steady-state simulations 3 results given the conditions in plot title. Simulation output is in appendix B.

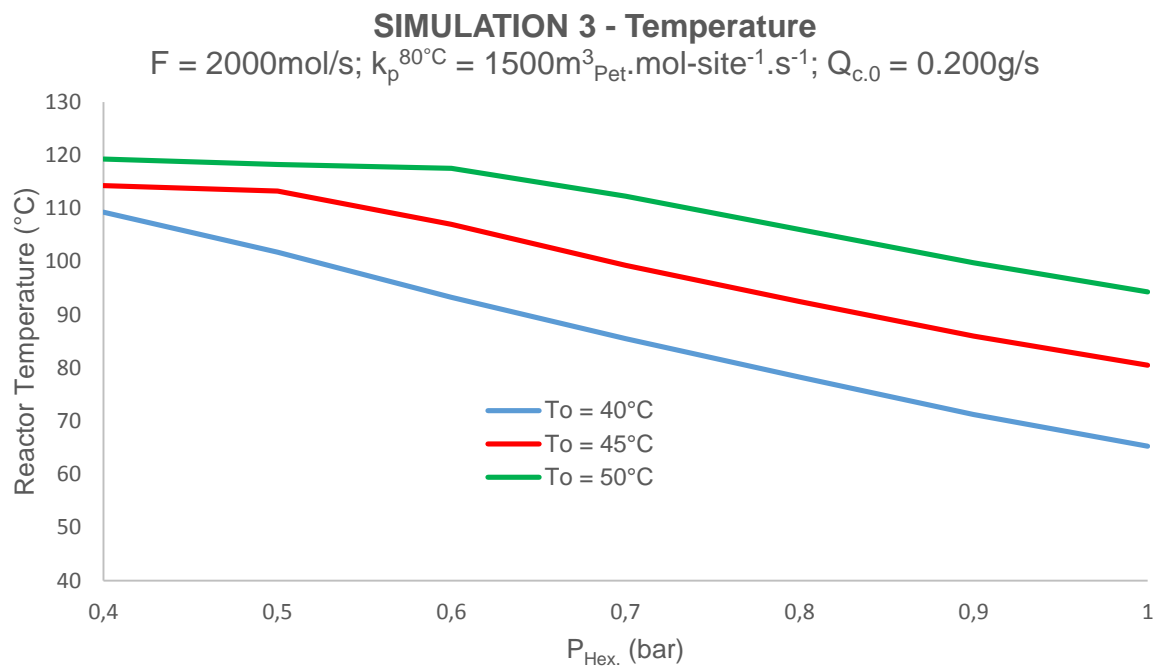


Figure 16 – Reactor temperature result simulation 3 given the conditions in plot title. Simulation output is in appendix B

Figure 15 shows there's small production difference especially between curves $T_0 = 45^\circ\text{C}$ and $T_0 = 50^\circ\text{C}$. Actually before condensing mode ($<0.5\text{bar}$ hexane), production is quite the same for 3 curves. Concerning case with $T_0 = 40^\circ\text{C}$, it starts to deviate from the others at 0.5bar hexane (its condensed mode beginning). The production increases with hexane pressure, although moderately, and it seems to stabilize near by the biggest hexane pressure tested (1.0bar). The other two curves start, in turn, to deviate from each other around 0.6bar hexane (starting cooling capacity for 45°C T_0 curve). Their individual evolution show an increasing polyethylene rate production with increasing hexane concentration in polymer phase. For example, for $T_0 = 45^\circ\text{C}$, the rate of polyethylene increasing is about 2.4% in average. Temperature decreases at a considerable rate with increasing hexane pressure. Again for $T_0 = 45^\circ\text{C}$, the average rate of decreasing is about 6%. 45°C and 50°C inlet streams have pointedly more productivities with increasing hexane pressure when compared with 40°C T_0 case. This clearly remarks the cooling capacity influence in polymer production. 40°C T_0 curve will have a too high liquid content and it'll quickly make production to decrease. On the other side, for example 45°C T_0 curve has less liquid content and it will allow bigger productions not only due to higher temperatures but also because hexane pressure is higher and its co-solubility effect will be more active. For the three inlet flow temperatures there is very high temperature relative variation between them. For example at 0.8bar hexane, when inlet temperature changes from 45°C to 50°C , there is a temperature relative variation of about 15%. And it is even higher between 40°C and 45°C (about 18%). These variations appear to decrease with increasing inlet temperature and increasing hexane pressure

This set of simulation indicates that differences in inlet temperature make substantial changes in production and reactor temperature. Basically, this happens because there's a big changing in flow composition in terms of liquid portion when the temperature changes, at least, 5°C (for instance, from 40 to 45°C). Even though hexane pressure gets higher – enhancing co-solubility effect and production in addition – if the liquid content in inlet flow is too high, it will soften the reaction. This may configure a direct warning on how important is to have good phase equilibria predictions so that simulation outputs come not too much skewed.

From all the three sets of simulations, the prominent indication is that, for a certain catalyst, inlet stream cooling capacity and hexane pressure should be correctly optimized. Increasing hexane pressure means increasing inlet stream liquid content and both of these factors will have a positive effect in production by favouring kinetics and heat removal. Notwithstanding, if the inlet stream liquid content is too high, the heat removal will make reaction temperature to fall down to a state where the kinetics is unfavoured even if the hexane concentration is promoting ethylene concentration in polymer phase. Naturally, it can exist higher cooling capacities following higher hexanes pressures; but the catalyst activity will have to be greater. In short, if one wants to take advantage of the co-solubility effect of hexane, heat removal should be properly designed.

PATENTS-SIMULATIONS COMPARISON

Table 7 and table 8 show condensed-mode FB operation results from some **patents** and the results from **simulation 3** of this work. They both have 2 cases, each one with different ICA pressure in order to realise the degree it affects production and temperature. First immediate consideration is that patents and simulations results are different because their conditions (and the ICA as well) are different too. For example, in patents the working total pressures are more than double the simulations. And ICA pressure is 3 times bigger in patents. On the other hand, ethylene pressure is quite similar. All these starting differences will lead to bigger productions in patents cases. Although it might be difficult to precisely compare these two sources of outputs, it's intended to bring out some trends and make some extrapolations. In all cases, there's no changing in catalyst flowrate or catalyst itself either (at least patent does not indicate it).

Case	Patent US 5.436.304 (1995)			SIMULATION 3		
	1	2	% $\Delta_{rel.}$	1	2	% $\Delta_{rel.}$
P (bar)	21.7	21.6	-	9.0	8.9	-
P _{et.} (bar)	7.40	9.50	28.4	7	7	-
P _{N2} (bar)	2.04	3.22	57.8	1	1	-
ICA	Isopentane	Isopentane	-	n-hexane	n-hexane	-
P _{ICA.} (bar)	3.06	2.07	-32.4	1.0	0.9	-10.0
T (°C)	81.1	84.3	3.95	94.3	71.3	-6.19
R _p (kg.m ⁻³ .h ⁻¹)	Z	1.28xZ	27.6	1.09xY	Y	-9.0
T ₀ (°C)	57.2	45.7	-20.1	50.0	40.0	-20.0
Gas DewP. (°C)	72.3	64.7	-10.5	63.1	59.7	-5.39
Liq. in gas (wt.)	21.8	24.4	-	15.0	20.9	-
Q _c (g/s)	W	W	-	0.200	0.200	-
K _p C ₀ [*] ($\bar{}$)	L	L	-	M	M	-
u _g (m/s)	0.53	0.53	-	0.54	0.54	-
ρ_g (kg/m ³)	27.1	29.0	-	11.0	10.7	-
ρ (kg/m ³)	251.5	305.7	13.0	411.5	412.4	-
d _p (μ m)	660	733	11.1	500	500	-
h _b (m)	13.5	13.9	-	10.7	10.7	-

Table 7 – comparison between simulation 3 results and an industrial patent. Patent partial pressures are calculated using ideal gas law given the molar fractions in its examples. Z, Y, W, L and M mean a certain numerical value.

Table 7 has a patent of a condensed-mode process for polymerizing monomers in FB's in a presence of a Ziegler-Nata catalyst. It's used isopentane as ICA and the level of condensed liquid in inlet flow is bigger than 20% weight. They reported that excessive amounts of isopentane leads to changes in the FB and ultimately to its rupture necessitating reactor shut-down. As the concentration of isopentane increases, the FB bulk density decreases making necessarily the bed height to increase. They also address the importance of superficial gas velocity in space-time yield. For example, when they changed superficial gas velocity from 0.52m/s to 0.72m/s (even decreasing a bit the level of condensing liquid) they estimated space-time yield would be about 20% relatively higher.

Specifically for patent cases shown in table 7, from case 1 to case 2, the superficial gas velocity is kept the same, there's an increase of ethylene pressure about 28% and a decreasing of about 30% in isopentane. Although the pressure of isopentane decreases, the amount of condensed liquid increases due to inlet temperature lowering. As a result, there's a space-time yield (R_p) relative increase of 28%. This case corroborates the decisive cooling capacity aspect provided by the inlet stream temperature.

Regarding simulation 3 scenario, from case 1 to case 2, the superficial gas velocity is kept the same (like in patent but 0.01m/s higher), the ethylene pressure is also kept the same and the hexane pressure is relatively decreased in 10%. In line with patent, there's increasing in level of condensed liquid as a result of inlet stream temperature reducing. The inlet temperature difference between case 1 and 2 is about 12°C in patent and 10°C in Simulation. The bulk density also increases with increasing hexane pressure yet very softly. The resulting polymerization rate (R_p) relative variation from case 1 to case 2 is about -9.0%. Here, unlike patent, there's a lowering in R_p at smaller hexane pressure. Despite the smaller liquid content (less stream cooling capacity), there's more hexane pressure and at higher reaction temperature. And so, in such conditions, catalyst activity and co-solubility effect are apparently enhancing polymerization more than cooling capacity is shrinking it. In patent, the ICA isopentane is not as soluble in polymer as n-hexane (see table 9). The production will rely more in cooling capacity and temperature. Overall, since the hexane pressure and ethylene as well are substantially higher in patent scenario, higher yields naturally are expected in comparison with simulations. Finally one points out that particle diameter, d_p , and bed height do no change in simulation cases once the considered simulation model does not take them into account and calculations are just made keeping them always constant.

There's another comparison for simulation and a literature patent in table 8. This patent highlights the capacity of operating in condensed-mode without causing the produced polymer to reach the stickiness limit. In general, it would be desirable to have a high proportion of ICA in the gas stream, to enhance the heat-removal from the reactor. Within the polymer particles, there is dissolved ICA, comonomers, other hydrocarbons, and even monomers, with quantities depending on the types of those species and the gas composition. Usually the amount of ICA is one of the most important factors that affect the overall quantity of the dissolved species in the polymer. At certain levels of ICA, an excess amount of the ICA is dissolved into the polymer produced, making the polymer sticky. Each ICA has a different solubility in each specific polymer product, and in general, it is desirable to utilize an ICA having relatively low solubility in the produced polymer, so that more of the ICA can be utilized in the gaseous stream before reaching the stickiness limit.

Case	Patent US 2005/0137364 A1			SIMULATION 3		
	1	2	% $\Delta_{rel.}$	1	2	% $\Delta_{rel.}$
P (bar)	24.1	24.1	-	8.8	9.0	-
P _{et.} (bar)	5.95	5.95	-	7	7	-
ICA	Isopentane	n-butane	-	n-hexane	n-hexane	-
P _{ICA.} (bar)	2.74	6.29	129.6	0.9	1.0	11.1
T (°C)	91.0	91.0	-	86.0	80.5	2.28
Prod. (ton.h ⁻¹)	Z	2.28xZ	128	Y	1.03xY	3.0
T ₀ (°C)	47.3	47.3	-	45.0	45.0	-
Gas DewP. (°C)	65.8	63.3	-3.80	59.7	63.1	5.70
Liq. in gas (wt.)	20.0	26.2	31.0	16.3	19.8	21.5
u _g (m/s)	0.73	0.73	-	0.54	0.54	-
d (m)	4.42	4.42	-	4.0	4.0	-

Table 8 – comparison between simulation 3 results and an industrial patent. Patent partial pressures are calculated using ideal gas law given the molar fractions in its examples. In patent case 1, the ICA is isopentane. In patent case 2, the ICA is n-butane

Table 9 has some useful data to help to understand and discuss the information in table 8 concerning patent and simulation cases. Vaporization heat and heat capacity are pretty similar to every components presented in table. Their solubility in polyethylene, nevertheless, are a bit different between n-hexane and the other two. This solubility in polyethylene was taken from the patent under analysis in table 8.

P(bar)	1	T _{boil.} (°C)	Vaporization heat (kJ/kg)	Heat capacity (kJ/kg.°C)	Solubility in Polyethylene (kg ICA/kg Polymer)*
Isopentane		28.0	342	2.3	1.63
n-butane		-0.5	385	1.6	0.94
n-hexane		68.7	335	1.7	28.5

Table 9 – vaporization heat and heat capacity for the ICA's compared in patents (isopentane, n-butane and n-hexane). They are referred to the boiling point temperature at 1 bar pressure. (Shell, 2014); (Cameo, 2014); * (US Patente N° 2005/013764 A1)

Globally, in the examples of the patent expressed in table 8, inventors use different ICA's and compare what's the difference in relative production rate for each one. The two ethylene polymerization patent cases occurred in a presence of a Ziegler-Nata catalyst, at 47.3°C inlet temperature, 0.73m/s gas superficial velocity, 5.95bar ethylene pressure in a 24.1bar total pressure and the reactor temperature T is 91°C. From case 1 to case 2, there's a very large relative variation of ICA pressure about 130% and the dew-point temperature of recycle flow relatively varies about -4%. The result in production rate output is a positive increase of 128%. The fact there's less nitrogen (incondensable) and, especially, because n-butane has a lower boiling point than isopentane, it will rise condensable liquid portion from case 1 to case 2. The n-butane pressure (case 2) is significantly higher that isopentane (case 1) because n-butane

has a lower solubility in polymer (table 9). And more ICA pressure allows more polymerization heat removal and, consequently, productivity goes up. Whether it's isopentane or n-butane, they are much less soluble in polyethylene than n-hexane. If identical concentration of all them are necessary to help solubilizing more ethylene in polymer phase, n-hexane takes advantage given its superior solubility. So n-butane and isopentane may not have a so high co-solubility potential effect as n-hexane and their contribution to higher productivities will lie in cooling capacity. In addition, like patent mentions, in general it is desirable to utilize a less soluble ICA in the growing polymer (for operational reasons). And here, isopentane and n-butane are also in advantage towards n-hexane. It's safer to use isopentane or n-butane in order to avoid particle stick phenomena.

Regarding simulation 3 results, from case 1 to case 2, there's a relative variation of 11% in hexane pressure and about 6% in dew point temperature. The gas recycle liquid content changes from 16.3 to 19.8%. Given these inputs, the productivity varies positively 3.0% from case 1 to case 2. If hexane pressure increased, for example, from 0.9bar 1.8bar, the relative variation of productivity would be about 55%. Once the ICA patent needs to vary 2.74bar to 5.29bar to achieve 128% relative variation in productivity and the liquid content variation of patent is bigger and gas superficial velocity as well, n-hexane appears to have a more pronounced effect in productivity. It has a higher boiling point temperature which may increase more easily the liquid content in recycle stream at moderate pressures. As already mentioned, its larger solubility may potentiate the co-solubility effect more than the other ICA's. And since it requires less pressure and less inlet stream temperature, it may be regarded as more advantageous in economic terms. Again, larger solubility might mean higher tendency to polymer stick phenomena and more degasing polymer process downstream. In a word, operating condensed-mode gas-phase ethylene polymerization with n-hexane may be more productive but it will need more rigorous reactor design and bed instability control as well.

3.3.2. Sensitive analysis

The steady-state model simulated in this work naturally involves some physical quantities. And some of them may not be properly estimated for the work temperature and/or pressures. The sensitive analysis will provide the information on equation balances terms that may have bigger deviations. Those ones should deserve more attention in the future for having better predictions and consequently allowing accurate reactor simulations. In a simulation like this, where the model is relatively simple, the sensitive analysis can be a crucial test to make it valid and appropriate to study the phenomena. It's going to be tested:

- Vaporization enthalpies
- Heat capacities
- Phase equilibrium fractions
- Polymerization heat
- Ethylene concentration in polymer phase

It was considered from the beginning that the liquid phase in recycling inlet gas stream was composed not only by n-hexane but also ethylene. This assumption was set due to Redlich Kwong-Soave EOS prediction for the reactor pressures and inlet gas temperatures. It follows immediately a big concern: is the equation of state predicting reasonable equilibrium fractions for both components? Is ethylene actually also in liquid phase?

The vaporization enthalpy for this mixture was calculated as the pure components weighted average vaporization enthalpy. And in turn, each of these enthalpies used correlations for pressures different from the ones used in this study. For example, the n-hexane vaporization enthalpy is based in a correlation for 1 bar total pressure. Nevertheless it's known that pressure has no significant importance in vaporization enthalpies. Particularly if the pressures are not much different from each other. The bigger unknown in this topic is definitely the phase equilibria prediction and if the mixture vaporization enthalpy is well approximated by the pure components weighted average vaporization enthalpy. Since this a critical aspect in cooling down the reactor it surely deserves a careful attention.

Concerning heat capacities they were predicted by SL EOS at reactor pressures and 80°C. Since the simulation results have different temperature solutions, the heat capacities will change too. And especially for gas heat capacity. Once gas mass rate is very big, even small changes in this heat capacity are expected to cause substantial changings in operation polyethylene mass rate and reactor temperature outputs.

The polymerization heat is, for the obvious reason, a parameter very important. Its value is naturally widely described in literature and so it's expected to be in good agreement with the reality. However it may vary when the operating conditions are considerably different from the ones of its measurements/simulations. So it will be also perturbed in this sensitive analysis and its impact in reactor outputs will be checked.

The concentration of ethylene is another crucial parameter in the model. And it is coupled with hexane concentration. So if one deviates the other will be too. Anyway SL EOS indicates a reasonable agreement with experimental evidence like we've seen in Arash work. It's, nonetheless, important to verify the numerical importance of ethylene concentration in productivity and reactor temperature.

Table 10 contains the model parameters intended to be tested by varying its original simulation numerical value in a certain amount (percent). For a certain percent deviation, it's then indicated the polyethylene mass rate absolute variation, Δm_{Pet} , the polyethylene mass rate relative variation, Δm_{Pet} (%), the reactor temperature absolute variation, ΔT , and reactor temperature relative variation, ΔT (%). The parameters perturbed are those at 0.6bar hexane and 0.9bar hexane conditions, both related to simulation 1 results. The two different hexane pressure conditions will capture the sensitiveness of parameters at 2 different hexane pressures.

P_{hex.} (bar)	0.6	Conditions of simulation 1				
Testing Parameter	Parameter deviation (%)	New simulation results relative deviation				
		Δm_{Pet} (ton/h)	Δm_{Pet} (%)	ΔT (°C)	ΔT (%)	
$\Delta H_{v,\text{et}}$ (kJ/mol)	200	-0.039	-0.67	-1.50	-1.76	
$\Delta H_{v,\text{hex}}$ (kJ/mol)	20	-0.050	-0.80	-3.00	-3.50	
x_{hex,T^0}	15	0.014	0.20	0.75	0.90	
y_{hex,T^0}	15	0.055	0.90	5.00	5.90	
$C_{p,g}$ (kJ.kg ⁻¹ .K ⁻¹)	20	-0.137	-2.30	-8.25	-9.70	
$C_{p,p}$ (kJ.kg ⁻¹ .K ⁻¹)	100	-0.027	-0.50	-1.50	-1.80	
ΔH_r (kJ/kg)	10	0.074	1.20	6.50	7.60	
$C_{\text{et},P}$ (mol/m ³ _p)	5	0.339	5.73	3.25	3.82	
P_{hex.} (bar)	0.9	Conditions of simulation 1				
$\Delta H_{v,\text{et}}$ (kJ/mol)	200	-0.117	-1.67	-3.75	-5.32	
$\Delta H_{v,\text{hex}}$ (kJ/mol)	20	-0.288	-4.13	-8.50	-12.06	
x_{hex,T^0}	15	0.041	0.59	1.50	2.13	
y_{hex,T^0}	15	0.136	1.94	4.75	6.74	
$C_{p,g}$ (kJ.kg ⁻¹ .K ⁻¹)	20	-0.202	-2.89	-6.25	-8.87	
$C_{p,p}$ (kJ.kg ⁻¹ .K ⁻¹)	100	-0.050	-0.71	-1.75	-2.48	
ΔH_r (kJ/kg)	10	0.202	2.90	8.00	11.35	
$C_{\text{et},P}$ (mol/m ³ _p)	5	0.460	6.60	4.00	5.67	

Table 10 – Sensitive analysis output for simulation 1

Table 10 shows that sensitive analysis for ethylene vaporization heat, $\Delta H_{v,\text{et}}$ and heat capacity of polymer phase, $C_{p,p}$, do not have a relevant influence in model output. They were considerably perturbed in 200 and 100% respectively varying only -0.67% and -0.50% in production for 0.6bar hexane condition. In opposite direction, solely 5% ethylene concentration in polymer phase, $C_{\text{et},P}$, perturbation leads to relative variation of 5.73% in production and 3.82% in reactor temperature. Reaction enthalpy, ΔH_r , hexane equilibrium gas fraction in inlet stream, y_{hex,T^0} and hexane vaporization heat, $\Delta H_{v,\text{hex}}$, make reasonable changes in temperature. When they are, for the following order, perturbed in 10, 15 and 20%

they alter the reactor temperature in 6.50, 5.00 and -3.0°C. With the largest difference in temperature from the original values comes gas heat capacity, $C_{p,g}$. deviation. When it varies 20%, the reactor temperature changes about -9.7°C. This may be explained with the fact the gas flowrate crossing the reactor is very big. There's in consequence a big amount of sensitive heat and heat capacity becomes a sensitive parameter in the context of this analysis.

Hexane liquid equilibrium fraction in inlet stream, x_{hex}^{T0} , is not causing great impact because it is a big percent. The mass balance to gas in reactor (see appendix A.2) may elucidate it:

$$\begin{cases} L = F - G \\ G = \frac{z - x}{y - x} F \end{cases} \quad (36)$$

Or equivalently:

$$L = F \left[1 - \left(\frac{z - x}{y - x} \right) \right] \quad (37)$$

So, for the original conditions of simulation 1 at 0.6 bar hexane, with x_{hex}^{T0} equals 85.6%, the liquid flow in inlet gas stream is $L = 7.16\text{kg/s}$. If x_{hex}^{T0} equals 98.5%, $L = 6.86\text{kg/s}$. The difference is not significant to make the vaporization heat bigger/smaller and reactor temperature (and production) as well. On the other hand, the hexane gas equilibrium fraction, y_{hex}^{T0} , may affect greatly the temperature and production. Again, using eq. 32 and for the conditions of simulation 1 with $y_{\text{hex}}^{T0} = 4.86\%$ original value, $L = 7.16$; varying 15% to $y_{\text{hex}}^{T0} = 5.59\%$, $L = 4.73$. It's a more noticeable difference which impacts more in the vaporization heat and, in turn, in reactor temperature.

In what concerns $C_{\text{et},p}$, the mere 5% deviation would mean changing from 97.41 mol/m^3_p to 102.3 mol/m^3_p . It's just a small difference but it has a big impact in polyethylene production and in temperature as seen before. This emphasizes the importance of using good predictions for this quantity.

3.4. Conclusions & Perspectives

A gas-phase ethylene polymerization reactor working in condensed mode was simulated using a simple pseudo-homogeneous CSTR model. The main purpose was to analyse the impact of n-hexane (ICA) in productivity and reactor temperature. The model included a simple approach composed by a single-site kinetics where the first-order ethylene concentration was predicted by Sanchez-Lacombe EOS. The particular aspect here was using an ethylene solubility Sanchez-Lacombe prediction for the ternary system – ethylene, n-hexane and polyethylene. This way the simulations for polymer production and reactor temperature were taking into account the co-solubility effect of n-hexane.

A global evaluation of simulations indicates an increasing of about **2%** of production as the n-hexane pressure increases **0.1bar** while there's no too much cooling capacity able to ease kinetics. With respect to temperature, there's a significant decreasing of about **8%** when the reactor is operating in condensed-mode in contrast with only **1.5%** when it is operating in a dry regime. The n-hexane fast evaporation removes significant latent heat; and as hexane pressure rises, more liquid hexane is available and the inlet stream cooling capacity is enlarged. At some point of inlet liquid content – associated with higher hexane pressures – the heat removal makes the reaction temperature to fall down too much and kinetics is diminished. The several inputs (catalyst flowrates, inlet temperature streams, reactor sizes, bulk densities) and outputs (reactor temperature, conversion, particle residence time, gas superficial velocity) were always comprised within the industrial operation range.

The simulations tested different **kinetic constants (k_p)**, different **catalyst flowrates** and different **inlet gas temperatures**. The changing of kinetic constants led to a relative variation between them of **15%** for production and **10%** for temperature. Changing the catalyst flowrate meant a relative variation of **9%** for production and **7%** for temperature. On the other way, when the inlet temperature is changed, the polymer production is differently trended: for the lowest inlet stream temperature, production grows less and decreases faster. The other two inlet temperatures tested seem to be more production maximized given the operation conditions. The simulation 3 was also crossed with 2 industrial patents. Using n-hexane as ICA might be more advantageous in comparison with isopentane and n-butane since it's more soluble in polymer (amorphous) phase – enhancing co-solubility effect and it has higher boiling point – likely to favour inlet stream liquid content. However, it's necessary to be particularly careful with sticking phenomena when n-hexane is utilized.

From the sensitive analysis, the main parameters causing bigger deviations are hexane vaporization heat - influencing productivity and temperature, gas heat capacity – influencing productivity and temperature, vapour composition of inlet flow gas – influencing temperature, as well as polymerization heat influencing a lot temperature. The concentration of ethylene in polymer phase have a pronounced impact on production and temperature.

It would be interesting to simulate the model with other alkanes with different heat capacities and co-solubility effects than from those of n-hexane, namely isopentane and n-butane. In addition, for similar co-solubility and heat removal behaviour, economic and n-alkane easier degasing operation from

polymer particles may also be a factor for ICA's choosing. As it was referred, n-hexane has a very high solubility in polyethylene compared with other similar n-alkanes. This will promote the co-solubility effect (positive) but it also intensifies the degasing operation of polymer particles (negative).

The reactor simulations in this thesis are based on a very simple reactor model. Continuing the current work will mean adopting more realistic reactor models working in a dynamic way where they can combine not only later polymerization times but also initial ones (with related kinetics). Catalyst size distribution as well as catalyst residence time should incorporate such models since industrial catalyst particles are not all uniform in their size and they remain different times in the reactor. This factors affect kinetics and productivity/temperature by extension. Howsoever the results obtained here were suitable for reproducing the effect of the ICA n-hexane in PE productivity and temperature and they may be also a comparison basis for other works in this field.

3.5. References

- Albizzati, E., & Galimberti, M. (1998). Catalysts for olefins polymerization. *Catalysis Today*, 41, 159-168.
- Alizadeh, A. (2014). *Study of sorption, heat and mass transfer during condensed-mode operation of gas phase ethylene polymerization on supported catalyst*. Kingston, Ontario.
- Alizadeh, A. (2014, Figure 2.3). *Study of sorption, heat and mass transfer during condensed-mode operation of gas phase ethylene polymerization on supported catalyst*. Kingston, Ontario.
- Alizadeh, A. (2014, Figure 4.3). *Study of sorption, heat and mass transfer during condensed-mode operation of gas phase ethylene polymerization on supported catalyst*. Kingston, Ontario.
- Alizadeh, A., & McKenna, T. F. (2013). Condensed Mode Cooling in Ethylene Polymerization: droplet evaporation. *Macromol. Symp.*, 333, 242-247.
- Alizadeh, M., Mostoufi, N., Pourmahdian, S., & Sotudeh-Gharebagh, R. (2004). Modeling of fluidized bed reactor of ethylene polymerization. *Chemical Engineering Journal*, 97, 27-35.
- Banat et al. (2014). *US Patent No. 8.669.334 B2*.
- Bashir, A. M., Ali, M. A.-h., Kanellopoulos, V., & Seppälä, J. (2013). Modelling of multicomponent olefins solubility in polyolefins using Sanchez–Lacombe equation of state. *Fluid Phase Equilibria*, 358, 83-90.
- Cai et al. (2005). *US Patent No. 2005/013764 A1*.
- Cameo, C. (2014, October). Retrieved from <http://cameochemicals.noaa.gov/chris/HXA.pdf>
- Chapman, W., Gubbins, K., Jackson, G., & Radosz, M. (1989). SAFT: Equation-of-State Solution Model for Associating Fluids. *Fluid phase equilibria journal*, 52, 31-38.
- Chemistry Department at the University of York. (2014, November 10). *Greener industry*. Retrieved from [http://www.greener-industry.org.uk/pages/poly\(ethene\)/8_polyethene_PM_HDPE.htm](http://www.greener-industry.org.uk/pages/poly(ethene)/8_polyethene_PM_HDPE.htm)
- Chinh et al. (1977). *UK Patent No. 5.668.228*.
- Chiovetta, M. G., & Estenoz, D. A. (2004). Behavior of Active Sites in a Changing, Supported Metallocene Catalyst Particle: Modeling Monomer Transport and Kinetics. *Macromolecular Materials and Engineering*, 289, 1012-1026.
- Choi, K., & Ray, W. (1985). The dynamic behaviour of fluidized bed reactors for solid catalyzed gas phase olefin polymerization. *Chemical Engineering Science*, 40, 2261-2279.
- Chung, J. S., Tairova, G., Zhang, Y., Hsu, J. C., McAuley, K. B., & Bacon, D. W. (2002). Polymer-Supported Metallocene Catalysts for Gas-Phase Ethylene Polymerization. *Korean Journal of Chemical Engineering*, 19, 597-600.
- Dow, c. c. (2009). Retrieved from http://msdssearch.dow.com/PublishedLiteratureDOWCOM/dh_0376/0901b80380376be5.pdf?filepath=/254-21151.pdf&fromPage=GetDoc

- Farag, H., Ossman, M., & Farid, Y. (2013). Modeling of fluidized bed reactor for ethylene polymerization: effect of parameters on the single-pass ethylene conversion. *International Journal of Industrial Chemistry*, 4-20.
- Fernandes, F. A., & Lona, L. M. (2001). Heterogeneous modelling for fluidized bed polymerization reactor. *Chemical Engineering Science*, 56, 963-969.
- Floyd, S., Choi, K., Taylor, T., & Ray, W. (1986). Polymerization of olefins through heterogeneous catalysts. Polymer particle modelling with an analysis of intraparticle heat and mass transfer effects. *Journal of Applied Polymer Science*, 32, 2935-2960.
- Fontes, C., & Mendes, M. J. (2001). Modelling and simulation of an industrial slurry reactor for ethylene polymerization. *Latin American Applied Research*, 31, 345-332.
- Frederic, M. P., Agnes, V. F., & McBrewster, J. (2010). *Flory-Huggins Solution Theory*. VDM Publishing.
- Greene, J. P. (2014). Sustainable Plastics: Environmental Assessments of Biobased, Biodegradable and recycled plastics. Wiley. Retrieved from <http://wpage.unina.it/avitabil/testi/PE.pdf>
- Griffin et al. (1995). *US Patent No. 5.462.999*.
- Griffin, J. R., & DeChellis, M. L. (1995). *US Patent No. 5.436.304*.
- Gross, J., & Sadowski, G. (2001). Perturbed-Chain SAFT: An Equation of State Based on a Perturbation Theory for Chain Molecules. *Ind. Eng. Chem. Res.*, 40, 1244-1260.
- Grosso, W. E., & Chiovetta, M. G. (2005). Modelling a fluidized-bed reactor for the catalytic polymerization of ethylene: particle size distribution effects. *Latin American Applied Research*, 35, 67-76.
- Harrison et al. (1998). Olefin polymerization using supported metallocene catalysts: development of high activity catalysts for use in slurry and gas phase ethylene polymerizations. *Journal of Molecular Catalysis*, 128, 65-77.
- Haslam, A. J., Solms, N. V., Adjiman, C. S., Galindo, A., Jackson, G., Paricaud, P., . . . Kontogeorgis, G. M. (2006). Predicting enhanced absorption of light gases in polyethylene using simplified PC-SAFT and SAFT-VR. *Elsevier*, 243, 74-91.
- Hatzantonis, H., Yiannoulakis, H., & Yiagopoulos, A. (2000). Recent developments in modeling gas-phase catalyzed olefin. *Chemical Engineering Science*, 55, 3237-3259.
- Ibrehem, A. S., Hussain, M. A., & Ghasem, N. M. (2009). Modified mathematical model for gas phase olefin polymerization in fluidized-bed catalytic reactor. *Chemical Engineering Journal*, 149, 353-362.
- J. Smulaka, R. S. (2001). New equation of state for ethylene covering the fluid region for temperatures from the melting line to 450K at pressures up to 300Mpa. *AIP publishing*, 1057-1097.
- Jafari, R., Sotudeh-Gharebagh, R., & Mostoufi, N. (2004). Modular simulation of fluidized bed reactors. *Chemical Engineering and Technology*, 27, 123-129.
- Jenkins et al. (1985). *US Patent No. 4.543.399*.
- Jenkins, J., Jones, R., & Jones, T. (1986). *US Patent No. 4,588,790*.

- Jiang, Y., McAuley, K. B., & Hsu, C. C. (1997). Heat Removal from Gas-Phase Polyethylene Reactors in the Supercondensed Mode. *Ind. Eng. Chem. Res.*, *36*, 1176-1180.
- Kanellopoulos, V., Dompazis, G., Gustafsson, B., & Kiparissides, C. (2004). A comprehensive analysis of single particle growth in heterogeneous olefin polymerization: the random pore polymeric flow model. *Workshop of CPERI*. Thessaloniki, Greece.
- Kiashemshaki, A., Mostoufi, N., & Sotudeh-Gharebagh, R. (2006). Two-phase modelling of a gas phase polyethylene fluidized bed reactor. *Chemical Engineering Science*, *61*, 3997-4006.
- Kim, J. Y., & Choi, K. Y. (2001). Modeling of particle segregation phenomena in a gas phase fluidized bed olefin polymerization reactor. *Chemical Engineering Science*, *56*, 4069-4083.
- Kosek, J., Grof, Z., Novák, A., Stepánek, F., & Marek, M. (2001). Dynamics of particle growth and overheating in gas-phase polymerization reactors. *Chemical Engineering Science*, *56*, 3951-3977.
- Kunni, D., & Levenspiel, O. (1991). *Fluidization engineering*. London: Butterworth Heinemann.
- Lloyd, L. (2011). *Handbook of Industrial Catalysts*. Springer.
- Lynch, D. T., & Wanke, S. E. (1991). Reactor design and operation for gas-phase ethylene polymerization using Ziegler-Natta catalysts. *Canadian Journal of Chemical Engineering*, *69*, 332-339.
- Lyondel Chemical, C. (2014). *Introduction to polyethylene*. Houston, Texas.
- McAuley, K. B., Talbot, J. P., & Harris, T. J. (1994). A comparison of two-phase and well-mixed models for fluidized bed polyethylene reactors. *Chemical Engineering Science*, *49*, 2035-2045.
- McKenna, T. F., & Soares, J. B. (2001). Single particle modelling for olefin polymerization on supported catalysts: a review and proposals for future developments. *Chemical Engineering Science*, *56*, pp. 3931-3949.
- MENG, W., LI, J., CHEN, B., & LI, H. (2013). Modeling and Simulation of Ethylene Polymerization in Industrial. *Chinese Journal of Chemical Engineering*, *21*, 850-859.
- Mirzaei, A., Kiashemshaki, A., & Emani, M. (2007). Fluidized Bed Polyethylene Reactor Modeling in Condensed Mode Operation. *Macromol. Symp.*, *259*, 135-144.
- Nath, S. K., Banaszak, B. J., & de Pablo, J. J. (2001). Simulation of Ternary Mixtures of Ethylene, 1-Hexene, and Polyethylene. *Macromolecules*, *34*, 7841-7848.
- NIST, N. I. (2014, September 8). *NIST, National Institute of standards and technology*. Retrieved from <http://webbook.nist.gov/cgi/cbook.cgi?ID=C110543&Mask=4>
- NOVA Chemicals. (2014, Outubro 30). *Nova Chemicals*. Retrieved from Nova Chemicals: <http://www.novachem.com/Pages/markets-and-applications/markets-and-applications.aspx>
- Nowlin, T. E. (2014). *Business and technology of the global polyethylene industry*. Massachusetts: Scrivener publishing.
- Ramanathan, A. S. (1998). Design Issues in Converting to Super-Condensed Mode Operation for Polyethylene. *AIChE Spring 98 Meeting*, (pp. 1-6). New Orleans.

- Rappaport, H. (2011, May). *SPI Film & bag*. Retrieved from <http://spi.files.cms-plus.com/about/fbf/H%20Rappaport%20SPI%20Film%20%26%20Bag%2005%2011.pdf>
- Ray, W., & Hutchinson, R. (1990). Polymerization of olefins through heterogeneous catalysis. VIII. Monomer sorption effects. *Journal of Applied Polymer Science*, *41*, 51-81.
- Sabic, E. (2005). A to Z of Polyethylene.
- Sanchez, I. C., & Lacombe, R. H. (1978). Statistical thermodynamics of Polymer solutions. *Macromolecules*, *11*, 1145-1156.
- Shamiri, A., Chakrabarti, M. H., Jahan, S., Hussain, M. A., Kaminsky, W., Aravind, P. V., & Yehye, W. A. (2014). The Influence of Ziegler-Natta and Metallocene Catalysts on Polyolefin Structure, Properties, and Processing Ability. *Materials*, *7*, 5069-5108.
- Shell, C. (2014, 10). Retrieved from <http://www.shell.com/content/dam/shell/static/chemicals/downloads/products-services/datasheet-paraffinsisopentaneurope.pdf>
- Suba, P., Árva, P., & Németh, S. (2007). The effect of a Ziegler-Natta catalyst and the polymerization parameters on the basic properties of polyethylene. *Hungarian journal of industrial chemistry*, *35*, 31-37.
- Trischler, H., Ruff, M., & Paulik, C. (2012). Influence of Co-Catalyst Concentration on the Formation of Active Centers and the Polymerization Rate in Catalytic Ziegler Natta Ethene Slurry Polymerization. *Journal of Materials Science and Engineering*, *A2*, 511-518.
- Wagner, B., Goeke, G., & Karol, F. (1981). *US Patent No. 4.303.771*.
- Weckhuysen, B. M., & Schoonheydt, R. A. (1999). Olefin polymerization over supported chromium oxide catalysts. *Catalysis Today*, *51*, 215-221.
- Wu, L., Zhou, J.-M., Lynch, D. T., & Wanke, S. E. (2005). Polymer-supported metallocene catalysts for gas-phase ethylene/1-hexene polymerization. *Applied Catalysis*, *293*, 180-191.
- Wu, S. Y., & Baeyens, J. (1998). Segregation by size difference in gas fluidized beds. *Powder Technology*, *98*, 139-150.
- Xie, T., McAuley, K. B., Hsu, J. C., & Bacon, D. W. (1994). Gas phase ethylene polymerization: Production processes, polymer properties and reactor modelling. *Ind. Eng. Chem. Res*, *33*, 449-479.
- Yang, Y. R., Yang, J. Q., Chen, W., & Rong, S. X. (2002). Instability Analysis of the Fluidized Bed for Ethylene Polymerization with Condensed Mode Operation. *Ind. Eng. Chem. Res.*, *41*, 2579-2584.
- Yao, W., Hu, X., & Yang, Y. (2007). Modeling solubility of gases in semicrystalline polyethylene. *Journal of applied polymer science.*, *103*, 1737-1744.
- Yao, W., Hu, X., & Yang, Y. (2007). Modeling the solubility of ternary mixtures of ethylene iso-pentane nhexane in semicrystalline polyethylene. *Journal of applied polymer science*, *104*, 3654-3662.
- Yiannoulakis, H., Yiagopoulos, A., & Kiparissides, C. (2001). Recent developments in the particle size distribution modeling of fluidized-bed olefin polymerization reactors. *Chemical Engineering Science*, *56*, 917-925.

Zhou, Y.-f., Wang, J.-d., Yang, Y.-r., & Wu, W.-q. (2013). Modeling of the Temperature Profile in an Ethylene Polymerization Fluidized-Bed Reactor in Condensed-Mode Operation. *Ind. Eng. Chem. Res.*, 52, 4455-4464.

4. Appendix

A. Thermodynamics considerations

In appendix A will be exposed correlations, some results and other considerations regarding thermodynamics phenomena necessary in this thesis.

A.1. Thermodynamics parameters related to polymer particle (amorphous polymer phase)

Table A.1 incorporates original data for ethylene and hexane concentration in polymer phase at several hexane pressures. The original data is in bold. It was extracted from Alizadeh work (Alizadeh A., 2014). The data was fitted using a 3rd degree polynomial – $aP^3 + bP^2 + cP + d$ – using the software *Excel*, where a, b, c and d are the regression parameters. The coefficient of determination, R^2 , is also indicated in the table. The top of the table has the pressure of the other components in ternary system and the temperature ($T_{ref.}$) where original data was measured/calculated. The first column of the table has the hexane pressure variable, 2nd and 3rd are related to polymer phase ethylene concentration and 4th and 5th are respected to polymer phase hexane concentration.

P _{et.} (bar) 7		P _{N2} (bar) 1			T _{ref.} (°C) 80		
Regression Parameters	a _{et.} 6.4306	b _{et.} 1.6014	R ² 1	a _{hex.} 132.74	b _{hex.} -14.185	R ² 1	
	C _{et.} 18.641	d _{et.} 84.26		C _{hex.} 409.51	d _{hex.} -10 ⁻¹¹		
P _{hex.} (bar)	C ^{P_{et.}} (mol/m ³ _p)	C ^{P_{et.} int.} (mol/m ³ _p)	C ^{P_{hex.}} (mol/m ³ _p)	C ^{P_{hex.} int.} (mol/m ³ _p)			
0.00	84.26	84.26	0.00	0.00			
0.10		86.15		40.94			
0.20		88.10		84.40			
0.30	90.17	90.17	125.16	125.16			
0.40		92.38		170.03			
0.50		94.78		217.80			
0.60	97.41	97.41	269.27	269.27			
0.70		100.30		325.24			
0.80	103.49	103.49	386.49	386.49			
0.90		107.02		453.84			
1.00		110.93		528.06			

Table A. 1 – ethylene concentration and hexane concentration in polymer phase at different hexane pressures, calculated by fitting 4 known values (in bold) for each quantity in analysis.

The resulting equation from ethylene concentration fitting is:

$$C_{et}^P \text{ (mol/m}^3\text{)} = 6.4306P_{hex.}^3 + 1.6014P_{hex.}^2 + 18.641P_{hex.} + 84.26, 0.00 < P_{hex.} \text{ (bar)} < 0.80. \quad (a)$$

And from hexane concentration fitting it translates in:

$$C_{hex}^P \text{ (mol/m}^3\text{)} = 132.74P_{hex.}^3 - 14.185P_{hex.}^2 + 409.51P_{hex.} - 10^{-11}, 0.00 < P_{hex.} \text{ (bar)} < 0.80. \quad (b)$$

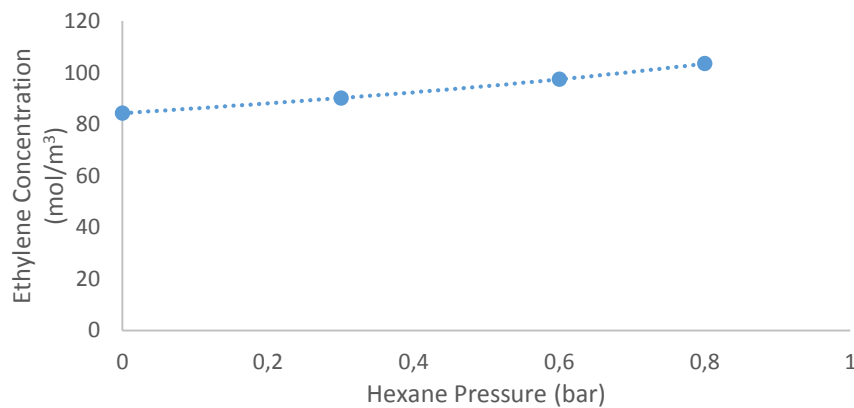


Figure A. 1 – ethylene concentration original values (markers) and respective polynomial fitting

In the body of the thesis, these equations were extrapolated for the values of 0.10, 0.90 and 1.00bar hexane pressure.

Table A.2 incorporates original data for polymer density, ρ_p , and heat capacity of gas phase, $c_{p,g}$, at different hexane pressures. The original data is in bold and it was extracted from Alizadeh work (Alizadeh A. , 2014). The data was fitted using a 2nd degree polynomial – $aP^2 + bP + c$ – using the software *Excel*. The coefficient of determination, R^2 , is also indicated in the table. The top of the table has the pressure of the other components in ternary system and the temperature ($T_{ref.}$) where the original data was measured/calculated. The first column of the table has the hexane pressure variable, 2nd and 3rd are related to polymer particle density and 4th and 5th are respected to gas heat capacity.

P _{et.} (bar) 7		P _{N2} (bar) 1		T _{ref.} (°C) 80				
Regression Parameters	a _p	-5.899	b _p	-13.575	a _g	-32.48	b _g	128.06
	c _p	920.38	R ²	0.9999	c _g	1553.4	R ²	1
P _{hex.} (bar)	ρ_p . (kg/m ³)	$\rho_p^{int.}$ (kg/m ³)	$C_{p,g}$ (J.kg ⁻¹ .K ⁻¹)		$C_{p,g}^{int.}$ (J.kg ⁻¹ .K ⁻¹)			
0.00	920.4	920.4	1553.4		1553.4			
0.10		919.0			1565.9			
0.20		917.4			1577.7			
0.30	915.7	915.8	1589.1		1588.9			
0.40		914.0			1599.4			
0.50		912.1			1609.3			
0.60	910.2	910.1	1618.4		1618.5			
0.70		908.0			1627.1			
0.80	905.7	905.8	1635.2		1635.1			
0.90		903.4			1642.3			
1.00		900.9			1649.0			

Table A. 2 – polymer density and gas heat capacity at different hexane pressures, calculated by fitting 4 known values (in bold).

The resulting equation from polymer particle density fitting is:

$$\rho_p \text{ (kg/m}^3\text{)} = - 5.889P_{\text{hex.}}^2 - 13.575P_{\text{hex.}} + 920.38, 0.00 < P_{\text{hex.}} \text{ (bar)} < 0.80. \quad \text{(c)}$$

And from gas heat capacity fitting it gets:

$$c_{p,g} \text{ (J.kg}^{-1}\text{.K}^{-1}\text{)} = - 32.48P_{\text{hex.}}^2 + 128.06P_{\text{hex.}} + 1553.4, 0.00 < P_{\text{hex.}} \text{ (bar)} < 0.80. \quad \text{(d)}$$

In the body of the thesis, these equations were extrapolated for the values of 0.10, 0.90 and 1.00bar hexane pressure.

A.2. Inlet flow thermodynamic condition

The gas-phase system in this work consists of 3 components – **Ethylene**, **n-hexane** and **nitrogen**. Ethylene and nitrogen are always at the same pressure – **7** and **1 bar** respectively. To avoid a **ternary system** (actually I had no big choice once the data/simulation concerning it is scarce or even absent. Even in simulators like *Aspen*) I chose to join the ethylene and nitrogen in **one just pseudo-component**. Since ethylene pressure is considerably bigger than the nitrogen one and **total pressure** is not that high so that it can cause important deviations from the **ideal mixture of gases**, I assumed this approach. This way I took the thermodynamic system in a binary mode and took all the advantages on it, namely considerable data/simulation available.

So to obtain the equilibrium data I used the Aspen® binary systems simulator with the thermodynamic model **Redlich-Kwong-Soave**. This Equation of state is suitable for mixture of gases in moderate total pressures like the one of this simulation. I set the **total pressure to 8 bar** (7 + 1) + **hexane pressure** and simulated a composition vs. temperature phase diagram.

The output results come in table A.3.

Inlet Gas Thermodynamic Condition			
$P_{\text{hex.}}$ (bar)	$T_{\text{dew point}}$ (°C)	$y_{\text{hex. dew point}}$ (%)	$x_{\text{hex. dew point}}$ (%)
0.00	-	-	-
0.10	21.8	1.23	84.69
0.20	27.7	2.44	84.82
0.30	33.6	3.61	85.50
0.40	38.8	4.76	85.87
0.50	43.6	5.88	86.53
0.60	48.1	6.98	86.79
0.70	52.3	8.05	87.25
0.80	56.1	9.09	87.68
0.90	59.7	10.11	88.05
1.00	63.1	11.11	88.29

Table A. 3 – molar equilibrium fractions of hexane at dew point for ethylene + hexane + nitrogen system

For example, at **0.40bar** hexane pressure, the system ethylene + hexane + nitrogen starts to boil at **38.8°C** and equilibrium state is composed by a gas of **4.76%** molar of hexane and a liquid of **85.87%** molar of hexane. The ethylene and nitrogen are admitted to be always in the same proportion in the pseudo-component. In addition, it's considered nitrogen to be only in the gas phase. For example, at **0.40bar** hexane pressure, the gas consists of **95.24%** molar in pseudo-component (ethylene + nitrogen), which in turn has the molar composition associated to **7bar ethylene** and **1bar nitrogen**, considering **ideal gas**.

Given the dew-points for the (gas) compositions of interest, one wants to know the **liquid** and **gas** quantities at some inlet flow **temperature** below such dew points. Considering a flash vaporization, we can write a total balance and a component mass balance. This equation system is written as:

$$\begin{aligned} \text{Total Mass Bal. : } F &= L + G \\ \text{Hexane Mass Bal. : } zF &= xL + yG \end{aligned} \tag{e}$$

F is total molar rate, **L** and **G** are liquid and gas molar rate respectively. Applied to the reactor system in this thesis, the **total mass balance** is saying that the sum of liquid L and gas G in equilibrium at some temperature (below dew point) entering the reactor will be equal to the total molar flow exiting the reactor at its temperature. For the perspective of **hexane component balance**, the liquid and gas containing determined equilibrium fractions of hexane at some temperature (below dew point) going into the reactor will be equal to the total flow F containing a determined equilibrium fraction of hexane at reactor temperature. Rearranging (e) for **L** and **G** it gets:

$$\begin{cases} L = F - G \\ G = \frac{z - x}{y - x} F \end{cases} \tag{f}$$

It's intended there to be a determined gas composition of hexane in the reactor. So the equilibrium fraction **z**, corresponding to some hexane pressure, is set. Noticing this **z** is the hexane composition immediately before dew-point. But for practical purposes it is the value corresponding to the hexane pressure desired in gas-phase. (For further information on dew-point considerations, check some relevant literature.)

Then according to the thermodynamics condition of inlet flow, the Liquid and Gas amounts are calculated. The total mass flow, **F** is a sort of decision variable that can play a role in terms of removing heat. On the other way, bigger molar/mass flows imply bigger volumetric flows and less conversions. The liquid portion is expected to flashily vaporize as soon as it enters the reactor.

The amount of liquid and gas in inlet flow at working temperatures and total flows F, for each hexane pressure, are in table A.4. Table has 2 half. 1st half is directed for 3 different total molar flowrates, F. The 2nd has 2 inlet temperatures, T₀, under analysis.

Inlet Gas Thermodynamic Condition							
T ₀ (°C)	40.0	Molar Gas flow rate, F (mol/s)					
		2300		2500		2540	
P _{hex.} (bar)		m _{Liq.} (kg/s)	m _{Gas} (kg/s)	m _{Liq.} (kg/s)	m _{Gas} (kg/s)	m _{Liq.} (kg/s)	m _{Gas} (kg/s)
0.00		-	-	0	65.7	0	66.8
0.10		-	-	0	68.7	0	69.8
0.20		-	-	0	71.6	0	72.8
0.30		-	-	0	74.5	0	75.7
0.40		0	71.1	0	77.2	0	78.5
0.50		2.88	70.7	3.13	76.8	3.18	78.1
0.60		6.58	69.4	7.16	75.5	7.27	76.7
0.70		10.2	68.2	11.1	74.1	11.3	75.3
0.80		13.7	67.0	14.9	72.8	15.2	74.0
0.90		17.4	65.7	18.8	71.4	19.1	72.5
1.00		20.6	64.6	22.4	70.3	22.8	71.4
F(mol/s)	2300	Inlet temperature, T ₀ (°C)					
		45		50			
		m _{Liq.} (kg/s)	m _{Gas} (kg/s)	m _{Liq.} (kg/s)	m _{Gas} (kg/s)		
0.00		-	-	-	-	-	-
0.10		-	-	-	-	-	-
0.20		-	-	-	-	-	-
0.30		-	-	-	-	-	-
0.40		0	71.1	0	71.1	0	71.1
0.50		0	73.6	0	73.6	0	73.6
0.60		2.63	73.4	0	76.0	0	76.0
0.70		6.31	72.1	2.05	76.3	2.05	76.3
0.80		9.90	70.8	5.70	75.0	5.70	75.0
0.90		13.50	69.5	9.32	73.7	9.32	73.7
1.00		16.85	68.4	12.8	72.5	12.8	72.5

Table A. 4 – mass amount of gas and liquid in the inlet flowrate entering the reactor for the different working conditions

The liquid mass, $m_{liq.}$, (or mol) fraction in total flow is:

$$m_{liq} = \frac{LM_{Liq.}}{FM_{WF}} = \frac{FM_F - GM_{Gas}}{FM_F} = \frac{FM_F \left(1 - \frac{z-x}{y-x}\right)}{FM_F} = \left(1 - \frac{z-x}{y-x}\right) \quad (g)$$

This is, the liquid mass fraction, $m_{liq.}$ is just dependent on thermodynamic conditions (as expected). This liquid mass in inlet flow can be an important parameter in designing equipment. If the inflow is too much wet there might problems in terms of mass flowing into the “flowing” equipments (compressors, feed gas injector, etc) and even the fluidized media proper working conditions can be affected. This may lead to a constraint in terms of inlet flow temperature.

A.3. Ethylene vaporization enthalpy fitting

Table A.5 contains data of ethylene heat vaporization at 10bar total pressure for several temperatures. Data was extracted from works of Smulaka (J. Smulaka, 2001). The data was fitted using a 2nd degree polynomial using the software *Excel*, where a, b, c and d are the regression parameters. The coefficient of determination, R², is also indicated in the table. The heat vaporizations in bold are original data and the correlated ones are just alongside it.

P (bar) 10			
Regression Parameters	a	b	c
	-0.0202	-72.836	11172
T (°C)	$\Delta H_{v.et.}$ (J/mol)	$\Delta H_{v.et.}^{int.}$ (J/mol)	Rel. var., Δ_r
-168,15	22873	22848	0,110%
-163,15	22533	22518	0,067%
-158,15	22192	22186	0,027%
-153,15	21852	21853	0,007%
-148,15	21512	21519	0,036%
-143,15	21173	21185	0,056%
-138,15	20834	20849	0,069%
-133,15	20497	20512	0,075%
-128,15	20160	20174	0,071%
-123,15	19823	19835	0,063%
-118,15	19486	19496	0,048%
-113,15	19150	19155	0,026%
-108,15	18815	18813	0,013%
-103,15	18475	18470	0,024%
-98,15	18136	18126	0,052%
-93,15	17795	17781	0,076%
-88,15	17453	17436	0,098%
-83,15	17108	17089	0,111%
-78,15	16760	16741	0,114%
-73,15	16408	16392	0,101%
-68,15	16053	16042	0,067%
-63,15	15692	15691	0,004%
-58,15	15325	15339	0,093%
-53,15	14950	14986	0,239%

Table A. 5 – Original ethylene vaporization enthalpy values (in bold) and fitting results for several temperatures

Fitted equation is:

$$\Delta H_{v.et.} = - 0.0202T^2 - 72.836T + 11172 \quad (h)$$

With interpolation range temperatures: $-168.15 < T(^{\circ}\text{C}) < - 53.15$

In the body of this thesis, this equation was extrapolated for the inlet stream conditions (40-50°C) and pressures [7-8]bar.

B. Outputs concerning Simulation results

The next tables contain all the relevant output simulation that are the source for the graphical results shown in Results chapter in this thesis. The values in it come from the model equations assumed in this work. Table B.1 shows numeric output for simulation II and table B.2 for simulation III.

Simulation II Results						
C_0^* (mol-site/m ³ _c)	$k_p^{80^\circ\text{C}}$ (m ³ _{Pet} ·mol-site ⁻¹ ·s ⁻¹)	T_0 (°C)	Molar Gas inflow rate, F (mol/s)			
0.55	1200	40.0	1800			
Catalyst flow rate (g/s) 0.222						
$P_{\text{hex.}}$ (bar)	m_{Pet} (ton/h)	T (°C)	% Conv.	R_P (kg _{Pet} ·m _c ⁻³ ·h ⁻¹)	$u_{g,0}$ (m/s)	σ (h)
0.20	5.536	111.0	3.57	424973	0.48	9.87
0.30	5.669	109.5	3.70	434415	0.48	9.57
0.40	5.809	108.3	3.83	444611	0.48	9.26
0.50	5.907	100.8	3.95	452715	0.48	9.03
0.60	5.989	92.0	4.05	459562	0.48	8.83
0.70	6.087	84.3	4.16	465980	0.48	8.60
0.80	6.140	76.7	4.24	471004	0.48	8.44
0.90	6.177	69.5	4.31	473876	0.48	8.29
1.00	6.211	63.3	4.38	475756	0.48	8.73
Catalyst flow rate (g/s) 0.236						
0.20	5.901	115.5	3.80	452437	0.48	9.26
0.30	6.030	113.8	3.93	462464	0.48	9.00
0.40	6.184	112.5	4.08	473368	0.48	8.70
0.50	6.297	105.0	4.21	482372	0.48	8.47
0.60	6.391	96.3	4.32	490320	0.48	8.27
0.70	6.502	88.5	4.44	498036	0.48	8.05
0.80	6.593	81.3	4.55	504989	0.48	7.86
0.90	6.669	74.3	4.66	510403	0.48	7.68
1.00	6.716	68.0	4.74	514807	0.48	7.53
Catalyst flow rate (g/s) 0.250						
0.20	6.268	120.0	4.04	479928	0.48	8.72
0.30	6.392	118.0	4.17	490548	0.48	8.47
0.40	6.540	116.5	4.32	502074	0.48	8.23
0.50	6.688	109.3	4.47	512073	0.48	7.98
0.60	6.795	100.5	4.59	521128	0.48	7.78
0.70	6.920	92.8	4.73	530147	0.48	7.57
0.80	7.023	85.5	4.85	538659	0.48	7.38
0.90	7.137	78.8	4.98	546413	0.48	7.18
1.00	7.223	72.8	5.10	553762	0.48	7.00

Table B. 1 – numerical results regarding the conditions of simulation II. The changing condition is catalyst flow rate

Simulation III Results						
C_0^* (mol-site/m ³ c)	$k_p^{80^\circ\text{C}}$ (m ³ Pet.mol-site ⁻¹ .s ⁻¹)		Catalyst flow rate (g/s)	Molar Gas inflow rate, F (mol/s)		
0.55	1500		0.200	2000		
T_0 (°C) 40						
$P_{\text{hex.}}$ (bar)	m_{Pet} (ton/h)	T (°C)	% Conv.	R_P (kg _{Pet} .m _C ⁻³ .h ⁻¹)	$u_{g,0}$ (m/s)	σ (h)
0.20	-	-	-	-	-	-
0.30	-	-	-	-	-	-
0.40	6.552	109.3	3.89	801828	0.54	8.21
0.50	6.666	101.8	4.01	511490	0.54	8.00
0.60	6.785	93.3	4.13	520264	0.54	7.79
0.70	6.899	85.5	4.24	528682	0.54	7.59
0.80	6.990	78.3	4.35	536312	0.54	7.41
0.90	7.064	71.3	4.44	542323	0.54	7.68
1.00	7.137	65.3	4.53	547906	0.54	7.09
T_0 (°C) 45						
0.20	-	-	-	-	-	-
0.30	-	-	-	-	-	-
0.40	6.566	114.3	3.90	503551	0.54	8.20
0.50	6.736	113.3	4.05	516308	0.54	7.92
0.60	6.885	107.0	4.19	528190	0.54	7.68
0.70	7.033	99.3	4.33	539804	0.54	7.45
0.80	7.214	92.5	4.49	552132	0.54	7.18
0.90	7.373	86.0	4.64	564676	0.54	6.95
1.00	7.548	80.5	4.80	578260	0.54	6.70
T_0 (°C) 50						
0.20	-	-	-	-	-	-
0.30	-	-	-	-	-	-
0.40	6.580	119.3	3.91	504979	0.54	8.18
0.50	6.750	118.3	4.06	517829	0.54	7.91
0.60	6.933	117.5	4.22	531955	0.54	7.63
0.70	7.114	112.3	4.38	546257	0.54	7.36
0.80	7.305	106.0	4.54	560687	0.54	7.09
0.90	7.518	99.8	4.73	576306	0.54	6.81
1.00	7.735	94.3	4.92	593325	0.54	6.54

Table B. 2 – numerical results regarding the conditions of simulation III. The changing condition is inlet temperature

These last tables have all in common hexane pressure as variable and the outputs, from left to the right, **polyethylene mass rate, reactor temperature, ethylene conversion, polymerization rate, superficial gas velocity** and **reaction media residence time**. In the top of the table there are the fixed parameters. The changing condition is 3 times displayed along the table. For example, in table B.2 (simulation III), the changing condition is inlet temperature, T_0 .

Table concerning **simulation I** is not displayed here because it's already in the body of the thesis.

Next tables – B.3, B.4 and B.5 – are again concerning Simulation Results. They exhibit the same template as the previous ones. These tables indicate, from left to the right, the following mass balance terms: **ethylene gas flowrate, hexane gas flowrate, dissolved ethylene in polymer particle, dissolved hexane in polymer particle and bulk density.**

The equations to calculate such quantities are remembered below:

$$\dot{m}_{et.} = \left(\dot{m}_{et.0} - \dot{m}_{Pet.} - C_{et.}^p(P) \frac{\dot{m}_{Pet.}}{\rho_p} M_{et.} \right) \quad (\text{i})$$

$$\dot{m}_{hex.} = \left(\dot{m}_{hex.0} - C_{hex.}^p(P) \frac{\dot{m}_{Pet.}}{\rho_p} M_{hex.} \right) \quad (\text{j})$$

$$\dot{m}_{et.d} = C_{et.}^p(P) \frac{\dot{m}_{Pet.}}{\rho_p} M_{et.} \quad (\text{k})$$

$$\dot{m}_{hex.d} = C_{hex.}^p(P) \frac{\dot{m}_{Pet.}}{\rho_p} M_{hex.} \quad (\text{l})$$

$$\rho = \rho_p + \varepsilon(\rho_g - \rho_p) \quad (\text{m})$$

In general, these tables all show same trends:

- decreasing of ethylene gas flowrate with increasing hexane pressure. When the hexane pressure increases, conversion increases making the ethylene gas flowing out the reactor to be less.
- increasing of hexane gas flowrate with increasing hexane pressure. Since there's more hexane gas entering the reactor and it does not react at all, the amount leaving the reactor will be greater.

Simulation I Results – Other operational calculations					
C_0^* (mol-site/m ³ c)	Catalyst flow rate (g/s)		T_0 (°C)	Molar Gas inflow rate, F (mol/s)	
0.55	0.222		40.0	2000	
$k_p^{80^\circ\text{C}}$ (m ³ Pet.mol-site ⁻¹ .s ⁻¹) 1200					
$P_{\text{hex.}}$ (bar)	$m_{\text{et.}}$ (kg/s)	$m_{\text{hex.}}$ (kg/s)	$m_{\text{et.d}}$ (kg/s)	$m_{\text{hex.d}}$ (kg/s)	ρ (kg/m ³)
0.00	56.3	0.00	1.25x10 ⁻³	0.00	419
0.10	55.3	1.08	2.37x10 ⁻³	0.18x10 ⁻²	419
0.10	54.3	4.12	3.64x10 ⁻³	1.08x10 ⁻²	418
0.20	53.2	7.48	4.84x10 ⁻³	1.99x10 ⁻²	418
0.30	52.2	11.1	5.08x10 ⁻³	3.09x10 ⁻²	417
0.40	51.2	14.6	5.35x10 ⁻³	4.32x10 ⁻²	416
0.50	50.2	18.0	5.65x10 ⁻³	5.69x10 ⁻²	416
0.60	49.2	21.4	5.97x10 ⁻³	7.23x10 ⁻²	415
0.70	48.1	24.7	6.23x10 ⁻³	8.98x10 ⁻²	414
0.80	47.0	27.8	6.74x10 ⁻³	1.10x10 ⁻¹	413
0.90	45.9	31.0	7.21x10 ⁻³	1.34x10 ⁻¹	412
1.00	-	-	-	-	-
$k_p^{80^\circ\text{C}}$ (m ³ Pet.mol-site ⁻¹ .s ⁻¹) 1350					
0.00	54.4	0.00	4.58x10 ⁻³	0.00	419
0.10	53.5	4.16	4.89x10 ⁻³	1.25x10 ⁻²	418
0.20	52.6	7.48	5.29x10 ⁻³	2.17x10 ⁻²	418
0.30	51.6	11.1	5.56x10 ⁻³	3.39x10 ⁻²	417
0.40	50.5	14.6	5.84x10 ⁻³	4.71x10 ⁻²	416
0.50	49.5	18.0	6.16x10 ⁻³	6.21x10 ⁻²	416
0.60	48.4	21.4	6.50x10 ⁻³	7.88x10 ⁻²	415
0.70	47.3	24.6	6.91x10 ⁻³	9.82x10 ⁻²	414
0.80	46.2	27.8	7.36x10 ⁻³	1.20x10 ⁻¹	413
0.90	45.0	30.9	7.89x10 ⁻³	1.47x10 ⁻¹	412
1.00	43.7	34.0	8.47x10 ⁻³	1.77x10 ⁻¹	412
$k_p^{80^\circ\text{C}}$ (m ³ Pet.mol-site ⁻¹ .s ⁻¹) 1500					
0.00	54.7	0.00	4.29x10 ⁻³	0.00	419
0.10	53.8	4.15	5.06x10 ⁻³	1.02x10 ⁻²	418
0.20	52.0	7.48	5.74x10 ⁻³	2.35x10 ⁻²	418
0.30	50.9	11.1	6.02x10 ⁻³	3.67x10 ⁻²	417
0.40	49.9	14.6	6.33x10 ⁻³	5.11x10 ⁻²	416
0.50	48.8	18.0	6.68x10 ⁻³	6.73x10 ⁻²	416
0.60	47.7	21.4	7.07x10 ⁻³	8.57x10 ⁻²	415
0.70	46.6	24.6	7.50x10 ⁻³	1.07x10 ⁻¹	414
0.80	45.4	27.8	7.98x10 ⁻³	1.31x10 ⁻¹	413
0.90	44.1	30.9	8.55x10 ⁻³	1.59x10 ⁻¹	412
1.00	42.8	34.0	9.20x10 ⁻³	1.92x10 ⁻¹	412

Table B. 3 – Other operational conditions such as ethylene outlet flow, product volumetric outlet flow, bulk density, etc

Simulation II Results – Other operational calculations					
C_0^* (mol-site/m ³ c)	$k_p^{80^\circ\text{C}}$ (m ³ Pet.mol-site ⁻¹ .s ⁻¹)		T_0 (°C)	Molar Gas inflow rate, F (mol/s)	
0.55	1200		40.0	1800	
Catalyst flow rate (g/s) 0.222					
$P_{\text{hex.}}$ (bar)	$m_{\text{et.}}$ (kg/s)	$m_{\text{hex.}}$ (kg/s)	$m_{\text{et.d}}$ (kg/s)	$m_{\text{hex.d}}$ (kg/s)	ρ (kg/m ³)
0.20	53.5	7.60	5.33x10 ⁻³	2.19x10 ⁻²	418
0.30	52.5	11.3	5.58x10 ⁻³	3.40x10 ⁻²	417
0.40	51.4	14.8	5.88x10 ⁻³	4.75x10 ⁻²	416
0.50	50.4	18.3	6.21x10 ⁻³	6.26x10 ⁻²	416
0.60	49.3	21.7	6.55x10 ⁻³	7.97x10 ⁻²	415
0.70	48.2	25.0	6.96x10 ⁻³	9.90x10 ⁻²	414
0.80	47.0	28.3	7.42x10 ⁻³	1.21x10 ⁻¹	413
0.90	45.8	31.4	7.93x10 ⁻³	1.47x10 ⁻¹	412
1.00	44.5	34.5	8.54x10 ⁻³	1.78x10 ⁻¹	412
Catalyst flow rate (g/s) 0.236					
0.20	52.9	7.60	5.81x10 ⁻³	2.38x10 ⁻²	418
0.30	51.8	11.3	6.10x10 ⁻³	3.71x10 ⁻²	417
0.40	50.7	14.8	6.41x10 ⁻³	5.17x10 ⁻²	416
0.50	49.6	18.3	6.76x10 ⁻³	6.81x10 ⁻²	416
0.60	48.5	21.7	7.16x10 ⁻³	8.67x10 ⁻²	415
0.70	47.3	25.0	7.59x10 ⁻³	1.08x10 ⁻¹	414
0.80	46.1	28.3	8.11x10 ⁻³	1.33x10 ⁻¹	413
0.90	44.9	31.4	8.66x10 ⁻³	1.61x10 ⁻¹	412
1.00	43.5	34.5	9.35x10 ⁻³	1.95x10 ⁻¹	412
Catalyst flow rate (g/s) 0.250					
0.20	52.2	7.59	6.31x10 ⁻³	2.59x10 ⁻²	418
0.30	51.1	11.3	6.61x10 ⁻³	4.02x10 ⁻²	417
0.40	50.0	14.8	6.96x10 ⁻³	5.62x10 ⁻²	416
0.50	48.8	18.3	7.34x10 ⁻³	7.39x10 ⁻²	416
0.60	47.7	21.7	7.76x10 ⁻³	9.41x10 ⁻²	415
0.70	46.5	25.0	8.26x10 ⁻³	1.17x10 ⁻¹	414
0.80	45.2	28.3	8.77x10 ⁻³	1.44x10 ⁻¹	413
0.90	43.9	31.4	9.42x10 ⁻³	1.75x10 ⁻¹	412
1.00	42.5	34.5	1.01x10 ⁻²	2.11x10 ⁻¹	412

Table B. 4 – Other operational conditions such as ethylene outlet flow, product volumetric outlet flow, bulk density, etc

Simulation III Results – Other operational calculations					
C_0^* (mol-site/m ³ c)	$k_p^{80^\circ\text{C}}$ (m ³ Pet.mol-site ⁻¹ .s ⁻¹)		Catalyst flow rate (g/s)	Molar Gas inflow rate, F (mol/s)	
0.55	1500		0.200	2000	
T_0 (°C) 40					
$P_{\text{hex.}}$ (bar)	$m_{\text{et.}}$ (kg/s)	$m_{\text{hex.}}$ (kg/s)	$m_{\text{et.d}}$ (kg/s)	$m_{\text{hex.d}}$ (kg/s)	ρ (kg/m ³)
0.20	-	-	-	-	-
0.30	-	-	-	-	-
0.40	46.5	13.4	5.35x10 ⁻³	4.32x10 ⁻²	416
0.50	45.6	16.6	5.65x10 ⁻³	5.69x10 ⁻²	416
0.60	44.6	19.7	5.96x10 ⁻³	7.22x10 ⁻²	415
0.70	43.6	22.7	6.33x10 ⁻³	9.00x10 ⁻²	414
0.80	42.5	25.6	6.74x10 ⁻³	1.10x10 ⁻¹	413
0.90	41.4	28.5	7.23x10 ⁻³	1.35x10 ⁻¹	412
1.00	40.3	31.3	7.77x10 ⁻³	1.62x10 ⁻¹	412
T_0 (°C) 45					
0.20	-	-	-	-	-
0.30	-	-	-	-	-
0.40	46.5	13.4	5.36x10 ⁻³	4.33x10 ⁻²	416
0.50	45.5	16.6	5.65x10 ⁻³	5.69x10 ⁻²	416
0.60	44.5	19.7	5.98x10 ⁻³	7.25x10 ⁻²	415
0.70	43.5	22.7	6.35x10 ⁻³	9.04x10 ⁻²	414
0.80	42.5	25.6	6.77x10 ⁻³	1.11x10 ⁻¹	413
0.90	41.4	28.5	7.26x10 ⁻³	1.35x10 ⁻¹	412
1.00	40.2	31.3	7.80x10 ⁻³	1.63x10 ⁻¹	412
T_0 (°C) 50					
0.20	-	-	-	-	-
0.30	-	-	-	-	-
0.40	46.5	13.4	5.35x10 ⁻³	4.32x10 ⁻²	416
0.50	45.5	16.6	5.66x10 ⁻³	5.70x10 ⁻²	416
0.60	44.5	19.7	5.98x10 ⁻³	7.25x10 ⁻²	415
0.70	43.5	22.7	6.34x10 ⁻³	9.02x10 ⁻²	414
0.80	42.4	25.6	6.79x10 ⁻³	1.11x10 ⁻¹	413
0.90	41.3	28.5	7.27x10 ⁻³	1.35x10 ⁻¹	412
1.00	40.1	31.3	7.83x10 ⁻³	1.63x10 ⁻¹	412

Table B. 5 – Other operational conditions such as ethylene outlet flow, product volumetric outlet flow, bulk density, etc

Next tables – B.6 and B.7 – concern relative variation of production and temperature for each hexane pressure. They are for Simulation 2 and simulation 3. Simulation 1 is in the body of thesis in results chapter (plot results).

To calculate the relative variation for polyethylene production, it was used the following formula:

$$\Delta \dot{m}_{Pet}(\%) = \frac{\dot{m}_{i+1} - \dot{m}_i}{\dot{m}_i} 100, 0.1 \leq i = P_{hex,i} \leq 1.0 \quad (n)$$

It's analogous for reaction temperature relative variation:

$$\Delta T(\%) = \frac{T_{i+1} - T_i}{T_i} 100, 0.1 \leq i = P_{hex,i} \leq 1.0 \quad (o)$$

SIMUL.2	m _{Pet.} Relative variation (%)			T relative variation (%)			Operation-mode
	Q _{c.0} (g/s)						
P _{hex.} (bar)	0.222	0.236	0.250	0.222	0.236	0.250	
0.20	-	-	-	-	-	-	-
0.30	2.40	2.17	1.97	-1.35	-1.52	-1.67	DRY
0.40	2.46	2.57	2.32	-1.14	-1.10	-1.27	DRY
0.50	1.70	1.82	2.27	-6.93	-6.67	-6.22	COND.
0.60	1.37	1.49	1.60	-8.68	-8.33	-8.01	COND.
0.70	1.64	1.74	1.83	-8.42	-8.05	-7.71	COND.
0.80	0.87	1.39	1.49	-8.90	-8.19	-7.82	COND.
0.90	0.61	1.15	1.62	-9.45	-8.62	-7.89	COND.
1.00	0.55	0.71	1.21	-8.99	-8.42	-7.62	COND.

Table B. 6 – Relative variation of polyethylene mass rate and reactor temperature for each hexane pressure with respect to simulation 2

SIMUL.3	m _{Pet.} Relative variation (%)			T relative variation (%)			Operation-mode
	T ₀ (°C)						
P _{hex.} (bar)	40	45	50	40	45	50	
0.40	-	-	-	-	-	-	-
0.50	<u>1.73</u>	2.48	2.58	<u>-6.86</u>	-0.88	-0.84	DRY/ <u>COND.</u>
0.60	<u>1.80</u>	<u>2.21</u>	2.72	<u>-8.35</u>	<u>-5.52</u>	-0.63	DRY/ <u>COND.</u>
0.70	1.67	2.16	2.60	-8.31	-7.24	-4.47	COND.
0.80	1.32	2.57	2.68	-8.48	-6.80	-5.57	COND.
0.90	1.07	2.20	2.92	-8.95	-7.03	-5.90	COND.
1.00	1.03	2.37	2.89	-8.42	-6.40	-5.51	COND.

Table B. 7 – Relative variation of polyethylene mass rate and reactor temperature for each hexane pressure with respect to simulation 3. For 0.50 and 0.60bar hexane pressures, the reactor operates in dry or condensed (numbers are underlined) mode depending on inlet temperature, T₀. From 0.6bar on, the reactor operates in condensed mode regardless the inlet temperature.